JPL Publication 83-39, Rev. 5

Observation Model and Parameter Partials for the JPL VLBI Parameter Estimation Software "MODEST"—1994

O. J. Sovers
C. S. Jacobs

August 1994

NASA
National Aeronautics and
Space Administration

Jet Propulsion Laboratory
California Institute of Technology
Pasadena California

The research described in this publication was carried out by the Jet Propulsion Laboratory, Cal
Institute of Technology, under a contract with the National Aeronautics and Space Administra

FOREWORD

This report is the fifth revision of the document *Observation Model and Parameter Partials for the JPL VLBI Parameter Estimation Software "MODEST" – 1991*, dated August 1, 1991, which it supersedes. A number of model revisions and improvements were made from 1991 to 1994. They are briefly enumerated in the abstract. The present document corresponds to MODEST version 278, which has been in use since June, 1994. The authors hope to publish revisions of this document in the future, as modeling improvements warrant.

ACKNOWLEDGMENTS

We would like to express our appreciation to Jack Fanselow who, together with Brooks Thomas and James Williams, initiated VLBI studies at JPL during the 1970s. Jack has now moved on to other areas, and leaves behind an excellent theoretical and practical foundation to build upon in the future. This document and the MASTERFIT/MODEST code are part of that legacy. Brooks and Jim continue to provide theoretical and practical guidance to JPL VLBI studies.

Whatever level of usefulness this document has achieved is due in substantial part to cooperation with colleagues in the Deep Space Tracking Group during the 1980s and '90s. In some sense the authors are merely a clearinghouse for ideas concerning clarification and additional modeling that were required as the experiments were refined. We have recently benefitted from the help of Gabor Lanyi concerning the various antenna effects which are becoming more important as higher measurement accuracy is approached. Likewise, Patrick Charlot and Jim Ulvestad contributed to the implementation of source structure corrections. Many other colleagues in Section 335 contributed to improvements and clarifications of the MASTERFIT code over the years. Among them are Steve Allen, Dick Branson, Rachel Dewey, Chad Edwards, Marshall Eubanks, Jean-François Lestrade, Kurt Liewer, Steve Lowe, Chuck Naudet, Jean Patterson, Larry Romans, Alan Steppe, Bob Treuhaft, and Mike Watkins.

ABSTRACT

This report is a revision of the document *Observation Model and Parameter Partials for the JPL VLBI Parameter Estimation Software "MODEST" – 1991*, dated August 1, 1991. It supersedes that document and its four previous versions (1983, 1985, 1986, and 1987). A number of aspects of the very long baseline interferometry (VLBI) model were improved from 1991 to 1994. Treatment of tidal effects is extended to model the effects of ocean tides on universal time and polar motion (UTPM), including a default model for nearly diurnal and semidiurnal ocean tidal UTPM variations, and partial derivatives for all (solid and ocean) tidal UTPM amplitudes. The time-honored "K_1 correction" for solid Earth tides has been extended to include analogous frequency-dependent response of five tidal components. Partials of ocean loading amplitudes are now supplied. The Zhu-Mathews-Oceans-Anisotropy (ZMOA) 1990-2 and Kinoshita-Souchay models of nutation are now two of the modeling choices to replace the increasingly inadequate 1980 International Astronomical Union (IAU) nutation series. A rudimentary model of antenna thermal expansion is provided. Two more troposphere mapping functions have been added to the repertoire. Finally, correlations among VLBI observations via the model of Treuhaft and Lanyi improve modeling of the dynamic troposphere. A number of minor misprints in Rev. 4 have been corrected.

CONTENTS

TABLES

SECTION 1

INTRODUCTION

In applications of radio interferometry to geodynamics and astrometry, observed values of group delay and phase delay rate obtained from observations of many different radio sources must be passed simultaneously through a multiparameter estimation routine to extract the significant model parameters. As the accuracy of radio interferometry has improved, increasingly complete models for the delay and delay rate observables have been developed. This report describes the current status of the delay model used in the Jet Propulsion Laboratory multiparameter estimation program "MODEST", which is the successor to the "MASTERFIT" code developed at JPL in the 1970s. It is assumed that the reader has at least a cursory knowledge of the principles of very long baseline interferometry (VLBI). Some references which provide an introduction are the book by Thompson, Moran, and Swenson (1986), and two reports by Thomas (1981, 1987).

The delay model is the sum of four major model components: geometry, clock, troposphere, and ionosphere. Sections 2 through 5 present our current models for these components, as well as their partial derivatives with respect to parameters that are to be adjusted by multiparameter fits to the data. The longest section (2) deals with the purely geometric portion of the delay and covers the topics of time definitions, tidal and source structure effects, coordinate frames, Earth orientation (universal time and polar motion), nutation, precession, Earth orbital motion, wave front curvature, gravitational bending, and antenna offsets. Section 6 describes the technique used to obtain the delay rate model from the delay model. Section 7 gives the values of physical constants used in MODEST, while Section 8 outlines model improvements that may be required by more accurate data in the future.

SECTION 2

GEOMETRIC DELAY

The geometric delay is that interferometer delay which would be measured by perfect instrumentation, perfectly synchronized, if there were a perfect vacuum between the observed extragalactic or Solar-System sources and the Earth-based instrumentation. For Earth-fixed baselines, this delay can be as large as 20 milliseconds, changing rapidly (by up to 3.1 μs per second) as the Earth rotates. In general the geometric component is by far the largest component of the observed delay. The main complexity of this portion of the model arises from the numerous coordinate transformations necessary to relate the reference frame used for locating the radio sources to the Earth-fixed reference frame in which station locations are represented.

In the following we will assume, unless otherwise stated, that "celestial reference frame" means a reference frame in which there is no net proper motion of the extragalactic radio objects which are observed by the interferometer. This is only an approximation to some truly "inertial" frame. Currently, this celestial frame implies a geocentric, equatorial frame with the equator and equinox of 2000 January 1.5 (J2000) as defined by the 1976 International Astronomical Union (IAU) conventions, including the 1980 nutation series (Seidelmann, 1982; Kaplan, 1981).

In this equatorial frame, some definition of the origin of right ascension must be made. We will not discuss that in this report, since one definition is at most a rotation from some other definition, and can be applied at any time. The important point is that consistent definitions must be used throughout the model development. The need for this consistency will, in all probability, eventually lead to our defining the origin of right ascension by means of the JPL planetary ephemerides, followed by our using interferometric observations of both natural radio sources and spacecraft at planetary encounters as a means of connecting the planetary and the radio reference frames (Folkner *et al.*, 1994; Dewey, 1991; Newhall *et al.*, 1986).

Also, unless otherwise stated, we will mean by "terrestrial reference frame" some reference frame tied to the mean surface features of the Earth. Currently, we are using a right-handed version of the Conventional International Origin (CIO) reference system with the pole defined by the 1903.0 pole. In practice, this is accomplished by defining the position of one of the interferometric observing stations (generally Deep Space Station (DSS) 15 at the Goldstone deep space tracking complex), and then by measuring the positions of the other stations under a constraint. This constraint is that the determinations of Earth orientation agree on the average with the International Earth Rotation Service (IERS) (1993) [and its predecessor, Bureau International de l'Heure (BIH) (1983)] measurements of the Earth's orientation over some substantial time interval ($\approx$ years). This procedure, or its functional equivalent, is necessary since the interferometer is sensitive only to the baseline vector. The VLBI technique does not have any preferred origin relative to the structure of the Earth. The rotation of the Earth does, however, provide a preferred direction in space which can be associated indirectly with the surface features of the Earth.

In contrast, geodetic techniques which involve the use of artificial satellites, or the Moon, are sensitive to the center of mass of the Earth as well as the spin axis. Thus, those techniques require only a definition of the origin of longitude. Laser ranging to the retroreflectors on the Moon allows a realizable practical definition of a terrestrial frame, accurately positioned relative to a celestial frame which is tied to the planetary ephemerides (Folkner *et al.*, 1994). The required collocation of the laser and VLBI stations is being provided by Global Positioning Satellite (GPS) measurements of baselines between VLBI and laser sites starting in the late 1980s (*e.g.*, Ray *et al.*, 1991). Careful definitions and experiments of this sort are required to realize a coordinate system of centimeter accuracy.

The relativistic delay formulation presented in this report is essentially identical to that in the original 1983 version (Fanselow, 1983). Special relativistic terms in the model delay have not been changed, but a small revision was made in the default gravitational correction starting with Rev. 3 (Sovers and Fanselow, 1987), when TDT (Temps Dynamique Terrestre) spatial coordinates were introduced (see Sec. 2.1.3). Among the estimated parameters, only baseline lengths were affected by this change, in that all distances were increased by the same factor of ≈ 2 parts in 10^8.

Except for subcentimeter relativistic complications caused by the locally varying Earth potential (as discussed below), calculation of the VLBI model for the observed delay can be summarized as:

1. Specify the proper locations of the two stations as measured in an Earth-fixed frame at the time that the wave front intersects station #1. Let this time be the proper time t_1' as measured by a clock in the Earth-fixed frame.
2. Modify the station locations for Earth-fixed effects such as solid Earth tides, tectonic motion, and other local station motion.
3. Transform these proper station locations to a geocentric celestial coordinate system with its origin at the center of the Earth, but moving with the Earth. This is a composite of 12 separate rotations, represented by a rotation matrix $Q(t)$.
4. Perform a Lorentz transformation of these proper station locations from the geocentric celestial frame to a frame at rest relative to the center of mass of the Solar System, and rotationally aligned with the celestial geocentric frame.
5. In this Solar-System-barycentric (SSB) frame, compute the proper time delay for the passage of the specified wave front from station #1 to station #2. Correct for source structure. Add the effective change in proper delay caused by the differential gravitational retardation of the signal.
6. Perform a Lorentz transformation of this SSB geometric delay back to the celestial geocentric frame moving with the Earth. This produces the adopted model for the geometric portion of the observed delay.
7. To this geometric delay, add the contributions due to clock offsets, to tropospheric delays, and to the effects of the ionosphere on the signal (see Sections 3 through 5).

As indicated in step 5, the initial calculation of delay is carried out in a frame at rest relative to the center of mass of the Solar System (SSB frame.) First, however, steps 1 through 4 are carried out in order to relate proper locations in the Earth-fixed frame to corresponding proper locations in the SSB frame. Step 4 in this process transforms station locations from the geocentric celestial frame to the SSB frame. This step incorporates special-relativistic effects to all orders of the velocity ratio v/c. In the presence of gravity, this transformation can be viewed as a special relativistic transformation between proper coordinates of two local frames (geocentric and SSB) in relative motion. For both frames, the underlying gravitational potential can be viewed approximately as the sum of locally constant potentials caused by all masses in the Solar System. The complications caused by small local variations in the Earth's potential are discussed below. Initial proper delay is then computed (step 5) in the SSB frame on the basis of these SSB station locations and an *a priori* SSB source location. A small proper-delay correction is then applied to account for the differential gravitational retardation introduced along the two ray paths through the Solar System, including retardation by the Earth's gravity. A final Lorentz transformation including all orders of v/c then transforms the corrected SSB proper delay to a model for the observed delay.

Since the Earth's potential varies slightly across the Earth ($\Delta U_E/c^2 \approx 4 \times 10^{-10}$ from center to surface), the specification of proper distance is not as straightforward with respect to the Earth's potential as it is with respect to the essentially constant potentials of distant masses. To overcome this difficulty, output station locations are specified in terms of the "TDT spatial coordinates" (Shahid-Saless *et al.*, 1991) used in Earth-orbiter models. Baselines modeled on the basis of this convention deviate slightly in length ($\leq$ 2 mm) from the proper values. A proper length that corresponds to a modeled baseline can be obtained through appropriate integration of the local metric (Shahid-Saless *et al.*, 1991). In practice, such a conversion is not necessary since comparison of baseline measurements obtained by different groups would be carried out in terms of TDT spatial coordinates.

The current model has been compared (Thomas, 1991; Treuhaft, 1991) with the "1-picosecond" relativistic model for VLBI delays developed by Shahid-Saless *et al.* (1991). When reduced to the same form, the model presented here is identical to that model at the picosecond level, term by term, with one exception. Treuhaft and Thomas (1991) show that a correction is needed to the Shahid-Saless *et al.* SSB system modeling of the atmospheric delay. This correction changes the Shahid-Saless *et al.* result by as much as 10 picoseconds. The remainder of this section provides the details for the first six steps of the general outline above.

2.1 TIME INTERVAL FOR THE PASSAGE OF A WAVE FRONT BETWEEN TWO STATIONS

The fundamental part of the geometric model is the calculation (step #5 above) of the time interval for the passage of a wave front from station #1 to station #2. This calculation is actually performed in a coordinate frame at rest relative to the center of mass of the Solar System. This part of the model is presented first to provide a context for the subsequent sections, all of which are heavily involved with the details of time definitions and coordinate transformations. We will use the same subscript and superscript notation which is used in Section 2.7 to refer to the station locations as seen by an observer at rest relative to the center of mass of the Solar System.

First, we calculate the proper time delay that would be observed if the wave front were planar. Next, we generalize this calculation to a curved wave front, and finally, we take into account the incremental effect which results from the fact that we must consider wave fronts that propagate through the various gravitational potential wells in the Solar System.

2.1.1 PLANE WAVE FRONT

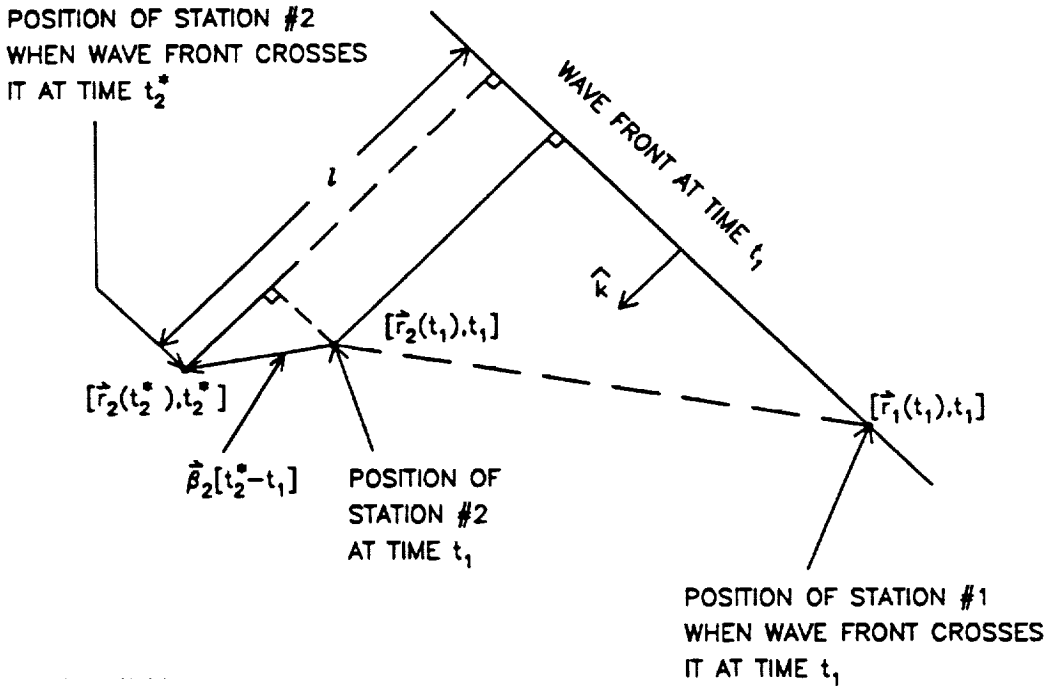

Figure 1. Geometry for calculating the transit time of a plane wave front

Consider the case of a plane wave moving in the direction, $\hat{\mathbf{k}}$, with station 2 having a mean velocity, $\boldsymbol{\beta}_2$, as shown in Figure 1. As mentioned above, distance and time are to be represented as proper coordinates in the SSB frame. The speed of light c is set equal to 1 in the following formulation. The proper time delay is the time it takes the wave front to move the distance l at speed c. This distance is the sum of the two solid lines perpendicular to the wave front in Figure 1:

$$t_2^* - t_1 = \hat{\mathbf{k}} \cdot [\mathbf{r}_2(t_1) - \mathbf{r}_1(t_1)] + \hat{\mathbf{k}} \cdot \boldsymbol{\beta}_2[t_2^* - t_1] \tag{2.1}$$

where the superscript $*$ serves to emphasize that station #2 has moved since t_1. This leads to the following expression for the geometric delay:

$$t_2^* - t_1 = \frac{\hat{\mathbf{k}} \cdot [\mathbf{r}_2(t_1) - \mathbf{r}_1(t_1)]}{1 - \hat{\mathbf{k}} \cdot \boldsymbol{\beta}_2} \tag{2.2}$$

The baseline vector, $\mathbf{r}_2(t_1) - \mathbf{r}_1(t_1)$, is computed on the basis of proper station locations calculated according to Eq. (2.183) in Sec. 2.7.

2.1.2 CURVED WAVE FRONT

In the case of a signal generated by a radio source within the Solar System it is necessary to include the effect of the curvature of the wave front. As depicted in Figure 2, let a source irradiate two Earth-fixed stations whose positions are given by $\mathbf{r}_i(t)$ relative to the Earth's center. The position of the Earth's center, $\mathbf{R}_c(t_1)$, as a function of signal reception time, t_1, at station #1 is measured relative to the position of the emitter at the time, t_e, of emission of the signal received at time t_1. While this calculation is actually done in the Solar System barycentric coordinate system, the development that follows is by no means restricted in applicability to that frame.

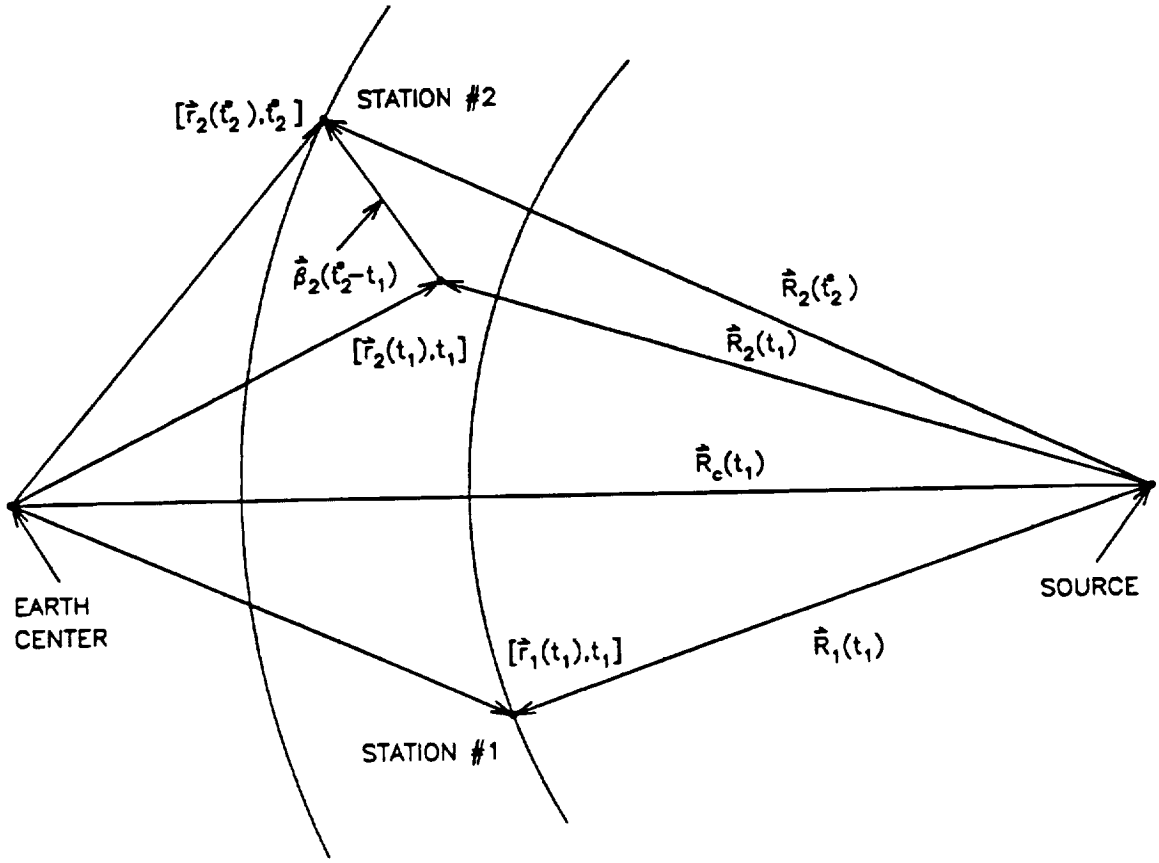

Figure 2. Geometry for calculating the transit time of a curved wave front

Suppose that a wave front emitted by the source at time t_e reaches station #1 at time t_1 and arrives at station #2 at time t_2^*. The geometric delay in this frame will be given by:

$$\tau = t_2^* - t_1 = |\mathbf{R}_2(t_2^*)| - |\mathbf{R}_1(t_1)| \tag{2.3}$$

where all distances are again measured in units of light travel time. If we approximate the velocity of station #2 by

$$\boldsymbol{\beta}_2 = \frac{\mathbf{R}_2(t_2^*) - \mathbf{R}_2(t_1)}{t_2^* - t_1} \tag{2.4}$$

and use the relation

$$\mathbf{R}_i(t_1) = \mathbf{R}_c(t_1) + \mathbf{r}_i(t_1) \tag{2.5}$$

we obtain:

$$\begin{aligned}\tau &= |\mathbf{R}_c(t_1) + \mathbf{r}_2(t_1) + \boldsymbol{\beta}_2\tau| - |\mathbf{R}_c(t_1) + \mathbf{r}_1(t_1)| \\ &= R_c(t_1)\ [\ |\hat{\mathbf{R}}_c + \boldsymbol{\varepsilon}_2| - |\hat{\mathbf{R}}_c + \boldsymbol{\varepsilon}_1|\ ]\end{aligned} \tag{2.6}$$

where

$$\boldsymbol{\varepsilon}_2 = \frac{\mathbf{r}_2(t_1) + \boldsymbol{\beta}_2\tau}{R_c(t_1)} \tag{2.7}$$

and

$$\boldsymbol{\varepsilon}_1 = \frac{\mathbf{r}_1(t_1)}{R_c(t_1)} \tag{2.8}$$

For ε_1 and $\varepsilon_2 \leq 10^{-4}$, we need to keep only terms of order ε^3 in a sixteen-place machine in order to expand the expression for τ in equation (2.6). This gives us:

$$\tau = \frac{\hat{\mathbf{R}}_c \cdot [\mathbf{r}_2(t_1) - \mathbf{r}_1(t_1)]}{[1 - \hat{\mathbf{R}}_c \cdot \boldsymbol{\beta}_2]} + \frac{R_c \Delta_c(\tau)}{2\ [1 - \hat{\mathbf{R}}_c \cdot \boldsymbol{\beta}_2]} \tag{2.9}$$

where to order ε^3

$$\Delta_c(\tau) = [\varepsilon_2^2 - \varepsilon_1^2] - [(\hat{\mathbf{R}}_c \cdot \boldsymbol{\varepsilon}_2)^2 + (\hat{\mathbf{R}}_c \cdot \boldsymbol{\varepsilon}_1)^2 + (\hat{\mathbf{R}}_c \cdot \boldsymbol{\varepsilon}_2)^3 - (\hat{\mathbf{R}}_c \cdot \boldsymbol{\varepsilon}_2)\varepsilon_2^2 - (\hat{\mathbf{R}}_c \cdot \boldsymbol{\varepsilon}_1)^3 + (\hat{\mathbf{R}}_c \cdot \boldsymbol{\varepsilon}_1)\varepsilon_1^2] \tag{2.10}$$

The first term in (2.9) is just the plane wave approximation, *i.e.*, as $R_c \rightarrow \infty$, $\hat{\mathbf{R}}_c \rightarrow \hat{\mathbf{k}}$, with the second term in brackets in (2.10) approaching zero as r^2/R_c. Given that the ratio of the first term to the second term is $\approx r/R_c$, wave front curvature is not calculable in a sixteen-place machine for $R > 10^{16} \times r$. For Earth-fixed baselines that are as long as an Earth diameter, requiring that the effects of curvature be less than 0.01 cm implies that the above formulation (2.10) must be used for $R < 1.4 \times 10^{15}$ km, or approximately 150 light years.

The procedure for the solution of (2.9) is iterative for $\varepsilon < 10^{-4}$, using the following:

$$\tau_n = \tau_0 + \frac{R_c \Delta_c(\tau_{n-1})}{2[1 - \hat{\mathbf{R}} \cdot \boldsymbol{\beta}_2]} \tag{2.11}$$

where

$$\tau_0 = \tau_{plane\ wave} \tag{2.12}$$

For $\varepsilon > 10^{-4}$, directly iterate on the equation (2.6) itself, using the procedure:

$$\tau_n = R_c|\hat{\mathbf{R}}_c + \boldsymbol{\varepsilon}_2(\tau_{n-1})| - R_c|\hat{\mathbf{R}}_c + \boldsymbol{\varepsilon}_1| \tag{2.13}$$

where again τ_0 is the plane wave approximation.

2.1.3 GRAVITATIONAL DELAY

Because a light signal propagating in a gravitational potential is retarded relative to its motion in field-free space, the computed value for the differential time of arrival of the signals at $\mathbf{r}_1(t_1)$ and $\mathbf{r}_2(t_2^*)$ must be corrected for gravitational effects. Gravitational potential effects and curved wave front effects are calculated independently of each other since the former are a small perturbation ($\approx$ 8.5 microradians or $\leq 1.''75$), even for Sun-grazing rays.

For the geometry illustrated in Figure 3, the required correction to *coordinate* time delay is given by Moyer (1971) as:

$$\Delta_{G_j} = \frac{(1 + \gamma_{PPN})\mu_j}{c^3} \cdot \left[\ln\left[\frac{r_s + r_2(t_2^*) + r_{s2}}{r_s + r_2(t_2^*) - r_{s2}}\right] - \ln\left[\frac{r_s + r_1(t_1) + r_{s1}}{r_s + r_1(t_1) - r_{s1}}\right] \right] \tag{2.14}$$

where r_{si} is defined as:

$$r_{si} = |\mathbf{r}_i(t_i) - \mathbf{r}_s(t_c)| \tag{2.15}$$

Here γ_{PPN} is the γ factor in the parametrized post-Newtonian gravitational theory (e.g. Misner *et al.*, 1973). In the Brans-Dicke theory,

$$\gamma_{PPN} = \frac{1+\omega}{2+\omega} \tag{2.16}$$

where ω is the coupling constant of the scalar field. For general relativity, $\gamma_{PPN} = 1$, *i.e.*, $\omega \to \infty$. However, we allow γ_{PPN} to be an estimated parameter so that by setting $\gamma_{PPN} = -1$, we also have the option of "turning off" the effects of general relativity on the estimate of the delay. This proves useful for software development. The gravitational constant, μ_p, is

$$\mu_p = Gm_p \tag{2.17}$$

where G is the universal gravitational constant, and m_p is the mass of the pth gravitating body.

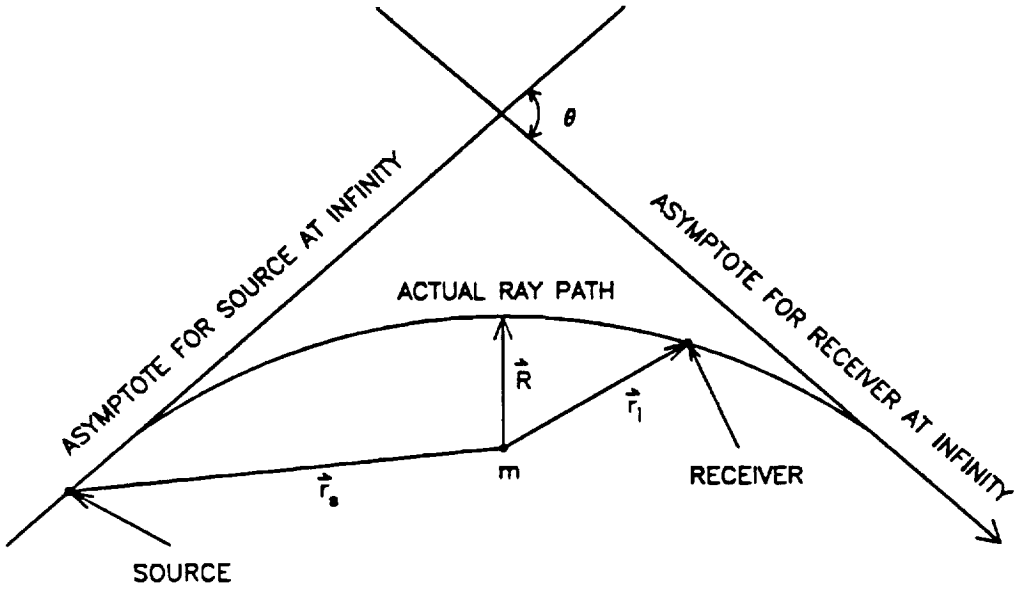

Figure 3. A schematic representation of the geodesic connecting two points in the presence of a gravitational mass

Depending on the particular source-receiver geometry in a VLBI experiment, a number of approximations are possible for the correction Δ_{Gp} of (2.14). Dropping the time arguments in (2.14), we have:

$$\Delta_{Gp} = \frac{(1+\gamma_{PPN})\mu_p}{c^3} \cdot \ln\left[\left[\frac{r_s + r_2 + r_{s2}}{r_s + r_1 + r_{s1}}\right]\left[\frac{r_s + r_1 - r_{s1}}{r_s + r_2 - r_{s2}}\right]\right] \tag{2.18}$$

This formulation is fine for $r_s \approx r_i \approx r_{si}$, but can be put in a computationally better form for the case of distant sources with closely spaced VLBI receivers, *i.e.*, $|\mathbf{r}_2 - \mathbf{r}_1|/r_1 \to 0, r_i/r_s \to 0$. For these sources, expand Δ_{Gp} in terms of r_i/r_s, r_{si}/r_s, and make use of the relationship

$$r_{si} = [\mathbf{r}_s^2 - 2\mathbf{r}_s \cdot \mathbf{r}_i + \mathbf{r}_i^2]^{1/2} \approx r_s - \mathbf{r}_i \cdot \hat{\mathbf{r}}_s \tag{2.19}$$

This leads to

$$\Delta_{Gp} = \frac{(1+\gamma_{PPN})\mu_p}{c^3} \cdot \ln\left[\frac{r_1 + \mathbf{r}_1 \cdot \hat{\mathbf{r}}_s}{r_2 + \mathbf{r}_2 \cdot \hat{\mathbf{r}}_s}\right] \tag{2.20}$$

for $r_i/r_s \to 0$.

If we further require that $|\mathbf{r}_2 - \mathbf{r}_1|/r_1 \to 0$, and make use of

$$\mathbf{r}_2 = \mathbf{r}_1 + \Delta\mathbf{r} \tag{2.21}$$

then:

$$\begin{aligned} r_2 + \mathbf{r}_2 \cdot \hat{\mathbf{r}}_s &= r_1\left[1 + 2\,\hat{\mathbf{r}}_1 \cdot \Delta\mathbf{r}/r_1 + (\Delta\mathbf{r}/r_1)^2\right]^{1/2} + \mathbf{r}_1 \cdot \hat{\mathbf{r}}_s + \Delta\mathbf{r} \cdot \hat{\mathbf{r}}_s \\ &\approx r_1\left(1 + \hat{\mathbf{r}}_1 \cdot \Delta\mathbf{r}/r_1\right) + \mathbf{r}_1 \cdot \hat{\mathbf{r}}_s + \Delta\mathbf{r} \cdot \hat{\mathbf{r}}_s \end{aligned} \tag{2.22}$$

In the limit of $\Delta\mathbf{r}/r_1 \to 0$:

$$r_2(1 + \mathbf{r}_2 \cdot \hat{\mathbf{r}}_s) \to r_1(1 + \mathbf{r}_1 \cdot \hat{\mathbf{r}}_s) + \Delta\mathbf{r} \cdot (\hat{\mathbf{r}}_1 + \hat{\mathbf{r}}_s) \tag{2.23}$$

Substituting into (2.20) and expanding the logarithm, we obtain:

$$\Delta_{Gp} = -\frac{(1+\gamma_{PPN})\mu_p}{c^3} \cdot \frac{(\mathbf{r}_2 - \mathbf{r}_1) \cdot (\hat{\mathbf{r}}_1 + \hat{\mathbf{r}}_s)}{r_1(1 + \hat{\mathbf{r}}_1 \cdot \hat{\mathbf{r}}_s)} \tag{2.24}$$

Using whichever of these three formulations (2.18, 2.20 or 2.24) is computationally appropriate, the model calculates a correction Δ_{Gp} for each of the major bodies in the Solar System (Sun, planets, Earth, and Moon).

Before the correction Δ_{Gp} can be applied to a proper delay computed according to Eq. (2.2), it must be converted from a coordinate-delay correction to a proper-delay correction appropriate to a near-Earth frame. For such proper delays, the gravitational correction is given to good approximation by

$$\Delta'_{Gp} = \Delta_{Gp} - (1+\gamma_{PPN})U\tau \tag{2.25}$$

where τ is the proper delay given by Eq. (2.2), and where U is the negative of the gravitational potential of the given mass divided by c^2, as observed in the vicinity of the Earth (U is a positive quantity). The $U\tau$ term is a consequence of the relationship of coordinate time to proper time, and the $\gamma_{PPN}U\tau$ term is a consequence of the relationship of coordinate distance to proper distance.

The total gravitational correction used is:

$$\Delta'_G = \sum_{p=1}^{N} \Delta'_{Gp} \tag{2.26}$$

where the summation to N is over the major bodies in the Solar System. For the Earth, the $(1+\gamma_{PPN})U\tau$ term in Eq. (2.25) is omitted if one wishes to conform with the "TDT spatial coordinates" used to reduce Earth-orbiter data. The scale factor $(1+\gamma_{PPN})U$ is approximately 1.97×10^{-8} for the Sun. A number of other conventions are possible. One of these, which does not omit the $(1+\gamma_{PPN})U\tau$ term for the Earth, but evaluates it at the Earth's surface, yields an additional scale factor of 0.14×10^{-8}. In either case, the model delay is decreased. Consequently, all inferred "measured" lengths increase by the same fraction relative to previous lengths (*e.g.* by 19.7 parts per billion or 21.1 ppb).

Some care must be taken in defining the positions given by $\mathbf{r}_s$, $\mathbf{r}_2(t_2^*)$, and $\mathbf{r}_1(t_1)$. We have chosen as the origin the position of the gravitational mass at the time of closest approach of the received signal to that object. The position, $\mathbf{r}_s$, of the source relative to this origin is the position of that source at the time, t_e, of the emission of the received signal. Likewise, the position, $\mathbf{r}_i(t_i)$, of the ith receiver is its position in this coordinate system at the time of reception of the signal. Even with

this care in the definition of the relative positions, we are making an approximation, and implicitly assuming that such an approximation is no worse than the approximations used by Moyer (1971) to obtain (2.14).

Some considerations follow, regarding the use of appropriate times to obtain the positions of the emitter, the gravitational object, and the receivers. For a grazing ray emitted by a source at infinity, using the position of the gravitating body G at the time of reception of the signal at station #1 rather than at the time of closest approach of the signal to G can cause a 15-cm error on baselines with a length of one Earth radius as shown by the following calculation. From Figure 4, the calculated distance of closest approach, R, changes during the light transit time, $t_{light\ transit}$, of a signal from a gravitational object at a distance R_{EG} by:

$$\Delta R \approx R_{EG}\dot{\Theta} \cdot t_{light\ transit} = \dot{\Theta} \cdot R_{EG}^2/c \tag{2.27}$$

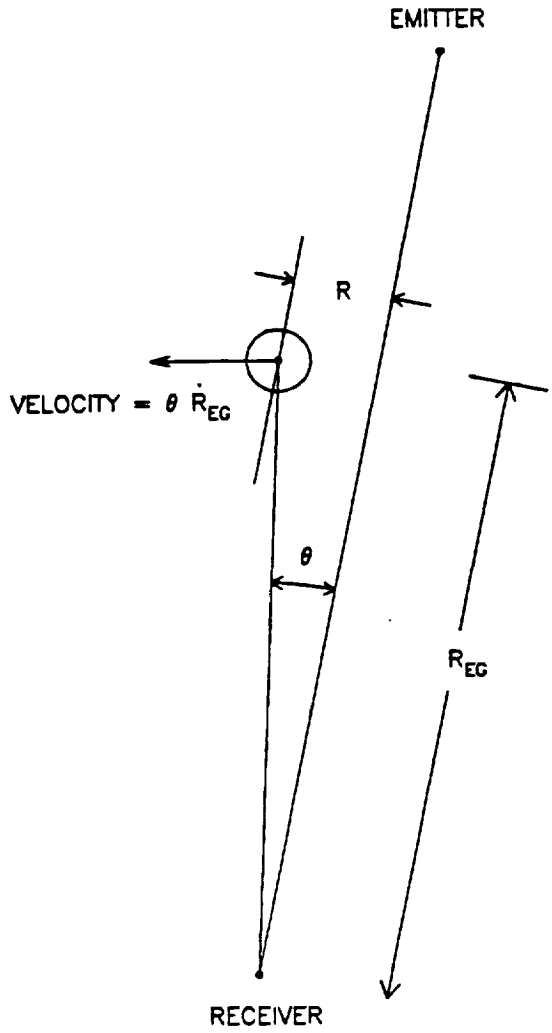

Figure 4. A schematic representation of the motion of a gravitating object during the transit time of a signal from the point of closest approach to reception by an antenna

Since the deflection is:

$$\Delta\Theta \approx 2\frac{(1+\gamma_{PPN})\mu_\odot}{c^3}\left[\frac{c}{R}\right] \tag{2.28}$$

$$\delta(\Delta\Theta) = -\Delta\Theta\left[\frac{\Delta R}{R}\right] = \Delta\Theta\left[\frac{\dot{\Theta} R_{EG}^2}{c R_{EG}\Theta}\right] = \Delta\Theta\left[\frac{R_{EG}}{c\Theta}\right]\frac{\partial\Theta}{\partial t} \tag{2.29}$$

We consider the two bodies of largest mass in the Solar System: the Sun and Jupiter. For grazing rays, their respective deflections $\Delta\Theta$ are 8480 and 73 nanoradians. The barycentric angular velocities $\frac{\partial\Theta}{\partial t}$ are estimated to be 0.06 and 17 nrad/s for the Sun and Jupiter. Note that Eq. (2.27) does not apply to the Sun. The Sun's motion in the barycentric frame has a period of 11 years with a radius on the order of the Sun's radius. Using approximate radii and distances from Earth to estimate R_{EG} and Θ, Eq. (2.29) gives 25 nrad for Jupiter; the corresponding value for the Sun is 0.07 nrad. For a baseline whose length equals the radius of the Earth, $\delta(\Delta\Theta)R_E$ is thus approximately 0.05 and 15 cm for the Sun and Jupiter, respectively. The effect is much smaller for the Sun in spite of its much larger mass, due to its extremely slow motion in the barycentric frame.

In view of the rapid decrease of gravitational deflection with increasing distance of closest approach, it is extremely unlikely that a routine VLBI observation would involve rays passing close enough to a gravitating body for this correction to be of importance. Exceptions are experiments specifically designed to measure planetary gravitational bending (Treuhaft and Lowe, 1991). In order to guard against such an unlikely situation in routine work, and to provide analysis capability for special experiments, the MODEST code always performs the transit-time correction for all planets. To obtain the positions of the gravitational objects, we employ an iterative procedure, using the positions and velocities of the objects at signal reception time. If $\mathbf{R}(t_r)$ is the position of the gravitational object at signal reception time, t_r, then that object's position, $\mathbf{R}(t_a)$, at the time, t_a, of closest approach of the ray path to the object was:

$$\mathbf{R}(t_a) = \mathbf{R}(t_r) - \overline{\mathbf{V}}[t_r - t_a] \tag{2.30}$$

$$t_r - t_a = \frac{|\mathbf{R}_c|}{c} \tag{2.31}$$

We do this correction iteratively, using the velocity, $\mathbf{V}(t_r)$, as an approximation of the mean velocity, $\overline{\mathbf{V}}$. Because $v/c \approx 10^{-4}$, an iterative solution,

$$\mathbf{R}_n(t_a) = \mathbf{R}(t_r) - \left[\frac{\mathbf{V}(t_r)}{c}\right] |\mathbf{R}_{n-1}(t_a)| \tag{2.32}$$

rapidly converges to the required accuracy.

2.2 TIME INFORMATION

Before continuing the description of the geometric model, a few words must be said about time-tag information and the time units which will appear as arguments below. A general reference for time definitions is the *Explanatory Supplement*, 1992. The epoch timing information in the data is taken from the UTC (Universal Coordinated Time) time tags in the data stream at station #1, UTC_1. This time is converted to Terrestrial Dynamic Time (TDT) and is also used as an argument to obtain an *a priori* estimate of Earth orientation. The conversion consists of the following components:

$$TDT = (TDT - TAI) + (TAI - UTC_{IERS}) + (UTC_{IERS} - UTC_{STD}) + (UTC_{STD} - UTC_1) + UTC_1 \tag{2.33}$$

The four offsets in (2.33) thus serve to convert the station 1 time tags to TDT. In turn, their meaning is the following:

1. $TDT - TAI$ is 32.184 seconds by definition; TAI (Temps Atomique International) is atomic time.
2. $TAI - UTC_{IERS}$ is the offset between atomic and coordinated time. The International Earth Rotation Service (IERS), its predecessor, Bureau International de l'Heure (BIH), and Bureau International des Poids et Mesures (BIPM) are the coordinating bodies responsible for upkeep and publication of standard time and Earth rotation quantities. $TAI - UTC_{IERS}$ is a published integer second offset (leap seconds) for any epoch after 1 January, 1972. Prior to that time, it is a more complicated function, which need not be discussed here since MODEST is only intended to model observations starting in the mid-1970s.
3. $UTC_{IERS} - UTC_{STD}$ is the offset in UTC between the coordinated time scales maintained by the IERS (BIPM) and secondary standards maintained by numerous national organizations. For VLBI stations in the U.S. this secondary standard is that of the National Institute of Standards and Technology (NIST) in Boulder, Colorado. These offsets can be obtained from BIPM Circular T (*e.g.* BIPM, 1990).
4. $UTC - UTC_1$ is the (unknown) offset between UTC kept by station 1 and the secondary national standard. This normally amounts to several μs, but may not be precisely known for each experiment. It is a source of modeling error: an error δt in epoch time causes an error of $\approx B\omega_E \Delta t = 7.3 \times 10^{-6}$ cm per km baseline per μs of clock error, where ω_E is the rotation rate of the Earth (Section 7). For the extreme case of a 10,000 km baseline, however, this amounts to only 0.07 cm per μs clock offset.

A priori UT1−UTC and pole positions are normally obtained by interpolation of the IERS Bulletin A smoothed values. However, any other source of UT1−UTC and pole position could be used provided it is a function of UTC, and is expressed in a left-handed coordinate system (see Section 2.6.1). Part of the documentation for any particular set of results should clearly state what were the values of UT1−UTC and pole position used in the data reduction process.

For the Earth model based on the new IAU conventions, the following definitions are employed throughout (Kaplan, 1981):

1. Julian date at epoch J2000 = 2451545.0.
2. All time arguments denoted by T below are measured in Julian centuries of 36525 days of the appropriate time relative to the epoch J2000, *i.e.*, $T = (JD - 2451545.0)/36525$.
3. For the time arguments used to obtain precession, nutation, or to reference the ephemeris, Barycentric Dynamic Time (TDB, Temps Dynamique Barycentrique) is used. This is related to Terrestrial Dynamic Time (TDT, Temps Dynamique Terrestre) by the following:

$$TDB = TDT + 0.^s001658 \sin(g + 0.0167 \sin(g)) \tag{2.34}$$

where

$$g = \frac{(357.^\circ528 + 35999.^\circ050\ TDT) \times 2\pi}{360^\circ} \tag{2.35}$$

2.3 STATION LOCATIONS

Coordinates of the observing stations are expressed in the Conventional International Origin (CIO) 1903.0 reference system, with the reference point for each antenna defined as in Sec. 2.8. The pre-1984 model considered the three coordinates of station i: r_{sp_i}, λ_i, z_i (radius off spin axis, longitude, and height above the equator, respectively) to be time-invariant. At the present accuracy level of space geodesy, it is imperative to account for tectonic motion. This is most simply done by estimating a new set of coordinates in the least-squares process for each VLBI session. Post-processing software then makes linear fits to these results to infer the time rate of change of the station location. Care must be taken that the correlations of coordinates estimated at different epochs are accounted for properly. The advantage of this approach is that the contribution of each session to the overall slope may be independently evaluated, since it is clearly isolated. An alternative second approach is to model tectonic motion directly, and to introduce time rates of change of the station coordinates as parameters in MODEST. The model is linear, with the cylindrical coordinates at time t expressed as

$$r_{sp_i} = r^0_{sp_i} + \dot{r}_{sp_i}(t - t_0) \tag{2.36}$$

$$\lambda_i = \lambda^0_i + \dot{\lambda}_i(t - t_0) \tag{2.37}$$

$$z_i = z^0_i + \dot{z}_i(t - t_0) \tag{2.38}$$

Here t_0 is a reference epoch, at which the station coordinates are $(r^0_{sp_i}, \lambda^0_i, z^0_i)$. If modeling is done in Cartesian coordinates, the analogous expressions are

$$x_i = x^0_i + \dot{x}_i(t - t_0) \tag{2.39}$$

$$y_i = y^0_i + \dot{y}_i(t - t_0) \tag{2.40}$$

$$z_i = z^0_i + \dot{z}_i(t - t_0) \tag{2.41}$$

with (x^0_i, y^0_i, z^0_i) being the station coordinates at the reference epoch t_0.

2.3.1 MODELS OF TECTONIC PLATE MOTION

As alternatives to estimating linear time dependence of the station coordinates, several standard models of tectonic plate motion are optionally available in MODEST. They all describe the motion as a rotation of a given plate about its rotation pole on the surface of a spherical Earth. Time dependence of the Cartesian station coordinates of station i which resides on plate j is expressed as

$$x_i = x^0_i + (\omega^j_y z^0_i - \omega^j_z y^0_i)(t - t_0) \tag{2.42}$$

$$y_i = y^0_i + (\omega^j_z x^0_i - \omega^j_x z^0_i)(t - t_0) \tag{2.43}$$

$$z_i = z^0_i + (\omega^j_x y^0_i - \omega^j_y x^0_i)(t - t_0) \tag{2.44}$$

where $\omega^j_{x,y,z}$ are the angular velocities.

Although these models are based on paleomagnetic data spanning millions of years, they have been found to provide a good quantitative characterization of present-day plate motions. The model due to Minster and Jordan (1978) was the first to be used in VLBI analyses. It is denoted AM0-2 in the original paper, and is also described in an addition to the MERIT standards document (Melbourne *et al.*, 1983, 1985). Table I gives a list of the rotation rates for the 11 plates in the AM0-2 model.

Table I

Plate Rotation Velocities: Minster-Jordan AM0-2 Model†

Plate	ω_x	ω_y	ω_z
AFRC	0.988	-3.360	4.192
ANTA	-0.923	-1.657	3.765
ARAB	4.867	-2.922	6.520
CARB	-0.486	-0.988	1.881
COCO	-11.122	-23.238	12.663
EURA	-0.536	-2.769	3.422
INDI	8.443	4.365	7.528
NAZC	-1.586	-9.299	11.006
NOAM	0.576	-3.984	-0.249
PCFC	-2.143	5.439	-11.438
SOAM	-0.978	-1.863	-1.508

† units are nrad/year

Note that the velocities are expressed in nanoradians per year rather than the microdegrees per year used in the original paper.

More recent models, denoted NUVEL-1 and NNR-NUVEL1, are due to DeMets *et al.* (1990) and Argus and Gordon (1991), respectively. In NUVEL-1, the Pacific plate is stationary, while NNR-NUVEL1 is based on the imposition of a no-net-rotation (NNR) condition. With some notable exceptions, the NUVEL models give rates that are very close to those of the AM0-2 model. The AM0-2 INDI plate has been split into AUST and INDI, and there are two additional plates: JDEF (Juan de Fuca) and PHIL (Philippine). The NUVEL-1 rotation rates are given in Tables II and III.

Table II

Plate Rotation Velocities: NUVEL-1 Model†

Plate	ω_x	ω_y	ω_z
AFRC	2.511	-8.303	14.529
ANTA	0.721	-6.841	14.302
ARAB	8.570	-5.607	17.496
AUST	9.777	0.297	16.997
CARB	1.393	-8.602	12.080
COCO	-9.323	-27.657	21.853
EURA	0.553	-7.567	13.724
INDI	8.555	-5.020	17.528
JDEF	6.81	3.32	5.31
NAZC	-0.023	-14.032	20.476
NOAM	1.849	-8.826	10.267
PCFC	0.000	0.000	0.000
PHIL	11.9	12.8	0.000
SOAM	0.494	-6.646	9.517

† units are nrad/year

Table III

Plate Rotation Velocities: NNR-NUVEL1 Model†

Plate	ω_x	ω_y	ω_z
AFRC	0.929	-3.239	4.098
ANTA	-0.862	-1.777	3.871
ARAB	6.987	-0.543	7.067
AUST	8.194	5.362	6.566
CARB	-0.190	-3.538	1.649
COCO	-10.907	-22.592	11.420
EURA	-1.030	-2.503	3.293
INDI	6.973	0.045	7.097
JDEF	5.227	8.386	-5.124
NAZC	-1.607	-8.968	10.046
NOAM	0.265	-3.761	-0.164
PCFC	-1.583	5.065	-10.430
PHIL	10.320	-7.700	-10.430
SOAM	-1.089	-1.581	-0.913

† units are nrad/year

A recent revision of the paleomagnetic time scale has led to a rescaling of the NUVEL rates. These "NUVEL-1A" and "NNR-NUVEL1A" model rates are equal to the NUVEL-1 and NNR-NUVEL1 rates of Tables II and III, respectively, multiplied by a factor of 0.9562 (DeMets *et al.*, 1994). Partial derivatives with respect to the plate velocities are given in Sec. 2.9.2.

2.4 TIDAL EFFECTS

As an initial step in calculating the geometric delay, we need to consider the effects of crustal motions on station locations. Among these deformations are solid Earth tides, tectonic motions, and alterations of the Earth's surface due to local geological, hydrological, and atmospheric processes. If only the crustal movement due to solid Earth tides and tectonic motion is modeled, then the remaining effects will manifest themselves as temporal changes of the Earth-fixed baseline. It is therefore important to model all crustal motions as completely as possible. The current level of mismodeling of these motions is probably one of the two biggest sources of systematic error (along with the troposphere) in analyses of VLBI data.

In the standard terrestrial coordinate system, tidal effects modify the station location $\mathbf{r}_0$ by an amount

$$\Delta = \Delta_{sol} + \Delta_{pol} + \Delta_{ocn} + \Delta_{atm} \tag{2.45}$$

where the four terms are due to solid Earth tides, pole tide, ocean loading, and atmosphere loading, respectively. Other Earth-fixed effects would be incorporated by augmenting the definition of Δ. All four tidal effects are most easily calculated in some variant of the VEN (vertical, East, North) local geocentric coordinate system. To transform them to the Earth-fixed coordinate frame, the transformation VW, given in the next section, is applied.

2.4.1 SOLID EARTH TIDES

Calculating the alteration of the positions of the stations caused by solid Earth tides is rather complicated due to the solid tides' coupling with the ocean tides, and the effects of local geology. We have chosen to gloss over these complications initially, and to incorporate the simple multipole response model described by Williams (1970), who used Melchior (1966) as a reference. Let $\mathbf{R}_p$ be the position of a perturbing source in the terrestrial reference system, and $\mathbf{r}_0$ the station position in the same coordinate system. To allow for a phase shift (ψ) of the tidal effects from its nominal value of 0, the phase-shifted station vector $\mathbf{r}_s$ is calculated from $\mathbf{r}_0$ by applying a matrix L, describing a right-handed rotation through an angle ψ about the Z axis of date, $\mathbf{r}_s = L\mathbf{r}_0$. This lag matrix, L, is:

$$L = \begin{pmatrix} \cos\psi & \sin\psi & 0 \\ -\sin\psi & \cos\psi & 0 \\ 0 & 0 & 1 \end{pmatrix} \tag{2.46}$$

By a positive value of ψ we mean that the peak response on an Earth meridian occurs at a time $\delta t = \psi/\omega_E$ after that meridian containing $\mathbf{r}_0$ crosses the tide-producing object, where ω_E is the angular rotation rate of the Earth. In the vertical component, the peak response occurs when the meridian containing $\mathbf{r}_s$ also includes $\mathbf{R}_p$.

The tidal potential at $\mathbf{r}_s$ due to the perturbing source at $\mathbf{R}_p$ is expressed as

$$\begin{aligned} U_{tidal} &= \frac{Gm_p}{R_p}\left[\left(\frac{r_s}{R_p}\right)^2 P_2(\cos\theta) + \left(\frac{r_s}{R_p}\right)^3 P_3(\cos\theta)\right] \\ &= U_2 + U_3 \end{aligned} \tag{2.47}$$

where only the quadrupole and octupole terms have been retained. Here, G is the gravitational constant, m_p is the mass of the perturbing source, P_2 and P_3 are Legendre polynomials, and θ is the angle between $\mathbf{r}_s$ and $\mathbf{R}_p$. While the quadrupole displacements are on the order of 50 cm, the mass and distance ratios of the Earth, Moon, and Sun limit the octupole terms to a few mm. The octupole terms are optionally included in the MODEST code, but partials with respect to the Love numbers are available only for the quadrupole terms. An estimate of the retardation correction (employing the position of the tide-producing mass at a time earlier than that of the observation by an amount equal to the light-travel time) shows that this correction is well below 1 mm, and can therefore be neglected.

In a local geocentric VEN coordinate system on a spherical Earth, the tidal displacement vector δ is

$$\delta = \sum_i [\, g_1^{(i)},\ g_2^{(i)},\ g_3^{(i)}]^T \tag{2.48}$$

where the $g_j^{(i)} (i = 2, 3)$ are the quadrupole and octupole displacements. The components of δ are obtained from the tidal potential as

$$g_1^{(i)} = h_i U_i / g \tag{2.49}$$

$$g_2^{(i)} = l_i \cos\phi_s \Big(\frac{\partial U_i}{\partial \lambda_s}\Big) / g \tag{2.50}$$

$$g_3^{(i)} = l_i \Big(\frac{\partial U_i}{\partial \phi_s}\Big) / g \tag{2.51}$$

where $h_i (i = 2, 3)$ are the vertical (quadrupole and octupole) Love numbers, $l_i (i = 2, 3)$ the corresponding horizontal Love numbers, and λ_s and ϕ_s are the station longitude and latitude, and g the acceleration due to gravity,

$$g = G m_E / r_s^2 \tag{2.52}$$

Using the relation between terrestrial and celestial coordinates,

$$\cos\theta = \sin\phi_s \sin\delta_p + \cos\phi_s \cos\delta_p \cos(\lambda_s + \alpha_G - \alpha_p) \tag{2.53}$$

with α_p, δ_p the right ascension and declination of the perturbing body, and α_G the right ascension of Greenwich, some algebra produces the following expressions for the quadrupole and octupole components of δ in terms of the coordinates of the station (x_s, y_s, z_s) and the tide-producing bodies (X_p, Y_p, Z_p):

$$g_1^{(2)} = \sum_p \frac{3\mu_p r_s^2}{R_p^5} \Big[\frac{(\mathbf{r}_s \cdot \mathbf{R}_p)^2}{2} - \frac{r_s^2 R_p^2}{6}\Big] \tag{2.54}$$

$$g_2^{(2)} = \sum_p \frac{3\mu_p r_s^3}{R_p^5} (\mathbf{r}_s \cdot \mathbf{R}_p)(x_s Y_p - y_s X_p)/\sqrt{x_s^2 + y_s^2} \tag{2.55}$$

$$g_3^{(2)} = \sum_p \frac{3\mu_p r_s^2}{R_p^5} (\mathbf{r}_s \cdot \mathbf{R}_p) \Big[\sqrt{x_s^2 + y_s^2}\ Z_p - \frac{z_s}{\sqrt{x_s^2 + y_s^2}} (x_s X_p + y_s Y_p)\Big] \tag{2.56}$$

$$g_1^{(3)} = \sum_p \frac{\mu_p r_s^2}{2R_p^7} (\mathbf{r}_s \cdot \mathbf{R}_p) \Big[5(\mathbf{r}_s \cdot \mathbf{R}_p)^2 - 3 r_s^2 R_p^2\Big] \tag{2.57}$$

$$g_2^{(3)} = \sum_p \frac{3\mu_p r_s^3}{2R_p^7} \Big[5(\mathbf{r}_s \cdot \mathbf{R}_p)^2 - r_s^2 R_p^2\Big] (x_s Y_p - y_s X_p)/\sqrt{x_s^2 + y_s^2} \tag{2.58}$$

$$g_3^{(3)} = \sum_p \frac{3\mu_p r_s^2}{2R_p^7} \Big[5(\mathbf{r}_s \cdot \mathbf{R}_p)^2 - r_s^2 R_p^2\Big] \Big[\sqrt{x_s^2 + y_s^2}\ Z_p - \frac{z_s}{\sqrt{x_s^2 + y_s^2}} (x_s X_p + y_s Y_p)\Big] \tag{2.59}$$

where μ_p is the ratio of the mass of the disturbing object, p, to the mass of the Earth, and

$$\mathbf{R}_p = [X_p, Y_p, Z_p]^T \tag{2.60}$$

is the vector from the center of the Earth to that body. The summations are over tide-producing bodies, of which we include only the Sun and the Moon.

The above formulation implicitly assumes that the Love numbers h_i and l_i are independent of the frequency of the tide-generating potential. Proper treatment entails a harmonic expansion of Eqs. (2.54)-(2.59) and using a different set of h_i, l_i for each frequency component. Presently, only

the first six largest nearly diurnal components are allowed to have Love numbers that differ from the standard values given in Sec. 7. Each harmonic term is denoted by its historical name, if it exists, and the Doodson code (IERS, 1992) (*e.g.*, K_1 and Doodson number = 165555). The Doodson notation classifies the tidal components according to increasing speed. The correction to the solid tidal radial displacement for the kth harmonic term at station s is given by

$$\delta h_2^{sk} = \delta h_2^k H_k(\sqrt{5/24\pi}) \cdot 3 \sin\phi_s \cos\phi_s \sin(\lambda_s + \theta_k) \tag{2.61}$$

where δh_2^k is the difference between the nominal quadrupole (h_2) Love number (0.609) and the frequency dependent Love number (Wahr, 1979), H_k is the amplitude of the kth harmonic term in the tide generating expansion from Cartwright and Edden (1973), ϕ_s is the geocentric latitude of the the station, λ_s is the East longitude of the station and θ_k is the kth harmonic tide argument. The Love numbers and tidal amplitudes are listed in Table IV.

Table IV

Frequency Dependent Solid Earth Tide Parameters

Component (k)	h_2^k	H_k (mm)
ψ_1 (166554)	0.937	3
(165565)	0.514	50
K_1 (165555)	0.520	369
(165545)	0.526	-7
P_1 (163555)	0.581	-122
O_1 (145555)	0.603	-262

These optional corrections yield (Naudet, 1994) additional purely vertical station displacements (in mm) of:

$$\psi_1 \text{ (166554)} \quad \delta g_1 = 0.37 \sin 2\phi_s \sin(\lambda_s + \alpha_G + l') \tag{2.62}$$

$$\text{(165565)} \quad \delta g_1 = -1.84 \sin 2\phi_s \sin(\lambda_s + \alpha_G - \Omega) \tag{2.63}$$

$$K_1 \text{ (165555)} \quad \delta g_1 = -12.68 \sin 2\phi_s \sin(\lambda_s + \alpha_G) \tag{2.64}$$

$$\text{(165545)} \quad \delta g_1 = 0.24 \sin 2\phi_s \sin(\lambda_s + \alpha_G + \Omega) \tag{2.65}$$

$$P_1 \text{ (163555)} \quad \delta g_1 = 1.32 \sin 2\phi_s \sin[\lambda_s + \alpha_G - 2(\Omega + F - D)] \tag{2.66}$$

$$O_1 \text{ (145555)} \quad \delta g_1 = 0.62 \sin 2\phi_s \sin[\lambda_s + \alpha_G - 2(\Omega + F)] \tag{2.67}$$

where ϕ_s, λ_s, α_G are the station latitude and longitude and Greenwich RA, respectively. The astronomical arguments l', F, D, Ω (mean anomaly of the Sun, mean argument of the latitude of the Moon, mean elongation of the Moon from the Sun, and the mean longitude of the ascending lunar node) are defined in Sec. 2.6.2. These displacements are then summed and used as the first order correction to each station's vertical displacement. Horizontal corrections are presently ignored. Note that the largest correction, the K_1 term, is identical to that already recommended in 1985 by the MERIT standards (Melbourne *et al.*, 1985).

To convert the locally referenced displacement, $\boldsymbol{\delta}$, which is expressed in the VEN system, to the Earth-fixed frame, two rotations must be performed. The first, W, rotates by an angle, ϕ_s (station geodetic latitude), about the y axis to an equatorial system. The second, V, rotates about the resultant z axis by angle, $-\lambda_s$ (station longitude), to bring the displacements into the standard geocentric coordinate system. The result is

$$\boldsymbol{\Delta}_{sol} = VW\boldsymbol{\delta} \tag{2.68}$$

where

$$W = \begin{pmatrix} \cos\phi_s & 0 & -\sin\phi_s \\ 0 & 1 & 0 \\ \sin\phi_s & 0 & \cos\phi_s \end{pmatrix} \tag{2.69}$$

and

$$V = \begin{pmatrix} \cos\lambda_s & -\sin\lambda_s & 0 \\ \sin\lambda_s & \cos\lambda_s & 0 \\ 0 & 0 & 1 \end{pmatrix} \tag{2.70}$$

Actually, the product of these two matrices is coded:

$$VW = \begin{pmatrix} \cos\lambda_s\cos\phi_s & -\sin\lambda_s & -\cos\lambda_s\sin\phi_s \\ \sin\lambda_s\cos\phi_s & \cos\lambda_s & -\sin\lambda_s\sin\phi_s \\ \sin\phi_s & 0 & \cos\phi_s \end{pmatrix} \tag{2.71}$$

MODEST code uses geodetic latitudes

$$\phi_s = \tan^{-1}\left[\frac{z_s}{r_{sp_s}(1-1/f)^2}\right] \tag{2.72}$$

where f is the geoid flattening factor. The difference between geodetic and geocentric latitude can affect this model on the order of (tidal effect)/(flattening factor) $\approx$ 0.1 cm.

2.4.2 POLE TIDE

One of the secondary tidal effects is the displacement of a station by the elastic response of the Earth's crust to shifts in the spin axis orientation. The spin axis is known to describe a circle of $\approx$ 20-m diameter at the north pole. Depending on where the spin axis pierces the crust at the instant of a VLBI measurement, the "pole tide" displacement will vary from time to time. This effect must be included if centimeter accuracy is desired.

Yoder (1984) and Wahr (1985) derived an expression for the displacement of a point at geocentric latitude ϕ_s, longitude λ_s due to the pole tide:

$$\begin{aligned} \delta = -\frac{\omega_E^2 R}{g}\big[&\sin\phi_s\cos\phi_s(x\cos\lambda_s + y\sin\lambda_s)\; h\,\hat{\mathbf{r}} \\ &+ \cos 2\phi_s(x\cos\lambda_s + y\sin\lambda_s)\; l\,\hat{\boldsymbol{\phi}} \\ &+ \sin\phi_s(-x\sin\lambda_s + y\cos\lambda_s)\; l\,\hat{\boldsymbol{\lambda}}\big] \end{aligned} \tag{2.73}$$

Here ω_E is the rotation rate of the Earth, R the radius of the (spherical) Earth, g the acceleration due to gravity at the Earth's surface, and h and l the customary Love numbers. Displacements of the instantaneous spin axis from the current average spin axis along the x and y axes are given by x and y. Eq. (2.73) shows how these map into station displacements along the unit vectors in the radial ($\hat{\mathbf{r}}$), latitude ($\hat{\boldsymbol{\phi}}$), and longitude ($\hat{\boldsymbol{\lambda}}$) directions. With the standard values $\omega_E = 7.292 \times 10^{-5}$ rad/sec, $R = 6378$ km, and $g = 980.665$ cm/sec^2, the factor $\omega_E^2 R/g = 3.459 \times 10^{-3}$. Since the maximum values of x and y are on the order of 10 meters, and $h \approx 0.6$, $l \approx 0.08$, the maximum displacement due to the pole tide is 1 to 2 cm, depending on the location of the station (ϕ_s, λ_s).

The locally referenced displacement δ is transformed via the suitably modified transformation (2.71) to give the displacement Δ_{pol} in the standard geocentric coordinate system. The pole tide effect has been coded as an optional part of the MODEST model. It is only applied if specifically requested, *i.e.*, the default model contains no pole tide contributions to the station locations.

2.4.3 OCEAN LOADING

This section is concerned with another of the secondary tidal effects, *i.e.*, the elastic response of the Earth's crust to ocean tides, which move the observing stations to the extent of a few cm. Such effects are commonly labeled "ocean loading." A model of ocean loading is incorporated in the MODEST code. It is general enough to accommodate a variety of externally derived parameters describing the tide phases and amplitudes at a number of frequencies. The present model entails deriving an expression for the locally referenced displacement δ due to ocean loading. In a local Cartesian coordinate system (the computer code accepts inputs related to unit vectors in the Up, North, and West directions) at time t,

$$\delta_j = \sum_{i=1}^{N} \xi_i^j \cos(\omega_i t + V_i - \delta_i^j) \tag{2.74}$$

The quantities ω_i (frequency of tidal constituent i) and V_i (astronomical argument of constituent i) depend only on the ephemeris information (positions of the Sun and Moon). The algorithm of Goad (IERS, 1989) is used to calculate these two quantities. On the other hand the amplitude ξ_i^j and Greenwich phase lag δ_i^j of each tidal component j are determined by the particular model assumed for the deformation of the Earth. The local displacement vector is transformed via Eqs. (2.71) and (2.68) to the displacement Δ_{ocn} in the standard geocentric frame.

Input to MODEST provides for specification of up to 11 frequencies and astronomical arguments ω_i and V_i, followed by tables of the local distortions and their phases, ξ_i^j and δ_i^j, calculated from the ocean tidal loading model of choice. The eleven components are denoted, in standard notation: K_2, S_2, M_2, and N_2 (all with approximately 12-hour periods), K_1, P_1, O_1, Q_1 (24 h), M_f (14 day), M_m (monthly), and S_{sa} (semiannual).

Three choices of ocean loading models have been used with MODEST. They differ in the displacements calculated and components considered, as well as in the numerical values that they yield for the ξ_i^js and δ_i^js. Scherneck's results (1983, 1990, 1991) are the most complete in the sense of considering both vertical and horizontal displacements and all eleven tidal components. They have now been adopted for the IERS standards (1992), and compose the default ocean loading model. Goad's model (1983) was adopted in the MERIT and early IERS standards (1989), but only considers vertical displacements. Pagiatakis' (1982, 1990) model, based on Pagiatakis, Langley, and Vanicek (1982), considers only six tidal components (S_2, M_2, N_2, K_1, P_1, and O_1).

An extension of the 1991 Scherneck model is also available in MODEST (Scherneck, 1993). The eleven tidal frequencies are modulated to an appreciable extent by multiples of N', the lunar nodal period (18.6 years). On the assumption that these additional terms yield ocean loading amplitudes which are in the same ratio to each main loading term as the companion tides are to the main tides, the additional station displacements can be written as

$$\delta_j' = \sum_{i=1}^{N} \sum_{k} r_{ki} \xi_i^j \cos\left[(\omega_i + n_{ki}\omega_{N'})t + V_i + n_{ki}N' - \delta_i^j)\right] \tag{2.75}$$

where the k summation extends over all integer multiples n_{ki} of the lunar node N', and r_{ki} is the ratio of the tidal amplitude of each companion k to the tidal amplitude of the parent i. Of 26 such components listed by Cartwright and Edden (1973), 20 are estimated to be significant in contributing to the largest ocean loading displacements at the 0.01 mm level. Table V shows the multiples n_{ki} and amplitude ratios r_{ki} for these 20 components.

Table V

Lunar Node Companions to Ocean Tides

i Component	n_{ki} Companion	r_{ki}: Relative Amplitude
K_2 (275555)	−1	−0.0128
	+1	+0.2980
	+2	+0.0324
S_2 (273555)	−1	+0.0022
M_2 (255555)	−2	+0.0005
	−1	−0.0373
N_2 (245655)	−1	−0.0373
K_1 (165555)	−1	−0.0198
	+1	+0.1356
	+2	−0.0029
P_1 (163555)	−1	−0.0112
O_1 (145555)	−2	−0.0058
	−1	+0.1885
Q_1 (135655)	−2	+0.0057
	−1	+0.1884
M_f (075555)	+1	+0.4143
	+2	+0.0387
M_m (065455)	−1	−0.0657
	+1	−0.0649
S_{sa} (057555)	+1	−0.0247

In pushing the limits of Earth modeling to below 1 cm accuracy in the mid-1990s, ocean loading station displacements are one aspect of the models that are undergoing close scrutiny. Initial trials indicate that ocean loading amplitudes can be derived from VLBI experiments at an approximate accuracy level of 1-2 mm (Sovers, 1994). Partial derivatives of the VLBI observables with respect to eight diurnal and semidiurnal amplitudes are considered in Sec. 2.9.2.1. When estimating parameters, however, great care must be used in order to avoid singularities due to the identity of components of station displacements ("confounding of parameters"). Since some components of ocean loading, solid Earth tides, and ocean tidally induced UTPM variations have the same frequencies, certain linear combinations of their station displacements are identical (see Sections 2.4.1 and 2.6.1.1.2).

2.4.4 ATMOSPHERE LOADING

By analogy with the ocean tides that were considered in the previous section, a time-varying atmospheric pressure distribution can induce crustal deformation. A paper by Rabbel and Schuh (1986) estimates the effects of atmospheric loading on VLBI baseline determinations, and concludes that they may amount to many millimeters of seasonal variation. In contrast to ocean tidal effects, analysis of the situation in the atmospheric case does not benefit from the presence of a well-understood periodic driving force. Otherwise, estimation of atmospheric loading via Green's function techniques is analogous to methods used to calculate ocean loading effects. Rabbel and Schuh recommend a simplified form of the dependence of the vertical crust displacement on pressure distribution. It involves only the instantaneous pressure at the site in question, and an average pressure over a circular

region C of radius $R = 2000$ km surrounding the site. The expression for the vertical displacement (mm) is:

$$\Delta r = -0.35 p_0 - 0.55 \bar{p} \tag{2.76}$$

where p_0 is the local pressure anomaly (relative to the standard pressure of 1013.25 mbar), and $\bar{p}$ is the pressure anomaly within the 2000-km circular region mentioned above (both quantities are in mbar). Note that the reference point for this displacement is the site location at standard (sea level) pressure. The locally referenced Δr is transformed to the standard geocentric coordinate system via the transformation (2.71).

It was decided to incorporate this rudimentary model into MODEST as an optional part of the model, with an additional mechanism for characterizing $\bar{p}$. The two-dimensional surface pressure distribution (relative to 1013.25 mbar) surrounding a site is described by

$$p(x, y) = p_0 + A_1 x + A_2 y + A_3 x^2 + A_4 xy + A_5 y^2 \tag{2.77}$$

where x and y are the local East and North distances of the point in question from the VLBI site. The pressure anomaly $\bar{p}$ may then be evaluated by the simple integration

$$\bar{p} = \int\int_C dx\, dy\; p(x, y) \;/ \int\int_C dx\, dy \tag{2.78}$$

giving

$$\bar{p} = p_0 + (A_3 + A_5) R^2/4 \tag{2.79}$$

It remains the task of the data analyst to perform a quadratic fit to any available area weather data to determine the coefficients A_{1-5}. Future advances in understanding the atmosphere-crust elastic interaction can probably be accommodated by adjusting the coefficients in Eq. (2.76). As an initial step along these lines, a station-dependent factor is introduced to scale the second coefficient in Eq. (2.76):

$$\Delta r = -0.35 p_0 - 0.55(1 + f) \bar{p} \tag{2.80}$$

This may account for differing geographical features surrounding different sites. In particular, f may depend on the fraction of ocean within the 2000 km radius.

In summary, models have been presented that describe the four tidal effects on the stations (solid, pole, ocean, and atmosphere). Each of the locally referenced tidal displacement vectors is then transformed to the standard geocentric coordinate system via rotations like (2.68). After this transformation, the final station location is

$$\mathbf{r}_t = \mathbf{r}_0 + \mathbf{\Delta}_{sol} + \mathbf{\Delta}_{pol} + \mathbf{\Delta}_{ocn} + \mathbf{\Delta}_{atm} \tag{2.81}$$

2.5 SOURCE STRUCTURE EFFECTS

Numerous astrophysical studies during the past decade have shown that compact extragalactic radio sources exhibit structure on a milliarcsecond scale (*e.g.*, Kellermann and Pauliny-Toth, 1981). Such studies are important for developing models of the origin of radio emission of these objects. Many radio source structures are found to be quite variable with frequency and time (Zensus and Pearson, 1987). If extragalactic sources are to serve as reference points in a stable reference frame, it is important to correct for the effects of their structures in astrometric VLBI observations.

MODEST modeling allows optional corrections for the effects of source internal structures, based on work by Thomas (1980), Ulvestad (1988), and Charlot (1989, 1990a). A non-point-like distribution of the intensity of a source yields time dependent corrections to the group delay and delay rate observables, $\Delta\tau_s$ and $\Delta\dot{\tau}_s$, that may be written in terms of the intensity distribution $I(\mathbf{s},\omega,t)$ as

$$\Delta\tau_s = \partial\phi_s/\partial\omega, \qquad \Delta\dot{\tau}_s = \partial\phi_s/\partial t \tag{2.82}$$

with

$$\phi_s = \arctan(-Z_s/Z_c) \tag{2.83}$$

and

$$Z_{\{{}^s_c\}} = \int\int d\Omega\; I(\mathbf{s},\omega,t)\left\{{\sin \atop \cos}\right\}(2\pi\mathbf{B}\cdot\mathbf{s}/\lambda) \tag{2.84}$$

Here ϕ_s is the correction to the phase of the incoming signal, $\mathbf{s}$ is a vector from the adopted reference point to a point within the source intensity distribution in the plane of the sky, ω and λ are the observing frequency and wavelength, $\mathbf{B}$ the baseline vector, and the integration is over solid angles Ω. Source intensity distribution maps are most conveniently parametrized in terms of one of two models: superpositions of delta functions or Gaussians. At a given frequency, the corresponding intensity distributions are written as

$$I(\mathbf{s}) = \sum_k S_k\,\delta(x - x_k, y - y_k) \tag{2.85}$$

or

$$I(\mathbf{s}) = \sum_k \frac{S_k}{2\pi a_k b_k}\exp\Big[-[(x-x_k)\cos\theta_k + (y-y_k)\sin\theta_k]^2/2{a_k}^2 - [-(x-x_k)\sin\theta_k + (y-y_k)\cos\theta_k]^2/2{b_k}^2\Big] \tag{2.86}$$

where S_k is the flux of component k, and $\mathbf{s_k}$ (with components x_k, y_k in the plane of the sky) is its position relative to the reference point. For Gaussian distributions, θ_k is the angle between the major axis of component k and the u axis (to be defined below), and (a_k, b_k) are the full widths at half maximum of the (major, minor) axes of component k normalized by $2\sqrt{2\log 2}$. The quantities $Z_{\{{}^s_c\}}$ entering the structure phase ϕ_s [Eq. (2.83)] are

$$Z_{\{{}^s_c\}} = \sum_k S_k\left\{{\sin \atop \cos}\right\}(2\pi\mathbf{B}\cdot\mathbf{s_k}/\lambda) \tag{2.87}$$

for delta functions, and

$$Z_{\{{}^s_c\}} = \sum_k S_k \exp[-2\pi^2(a_k^2U_k^2 + b_k^2V_k^2)]\left\{{\sin \atop \cos}\right\}(2\pi\mathbf{B}\cdot\mathbf{s_k}/\lambda) \tag{2.88}$$

for Gaussians. Here

$$U_k = u\cos\theta_k + v\sin\theta_k \tag{2.89}$$

$$V_k = -u\sin\theta_k + v\cos\theta_k \tag{2.90}$$

with u, v being the projections of the baseline vector $\mathbf{B}$ on the plane of the sky in the E-W, N-S directions, respectively.

MODEST accepts maps specified in terms of an arbitrary number of Gaussian or delta function components. At most, six parameters must be specified for each component: its polar coordinates and flux, and, for a Gaussian, its major and minor axes and the position angle of the major axis. The structural correction for phase is computed via Eqs. (2.83), (2.87), and (2.88). For the bandwidth synthesis (BWS) delay observable, the structure correction is the slope of a straight line fitted to the individual structure phases calculated for each frequency channel used during the observation. For example, for Mark III data there are typically 8 channels spanning ≈8.2 to 8.6 GHz at X band, and 6 channels spanning ≈2.2 to 2.3 GHz at S band. Delay rate structure corrections are calculated by differencing the structure phases at ±2 seconds (see Section 6). In the case of dual-band (S-X) experiments, a linear combination of the structure corrections calculated independently for each band is applied to the dual-band observables.

The practical question to be resolved is whether such structural corrections based on maps yield significant and detectable corrections to the observables at the present levels of experimental and modeling uncertainty. Maps are available for only a few of the hundreds of sources currently observed by VLBI. Some of the extended sources show time variability on a scale of months; since the corrections $\Delta\tau_s$ and $\Delta\dot{\tau}_s$ are quite sensitive to fine details of the structure, in such cases new maps may be required on short time scales. Depending on the relative orientation of the source and baseline, the delay correction can be as large as ≈1 ns, which is equivalent to tens of cm. Nevertheless, the prognosis appears to be good. Charlot (1990b) found that data from a multiple baseline geodynamics experiment are adequate to map source structures with high angular resolution. More recently Charlot (1993) has also shown that use of maps for the structure of the source 3C 273 improves the fit in analyses of geodetic experiments.

Empirical evaluation of the effects of unknown source structure on VLBI measurements could be made via the time rates of change of the source right ascension α and declination δ. A linear model of the motion of source coordinates

$$\alpha = \alpha_0 + \dot{\alpha}(t - t_0) \tag{2.91}$$

$$\delta = \delta_0 + \dot{\delta}(t - t_0) \tag{2.92}$$

is implemented in MODEST. Non-zero estimates of the rate parameters $\dot{\alpha}$ and $\dot{\delta}$ could arise either from genuine proper motion or from motion of the effective source centroid sampled by VLBI measurements. Proper interpretation of such results is problematic, but non-zero rates can be used as a crude diagnostic for the presence of structure effects.

MODEST code also provides the option of modeling source structure as a superposition of two δ functions centered at points $P_1(x_1, y_1)$ and $P_2(x_2, y_2)$ respectively, as in Eq. (2.85) above. The parameters describing the two components are: 1) flux ratio $K = S_2/S_1$, where S_k is the flux of the kth component, 2) component separation $s = |\mathbf{s}| = |\overrightarrow{P_1P_2}|$, and 3) position angle θ. The position angle is $\theta = 0°$ when $\overrightarrow{P_1P_2}$ is in the direction of increasing declination $\hat{\delta}$, and $\theta = 90°$ when $\overrightarrow{P_1P_2}$ is in the direction of increasing right ascension $\hat{\alpha}$. From Charlot (1990b), the group delay has the following dependence on the structural parameters:

$$\tau = \frac{2\pi K\ (1-K)}{\omega\ (1+K)} \cdot \frac{R[1-\cos(2\pi R)]}{[K^2 + 2K\cos(2\pi R) + 1]} \tag{2.93}$$

where

$$R = \mathbf{B} \cdot \mathbf{s}/\lambda \tag{2.94}$$

For evaluating partial derivatives of τ, the component separation $\mathbf{s}$ and baseline $\mathbf{B}$ are most conveniently written in terms of their components in the celestial system, as

$$\mathbf{s} = \hat{\alpha}\ s\ \sin\theta\ +\ \hat{\delta}\ s\ \cos\theta \tag{2.95}$$

$$\mathbf{B} = \hat{\alpha}\ u\ \lambda\quad\ +\ \hat{\delta}\ v\ \lambda \tag{2.96}$$

Then R becomes

$$R = s\ (u\ \sin\theta\ +\ v\ \cos\theta)\ /\ \lambda \tag{2.97}$$

2.6 TRANSFORMATION FROM TERRESTRIAL TO CELESTIAL COORDINATE SYSTEMS

The Earth is approximately an oblate spheroid, spinning in the presence of two massive moving objects (the Sun and the Moon) which are positioned such that their time-varying gravitational effects not only produce tides on the Earth, but also subject it to torques. In addition, the Earth is covered by a complicated fluid layer, and also is not perfectly rigid internally. As a result, the orientation of the Earth is a very complicated function of time, which to first order can be represented as the composite of a time-varying rotation rate, a wobble, a nutation, and a precession. The exchange of angular momentum between the solid Earth and the fluids on its surface is not readily predictable, and thus must be continually determined experimentally. Nutation and precession are well modeled theoretically. However, at the accuracy with which VLBI can determine baseline vectors, even these models are not completely adequate.

Currently, the rotational transformation, Q, of coordinate frames from the terrestrial frame to the celestial geocentric frame is composed of 6 separate rotations (actually 12, since the nutation, precession, and "perturbation" transformations, N, P, and Ω, consist of 3 transformations each) applied to a vector in the terrestrial system:

$$Q = \Omega PNUXY \tag{2.98}$$

In order of appearance in (2.98), the transformations are: the perturbation rotation, precession, nutation, UT1, and the x and y components of polar motion. All are discussed in detail in the following four sections. With this definition of Q, if $\mathbf{r}_t$ is a station location expressed in the terrestrial system, *e.g.*, the result of (2.81), that location, $\mathbf{r}_c$, expressed in the celestial system is

$$\mathbf{r}_c = Q\mathbf{r}_t \tag{2.99}$$

This particular formulation follows the historical path of astrometry, and is couched in that language. While esthetically unsatisfactory with modern measurement techniques, such a formulation is currently practical for intercomparison of techniques and for effecting a smooth inclusion of the interferometer data into the long historical record of astrometric data. Much more pleasing esthetically would be the separation of Q into two rotation matrices:

$$Q = Q_1 Q_2 \tag{2.100}$$

where Q_2 are those rotations to which the Earth would be subjected if all external torques were removed (approximately UXY above), and where Q_1 are those rotations arising from external torques (approximately ΩPN above). Even then, the tidal response of the Earth prevents such a separation from being perfectly realized. Eventually, the entire problem of obtaining the matrix Q, and the tidal effects on station locations should be done numerically. Note that the six rotations operating on a vector yield its components in a new coordinate system, and, since we rotate the Earth rather than the celestial sphere, the matrices Ω, P, and N will be the transposes of those used to rotate the celestial system of J2000 to a celestial system of date.

2.6.1 UT1 AND POLAR MOTION

The first transformation, Y, is a right-handed rotation about the x axis of the terrestrial frame by an angle Θ_2. Currently, the terrestrial frame is the 1903.0 CIO frame, except that the positive y axis is at 90 degrees east (Moscow). The x axis is coincident with the 1903.0 meridian of Greenwich, and the z axis is the 1903.0 standard pole.

$$Y = \begin{pmatrix} 1 & 0 & 0 \\ 0 & \cos\Theta_2 & \sin\Theta_2 \\ 0 & -\sin\Theta_2 & \cos\Theta_2 \end{pmatrix} \tag{2.101}$$

where Θ_2 is the y pole position published by IERS.

The next rotation in sequence is the right-handed rotation (through an angle Θ_1 about the y axis) obtained after the previous rotation has been applied:

$$X = \begin{pmatrix} \cos\Theta_1 & 0 & -\sin\Theta_1 \\ 0 & 1 & 0 \\ \sin\Theta_1 & 0 & \cos\Theta_1 \end{pmatrix} \tag{2.102}$$

In this rotation, Θ_1 is the IERS x pole position. Note that we have incorporated in the matrix definitions the transformation from the left-handed system used by IERS to the right-handed system we use. Note also that instead of IERS data used as a pole definition, we could instead use any other source of polar motion data provided it was represented in a left-handed system. The only effect would be a change in the definition of the terrestrial reference system.

The application of "XY" to a vector in the terrestrial system of coordinates expresses that vector as it would be observed in a coordinate frame whose z axis was along the Earth's ephemeris pole. The third rotation, U, is about the resultant z axis obtained by applying "XY". It is a rotation through the angle, $-H$, where H is the hour angle of the true equinox of date (*i.e.*, the dihedral angle measured westward between the xz plane defined above and the meridian plane containing the true equinox of date). The equinox of date is the point defined on the celestial equator by the intersection of the mean ecliptic with that equator. It is that intersection where the mean ecliptic rises from below the equator to above it (ascending node).

$$U = \begin{pmatrix} \cos H & -\sin H & 0 \\ \sin H & \cos H & 0 \\ 0 & 0 & 1 \end{pmatrix} \tag{2.103}$$

This angle H is composed of two parts:

$$H = h_\gamma + \alpha_E \tag{2.104}$$

where h_γ is the hour angle of the mean equinox of date, and α_E (equation of equinoxes) is the difference in hour angle of the true equinox of date and the mean equinox of date, a difference which is due to the nutation of the Earth. This set of definitions is cumbersome and couples the nutation and precession effects into Earth rotation measurements. However, in order to provide a direct estimate of conventional $UT1$ (universal time) it is convenient to endure this historical approach, at least for the near future.

$UT1$ is defined to be such that the hour angle of the mean equinox of date is given by the following expression (Aoki *et al.*, 1982; Kaplan, 1981):

$$\begin{aligned} h_\gamma = UT1 \; &+ \; 6^h \; 41^m \; 50^s.54841 \; + \; 8640184^s.812866 \; T_u \\ &+ \; 0^s.093104 \; T_u^2 \; - \; 6^s.2 \times 10^{-6} \; T_u^3 \end{aligned} \tag{2.105}$$

where the dimensionless quantity

$$T_u = \frac{(\text{Julian } UT1 \text{ date}) \; - \; 2451545.0}{36525} \tag{2.106}$$

The actual equivalent expression which is coded is:

$$\begin{aligned} h_\gamma = &2\pi(UT1 \text{ Julian day fraction}) + 67310^s.54841 \\ &+ 8640184^s.812866 \; T_u + 0^s.093104 \; T_u^2 - 6^s.2 \times 10^{-6} \; T_u^3 \end{aligned} \tag{2.107}$$

This expression produces a time, $UT1$, which tracks the Greenwich hour angle of the real Sun to within 16^m. However, it really is sidereal time, modified to fit our intuitive desire to have the Sun directly overhead at noon on the Greenwich meridian. Historically, differences of $UT1$ from a uniform

measure of time, such as atomic time, have been used in specifying the orientation of the Earth. Note that this definition has buried in it the precession constant since it refers to the mean equinox of date.

By the very definition of "mean of date" and "true of date", nutation causes a difference in the hour angles of the mean equinox of date and the true equinox of date. This difference, called the "equation of equinoxes", is denoted by α_E and is obtained as follows:

$$\alpha_E = \tan^{-1}\left(\frac{y_{\gamma'}}{x_{\gamma'}}\right) = \tan^{-1}\left(\frac{N_{21}^{-1}}{N_{11}^{-1}}\right) = \tan^{-1}\left(\frac{N_{12}}{N_{11}}\right) \tag{2.108}$$

where the vector

$$\begin{pmatrix} x'_\gamma \\ y'_\gamma \\ z'_\gamma \end{pmatrix} = N_{ij}^{-1}\begin{pmatrix} 1 \\ 0 \\ 0 \end{pmatrix} \tag{2.109}$$

is the unit vector, in true equatorial coordinates of date, toward the mean equinox of date. In mean equatorial coordinates of date, this same unit vector is just $(1,0,0)^T$. The matrix N_{ij}^{-1} is the inverse (or equally, the transpose) of the transformation matrix N, which will be defined below in Eq. (2.120), to effect the transformation from true equatorial coordinates of date to mean equatorial coordinates of date.

It is convenient to apply "UXY" as a group. To parts in 10^{12}, $XY = YX$. However, with the same accuracy $UXY \neq XYU$. Neglecting terms of $\mathcal{O}(\Theta^2)$ (which produce station location errors of approximately 6×10^{-4} cm):

$$UXY = \begin{pmatrix} \cos H & -\sin H & -\sin\Theta_1 \cos H - \sin\Theta_2 \sin H \\ \sin H & \cos H & -\sin\Theta_1 \sin H + \sin\Theta_2 \cos H \\ \sin\Theta_1 & -\sin\Theta_2 & 1 \end{pmatrix} \tag{2.110}$$

As for station coordinates, a time-linear model is also available for UTPM. If PM and UT1 are symbolized by Θ_{1-3}, and the reference time is t_0, then the model is

$$\Theta_i = \dot{\Theta}_i^0 + \dot{\Theta}_i(t - t_0) \tag{2.111}$$

where Θ_i^0 are the values of UTPM at the reference epoch.

2.6.1.1 Tidal UTPM Variations

Tidal shifts of mass in the solid Earth, oceans, and atmosphere produce angular momenta which must be redistributed to satisfy conservation of total angular momentum. The consequences are variations in the orientation and rotation rate of the Earth: modification of polar motion and UT1. Such small effects emerged above the detection threshold in space geodesy in the early 1990s. Modeling them is important if centimeter-level accuracy is to be obtained in interpretation of VLBI measurements.

Just as various tidal forces affect the station locations (Secs. 2.4.1 - 2.4.4), they also affect polar motion and UT1 (Θ_{1-3}). Equations similar to (2.45) may be written for each of the three components of Earth orientation:

$$\Theta_i = \Theta_{i0} + \Delta\Theta_{i_{sol}} + \Delta\Theta_{i_{ocn}} + \Delta\Theta_{i_{atm}} \tag{2.112}$$

where Θ_i (i=1,3) symbolizes each of the three components of UTPM, Θ_{i0} is its value in the absence of tidal effects, and the three Δ terms are the respective contributions of solid Earth, ocean, and atmospheric tides. The next two sections describe the current models of solid and ocean tide contributions that are implemented in MODEST. At present, not enough is known about atmospheric tidal effects.

2.6.1.1.1 Solid Earth Tide UTPM Variations

The pioneering work in tidal effects on Earth orientation was that of Yoder *et al.* (1981). It was limited to UT1, but included some ocean effects. Their calculated $\Delta UT1$ can be represented as

$$\Delta UT1 = \sum_{i=1}^{N}\left[A_i \sin\left[\sum_{j=1}^{5} k_{ij}\alpha_j\right]\right] \tag{2.113}$$

where N (=41) is chosen to include all terms with periods from 5 to 35 days. There are no other contributions until a period of 90 days is reached. However, these long-period terms are included by the measurements of the current Earth-orientation measurement services. The values for k_{ij} and A_i, along with the period involved, are given in Table VI. The α_i for $i = 1, 5$ are just the five fundamental arguments defined in Eqs. (2.123-2.127) as l, l', F, D, and Ω, respectively. In Table VI, the sign of the 14.73 day term has been changed [Yoder (1982)] to correct a sign error in Yoder *et al.* (1981). The BIH Annual Report for 1982 [BIH (1983)] is the first reference to give the correct table.

2.6.1.1.2 Ocean Tide UTPM Variations

Redistribution of the angular momentum produced by ocean tides affects the Earth's rotation pole position and velocity. This effect was first quantified by Brosche *et al.* (1989, 1991). The dominant effects on polar motion and UT1 are at diurnal, semidiurnal, fortnightly, monthly, and semiannual frequencies. Assuming that the frequencies slower than fortnightly are adequately accounted for either in modeling combined solid and ocean tidal effects (not strictly true with the Yoder model), or are already present in the *a priori* UTPM series, only the diurnal and semidiurnal frequencies need to be modeled. Further limiting the model to tidal components with apparent amplitudes larger than 1μs gives eight components.

For unified notation, define Θ_{1-3} = x, y polar motion and $UT1$, respectively. Then the ocean tidal effects $\Delta\Theta$ can be written as

$$\Delta\Theta_l = \sum_{i=1}^{N}\left[A_{il}\cos\left[\sum_{j=1}^{5} k_{ij}\alpha_j + n_i(h_\gamma + \pi)\right] + B_{il}\sin\left[\sum_{j=1}^{5} k_{ij}\alpha_j + n_i(h_\gamma + \pi)\right]\right] \tag{2.114}$$

A_{il} and B_{il} are the cosine and sine amplitudes that may be calculated from theoretical tidal models (as in the work of Brosche) or determined from data (Herring and Dong, 1991; Herring, 1992; Sovers, Jacobs and Gross, 1993). Theoretical calculations of polar motion ocean effects have only very recently appeared: Gross (1993) used Seiler's (1989-1991) ocean model to estimate $A_{i,1-2}$ and $B_{i,1-2}$ (i = 2 to 7). Table VII lists the eight terms currently included in the model. The numerical coefficients are taken from the results of Sovers *et al.* (1993); this is known in MODEST code as the JPL92 fast UTPM model.

The ocean tidal UTPM effects are also modulated by the 18.6-year lunar node variation (N'). As in the case of ocean loading station displacements (Sec. 2.4.3), the contributions $\Delta\Theta_l{}'$ of the companion tides to $\Delta\Theta_l$ can be written as

$$\Delta\Theta_l{}' = \sum_{i=1}^{N}\sum_{k} r_{ki}\left[A_{il}\cos\left[\sum_{j=1}^{5} k_{ij}\alpha_j + n_i(h_\gamma + \pi) + n_{ki}\omega_{N'})t + n_{ki}N'\right] + B_{il}\sin\left[\sum_{j=1}^{5} k_{ij}\alpha_j + n_i(h_\gamma + \pi) + n_{ki}\omega_{N'})t + n_{ki}N'\right]\right] \tag{2.115}$$

where the strengths of the companion tides r_{ki} are found in Table V. These corrections are optionally available in MODEST.

Since a rotational frequency of 1 (0) cycles per sidereal day (cpsd) in the celestial frame (S) is identical to a frequency of 0 (-1) cpsd in the Earth-fixed frame (B), nutations with space-fixed frequencies ω_S coincide with polar motions with body-fixed frequencies $\omega_B = -1 + \omega_S$. The polar motion terms with coefficients $A_{i1,2}$ and $B_{i1,2}$ corresponding to the diurnal tidal components listed in Table VIII (i = 5 to 8) are thus equivalent to components of the nutation model, and due care must be taken when both classes of parameters are estimated.

Table VI
Periodic Tidally Induced Variations in UT1
with Periods Less than 35 Days

Index i	Period (days)	Argument coefficient k_{i1}	k_{i2}	k_{i3}	k_{i4}	k_{i5}	A_i (0^s.0001)
1	5.64	1	0	2	2	2	-0.02
2	6.85	2	0	2	0	1	-0.04
3	6.86	2	0	2	0	2	-0.10
4	7.09	0	0	2	2	1	-0.05
5	7.10	0	0	2	2	2	-0.12
6	9.11	1	0	2	0	0	-0.04
7	9.12	1	0	2	0	1	-0.41
8	9.13	1	0	2	0	2	-0.99
9	9.18	3	0	0	0	0	-0.02
10	9.54	-1	0	2	2	1	-0.08
11	9.56	-1	0	2	2	2	-0.20
12	9.61	1	0	0	2	0	-0.08
13	12.81	2	0	2	-2	2	0.02
14	13.17	0	1	2	0	2	0.03
15	13.61	0	0	2	0	0	-0.30
16	13.63	0	0	2	0	1	-3.21
17	13.66	0	0	2	0	2	-7.76
18	13.75	2	0	0	0	-1	0.02
19	13.78	2	0	0	0	0	-0.34
20	13.81	2	0	0	0	1	0.02
21	14.19	0	-1	2	0	2	-0.02
22	14.73	0	0	0	2	-1	0.05
23	14.77	0	0	0	2	0	-0.73
24	14.80	0	0	0	2	1	-0.05
25	15.39	0	-1	0	2	0	-0.05
26	23.86	1	0	2	-2	1	0.05
27	23.94	1	0	2	-2	2	0.10
28	25.62	1	1	0	0	0	0.04
29	26.88	-1	0	2	0	0	0.05
30	26.98	-1	0	2	0	1	0.18
31	27.09	-1	0	2	0	2	0.44
32	27.44	1	0	0	0	-1	0.53
33	27.56	1	0	0	0	0	-8.26
34	27.67	1	0	0	0	1	0.54
35	29.53	0	0	0	1	0	0.05
36	29.80	1	-1	0	0	0	-0.06
37	31.66	-1	0	0	2	-1	0.12
38	31.81	-1	0	0	2	0	-1.82
39	31.96	-1	0	0	2	1	0.13
40	32.61	1	0	-2	2	-1	0.02
41	34.85	-1	-1	0	2	0	-0.09

Table VII
Ocean Tidally Induced Periodic Variations in Polar Motion (JPL92 Model)

Index i	Tide, period (hours)		Argument coefficient k_{i1}	k_{i2}	k_{i3}	k_{i4}	k_{i5}	n_j	A_{i1}	B_{i1}	A_{i2}	B_{i2} (μas)
1	K_2	11.967	0	0	0	0	0	-2	-2	65	44	-57
2	S_2	12.000	0	0	2	-2	2	-2	101	166	126	-89
3	M_2	12.421	0	0	2	0	2	-2	26	283	247	-2
4	N_2	12.658	1	0	2	0	2	-2	-15	56	19	-11
5	K_1	23.934	0	0	0	0	0	-1	-583	-2780	-2950	376
6	P_1	24.066	0	0	2	-2	2	-1	154	46	42	-17
7	O_1	25.819	0	0	2	0	2	-1	242	-152	2	-30
8	Q_1	26.868	1	0	2	0	2	-1	72	-32	26	7

Table VIII
Ocean Tidally Induced Periodic Variations in UT1 (JPL92 Model)

Index i	Tide, period (hours)		Argument coefficient k_{i1}	k_{i2}	k_{i3}	k_{i4}	k_{i5}	n_j	A_{i3}	B_{i3} ($0.1\mu s$)
1	K_2	11.967	0	0	0	0	0	-2	-9	26
2	S_2	12.000	0	0	2	-2	2	-2	-4	52
3	M_2	12.421	0	0	2	0	2	-2	-104	149
4	N_2	12.658	1	0	2	0	2	-2	-23	20
5	K_1	23.934	0	0	0	0	0	-1	35	151
6	P_1	24.066	0	0	2	-2	2	-1	-32	-64
7	O_1	25.819	0	0	2	0	2	-1	-135	-166
8	Q_1	26.868	1	0	2	0	2	-1	-40	-53

2.6.1.1.3 Interpolation of UTPM Values

Depending on the smoothing used to produce the *a priori* $UT1 - UTC$ series, the short-period (t < 35 days) fluctuations in $UT1$ due to changes in the latitude and size of the mean tidal bulge may or may not be smoothed out. Since we want as accurate an *a priori* as possible, it may be necessary to add this effect to the $UT1$ *a priori* obtained from the series $UT1_{smoothed}$. If this option is selected, then the desired *a priori* $UT1$ is given by

$$UT1_{a\ priori} = UT1_{smoothed} + \Delta UT1 \tag{2.116}$$

$UT1_{smoothed}$ represents an appropriately smoothed *a priori* measurement of the orientation of the Earth (*i.e.*, typically IERS Bulletin A smoothed or, even better, $UT1R$), for which the short period (t < 35 days) tidal effects have either been averaged to zero, or, as in the case of $UT1R$, removed before smoothing.

It might be appropriate at this point to describe the interpolation method used in MODEST to obtain *a priori* polar motion and $UT1$ values. These are normally available as tables at 5-day or

1-day intervals, from either IERS (*e.g.* IERS, 1993) or the International Radio Interferometric Surveying (IRIS) project of the International Association for Geodesy (IAG) (*e.g.* IAG, 1993). Linear interpolation is performed for all three quantities. If the short-period tidal terms $\Delta UT1$ are present in the tabular values, they are subtracted before interpolation, and added back to the final value. With the present accuracy of determinations of pole position and $UT1$ (<1 mas and 0.05 ms respectively), linear interpolation over a 5-day interval may be inadequate, possibly giving rise to 0.1 ms errors in $UT1$. Quadratic spline interpolation is a possible alternative. Even with the present code, however, the highest possible accuracy may be achieved by performing the interpolation externally to MODEST, and supplying it with tables of values more closely spaced in time for the final internal linear interpolation. The Kalman-filtered UTPM values of Gross (1992), with values given at 1-day intervals, are ideally suited for this purpose.

2.6.2 NUTATION

With the completion of the $UT1$ and polar motion transformations, we are left with a station location vector, $\mathbf{r}_{date}$. This is the station location relative to true equatorial celestial coordinates of date. The last set of transformations are nutation, N, precession, P, and the perturbation rotation, Ω, applied in that order. These transformations give the station location, $\mathbf{r}_c$, in celestial equatorial coordinates:

$$\mathbf{r}_c = \Omega P N \mathbf{r}_{date} \tag{2.117}$$

The transformation matrix N is a composite of three separate rotations (Melbourne *et al.*, 1968):

1. A(ε): true equatorial coordinates of date to ecliptic coordinates of date.

$$A(\varepsilon) = \begin{pmatrix} 1 & 0 & 0 \\ 0 & \cos\varepsilon & \sin\varepsilon \\ 0 & -\sin\varepsilon & \cos\varepsilon \end{pmatrix} \tag{2.118}$$

2. $C^T(\delta\psi)$: nutation in longitude from ecliptic coordinates of date to mean ecliptic coordinates of date.

$$C^T(\delta\psi) = \begin{pmatrix} \cos\delta\psi & \sin\delta\psi & 0 \\ -\sin\delta\psi & \cos\delta\psi & 0 \\ 0 & 0 & 1 \end{pmatrix} \tag{2.119}$$

where $\delta\psi$ is the nutation in ecliptic longitude.

3. $A^T(\bar{\varepsilon})$: ecliptic coordinates of date to mean equatorial coordinates.

In ecliptic coordinates of date, the mean equinox is at an angle $\delta\psi = \tan^{-1}(y_{\bar{\gamma}}/x_{\bar{\gamma}})$. The angle $\delta\varepsilon = \varepsilon - \bar{\varepsilon}$ is the nutation in obliquity, and $\bar{\varepsilon}$ is the mean obliquity (the dihedral angle between the plane of the ecliptic and the mean plane of the equator). "Mean" as used in this section implies that the short-period ($T \leq 18.6$ years) effects of nutation have been removed. Actually, the separation between nutation and precession is rather arbitrary, but historical. The composite rotation is:

$$N = A^T(\bar{\varepsilon}) C^T(\delta\psi) A(\varepsilon) \tag{2.120}$$

$$= \begin{pmatrix} \cos\delta\psi & \cos\varepsilon\sin\delta\psi & \sin\varepsilon\sin\delta\psi \\ -\cos\bar{\varepsilon}\sin\delta\psi & \cos\bar{\varepsilon}\cos\varepsilon\cos\delta\psi + \sin\bar{\varepsilon}\sin\varepsilon & \cos\bar{\varepsilon}\sin\varepsilon\cos\delta\psi - \sin\bar{\varepsilon}\cos\varepsilon \\ -\sin\bar{\varepsilon}\sin\delta\psi & \sin\bar{\varepsilon}\cos\varepsilon\cos\delta\psi - \cos\bar{\varepsilon}\sin\varepsilon & \sin\bar{\varepsilon}\sin\varepsilon\cos\delta\psi + \cos\bar{\varepsilon}\cos\varepsilon \end{pmatrix}$$

The 1980 IAU nutation model (Seidelmann, 1982; Kaplan, 1981) is used to obtain the values for $\delta\psi$ and $\varepsilon - \bar{\varepsilon}$. The mean obliquity is obtained from Lieske *et al.* (1977) or from Kaplan (1981):

$$\bar{\varepsilon} = 23^\circ\ 26'\ 21.''448 - 46.''8150\ T - 5.''9 \times 10^{-4} T^2 + 1.''813 \times 10^{-3} T^3 \tag{2.121}$$

$$T = \frac{(\text{Julian } TDB \text{ date}) - 2451545.0}{36525} \tag{2.122}$$

This nutation in longitude ($\delta\psi$) and in obliquity ($\delta\varepsilon = \varepsilon - \bar{\varepsilon}$) can be represented by a series expansion of the sines and cosines of linear combinations of five fundamental arguments. These are (Kaplan, 1981; Cannon, 1981):

1. the mean anomaly of the Moon:

$$\begin{aligned} \alpha_1 = l = {} & 485866''.733 + (1325^r + 715922''.633)\ T \\ & + 31''.310\ T^2 + 0''.064\ T^3 \end{aligned} \tag{2.123}$$

2. the mean anomaly of the Sun:

$$\begin{aligned} \alpha_2 = l' = {} & 1287099''.804 + (99^r + 1292581''.224)\ T \\ & - 0''.577\ T^2 - 0.''012\ T^3 \end{aligned} \tag{2.124}$$

3. the mean argument of latitude of the Moon:

$$\alpha_3 = F = 335778''.877 + (1342^r + 295263''.137)\,T - 13''.257\,T^2 + 0''.011\,T^3 \quad (2.125)$$

4. the mean elongation of the Moon from the Sun:

$$\alpha_4 = D = 1072261''.307 + (1236^r + 1105601''.328)\,T - 6''.891\,T^2 + 0''.019\,T^3 \quad (2.126)$$

5. the mean longitude of the ascending lunar node:

$$\alpha_5 = \Omega = 450160''.280 - (5^r + 482890''.539)\,T + 7''.455\,T^2 + 0''.008\,T^3 \quad (2.127)$$

where $1^r = 360^\circ = 1296000''$.

With these fundamental arguments, the nutation quantities can then be represented by

$$\delta\psi = \sum_{j=1}^{N}\left[(A_{0j} + A_{1j}T)\sin\left[\sum_{i=1}^{5} k_{ji}\alpha_i(T)\right]\right] \quad (2.128)$$

and

$$\delta\varepsilon = \sum_{j=1}^{N}\left[(B_{0j} + B_{1j}T)\cos\left[\sum_{i=1}^{5} k_{ji}\alpha_i(T)\right]\right] \quad (2.129)$$

where the various values of α_i, k_{ji}, A_j, and B_j are tabulated in Table A.I.

2.6.2.1 Corrections to the 1980 IAU Model

Additional terms can be optionally added to the nutations $\delta\psi$ and $\delta\varepsilon$ in Eqs. (2.128) and (2.129). These include the out-of-phase nutations, the free-core nutations (Yoder, 1983) with period ω_f (nominally 430 days), and the "nutation tweaks" $\Delta\psi$ and $\Delta\varepsilon$, which are arbitrary constant increments of the nutation angles $\delta\psi$ and $\delta\varepsilon$. Unlike the usual nutation expressions, the tweaks have no time dependence. The out-of-phase nutations, which are not included in the IAU 1980 nutation series, are identical to Eqs. (2.128) and (2.129), with the replacements sin $\leftrightarrow$ cos:

$$\delta\psi^o = \sum_{j=1}^{N}\left[(A_{2j} + A_{3j}T)\cos\left[\sum_{i=1}^{5} k_{ji}\alpha_i(T)\right]\right] \quad (2.130)$$

and

$$\delta\varepsilon^o = \sum_{j=1}^{N}\left[(B_{2j} + B_{3j}T)\sin\left[\sum_{i=1}^{5} k_{ji}\alpha_i(T)\right]\right] \quad (2.131)$$

Expressions similar to these are adopted for the free-core nutations:

$$\delta\psi^f = (A_{00} + A_{10}T)\sin(\omega_f T) + (A_{20} + A_{30}T)\cos(\omega_f T) \quad (2.132)$$

and

$$\delta\varepsilon^f = (B_{00} + B_{10}T)\cos(\omega_f T) + (B_{20} + B_{30}T)\sin(\omega_f T) \quad (2.133)$$

If the free-core nutation is to be retrograde, as expected on theoretical grounds, ω_f should be negative. The nutation model thus contains a total of 856 parameters: A_{ij} (i=0,3; j=1,106) and B_{ij} (i=0,3;

j=1,106) plus the free-nutation amplitudes A_{i0} (i=0,3), B_{i0} (i=0,3). The only nonzero *a priori* amplitudes are the A_{0j}, A_{1j}, B_{0j}, B_{1j} (j=1,106) given in Table A.I.

The nutation tweaks are just constant additive factors to the angles $\delta\psi$ and $\delta\varepsilon$:

$$\delta\psi \rightarrow \delta\psi + \Delta\psi \tag{2.134}$$

and

$$\delta\varepsilon \rightarrow \delta\varepsilon + \Delta\varepsilon \tag{2.135}$$

Several alternatives are available as MODEST options to correct deficiencies in the IAU nutation model. The first possibility is to use empirically determined values of $\Delta\psi$, $\Delta\varepsilon$ as part of the polar motion and $UT1$ input which was described in Section 2.6.1.1.3. If this option is selected, the user is relying on nutation angles that are determined from other VLBI experiments near the date of interest, and performing linear interpolation.

Other options are available to select one of the recently published replacements of the 1980 IAU series. Zhu *et al.* (1989, 1990) have refined the 1980 IAU theory of nutation both by reexamining the underlying Earth model and by incorporating recent experimental results. The Zhu *et al.* results are tabulated here in three parts: a) the original 106 terms of the 1980 IAU series with revised amplitudes in Table A.II, b) four sets of out of phase terms in Table A.III, and c) an additional 156 terms in Table A.IV. Herring (1991) has extended the work of Zhu *et al.* and used geophysical parameters from Mathews *et al.* (1991) to generate the ZMOA 1990-2 (Zhu, Mathews, Oceans, Anelasticity) nutation series. Tables A.V to A.VII list the coefficients of this series. Kinoshita and Souchay (1990) have reexamined the rigid-Earth nutation theory, and calculated all terms larger than 0.005 mas, including planetary terms not included in any previous theories. The 263 lunisolar terms listed in Table A.VIII have been corrected for Earth non-rigidity (Souchay, 1993); Table A.IX lists the 117 planetary terms.

Note that the paper of Kinoshita and Souchay gives expressions for the lunisolar tidal arguments that are at variance with the IAU formulas presented above in Eqs. (2.123-2.127). Their expressions for the five usual arguments l, l', F, D, and Ω, as well as five additional planetary arguments l_V, l_E, l_M, l_J, and l_S are given below (all in units of radians):

1. the mean anomaly of the Moon:

$$\alpha_1 = l = 2.35555590 + 8328.691427\,T \tag{2.136}$$

2. the mean anomaly of the Sun:

$$\alpha_2 = l' = 6.24006013 + 628.301955\,T \tag{2.137}$$

3. the mean argument of latitude of the Moon:

$$\alpha_3 = F = 1.62790523 + 8433.466158\,T \tag{2.138}$$

4. the mean elongation of the Moon from the Sun:

$$\alpha_4 = D = 5.19846674 + 7771.377147\,T \tag{2.139}$$

5. the mean longitude of the ascending lunar node:

$$\alpha_5 = \Omega = 2.18243920 - 33.757045\,T \tag{2.140}$$

The Kinoshita-Souchay planetary contributions to $\delta\psi$ and $\delta\varepsilon$ are

$$\delta\psi = \sum_{j=1}^{N}\left[S_{\psi j}\sin\left[\sum_{i=1}^{10} k_{ji}\beta_i(T)\right] + C_{\psi j}\cos\left[\sum_{i=1}^{10} k_{ji}\beta_i(T)\right]\right] \tag{2.141}$$

and

$$\delta\epsilon = \sum_{j=1}^{N} \left[S_{\epsilon j} \sin \left[\sum_{i=1}^{10} k_{ji}\beta_i(T) \right] + C_{\epsilon j} \cos \left[\sum_{i=1}^{10} k_{ji}\beta_i(T) \right] \right] \tag{2.142}$$

where the astronomical arguments are symbolized by β_i; the last four βs are identical with the αs defined above ($\beta_7 = D = \alpha_4$, $\beta_8 = F = \alpha_3$, $\beta_9 = l = \alpha_1$, $\beta_{10} = \Omega = \alpha_5$), while the first six are

1. the mean anomaly of Venus:

$$\beta_1 = l_V = 3.176146697 + 1021.3285546\,T \tag{2.143}$$

2. the mean anomaly of Earth:

$$\beta_2 = l_E = 1.753470314 + 628.30758492\,T \tag{2.144}$$

3. the mean anomaly of Mars:

$$\beta_3 = l_M = 6.203480913 + 334.06124315\,T \tag{2.145}$$

4. the mean anomaly of Jupiter:

$$\beta_4 = l_J = 0.599546497 + 52.96909651\,T \tag{2.146}$$

5. the mean anomaly of Saturn:

$$\beta_5 = l_S = 0.874016757 + 21.32990954\,T \tag{2.147}$$

6. general precession:

$$\beta_6 = p_a = 0.02438175\,T + 5.38691 \times 10^{-6}\,T^2 \tag{2.148}$$

For simulation purposes, the older Woolard nutation model is also available in MODEST. With the exception of the number, amplitudes, and arguments of the terms, the older series is exactly analogous to the 1980 IAU theory, *i.e.*, of the form of Eqs. (2.128) and (2.129). For completeness of documentation, the coefficients are listed in Table A.X.

No partial derivatives with respect to the Woolard or Zhu *et al.* amplitudes are currently calculated. It is emphasized that, for the present, the default nutation model in MODEST remains as just the 1980 IAU nutation model given in Table A.I.

2.6.3 PRECESSION

The next transformation in going from the terrestrial frame to the celestial frame is the rotation P. This is the precession transformation from mean equatorial coordinates of date to the equatorial coordinates of the reference epoch (*e.g.*, J2000). It is a composite of three rotations discussed in detail by Melbourne *et al.* (1968) and Lieske *et al.* (1977):

$$R(-Z) = \begin{pmatrix} \cos Z & \sin Z & 0 \\ -\sin Z & \cos Z & 0 \\ 0 & 0 & 1 \end{pmatrix} \tag{2.149}$$

$$Q(\Theta) = \begin{pmatrix} \cos\Theta & 0 & \sin\Theta \\ 0 & 1 & 0 \\ -\sin\Theta & 0 & \cos\Theta \end{pmatrix} \tag{2.150}$$

$$R(-\varsigma) = \begin{pmatrix} \cos\varsigma & \sin\varsigma & 0 \\ -\sin\varsigma & \cos\varsigma & 0 \\ 0 & 0 & 1 \end{pmatrix} \tag{2.151}$$

$$P = R(-\varsigma)Q(\Theta)R(-Z) \tag{2.152}$$

$$= \begin{pmatrix} \cos\varsigma\cos\Theta\cos Z - \sin\varsigma\sin Z & \cos\varsigma\cos\Theta\sin Z + \sin\varsigma\cos Z & \cos\varsigma\sin\Theta \\ -\sin\varsigma\cos\Theta\cos Z - \cos\varsigma\sin Z & -\sin\varsigma\cos\Theta\sin Z + \cos\varsigma\cos Z & -\sin\varsigma\sin\Theta \\ -\sin\Theta\cos Z & -\sin\Theta\sin Z & \cos\Theta \end{pmatrix}$$

The auxiliary angles ς, Θ, Z depend on precession constants, obliquity, and time as

$$\varsigma = 0''.5mT + 0''.30188\,T^2 + 0''.017998\,T^3 \tag{2.153}$$

$$Z = 0''.5mT + 1''.09468\,T^2 + 0''.018203\,T^3 \tag{2.154}$$

$$\Theta = nT - 0''.42665\,T^2 - 0''.041833\,T^3 \tag{2.155}$$

where the speeds of precession in right ascension and declination are, respectively,

$$m = p_{LS}\cos\varepsilon_0 - p_{PL} \tag{2.156}$$

$$n = p_{LS}\sin\varepsilon_0 \tag{2.157}$$

and p_{LS} = the luni-solar precession constant, p_{PL} = planetary precession constant, ε_0 = the obliquity at J2000, and T [Eq. (2.122)] is the time in centuries past J2000. Nominal values at J2000 are p_{LS} = 5038".7784/cy, p_{PL} = 10".5526/cy; these yield the expressions given by Lieske *et al.* (1977) and Kaplan (1981):

$$\varsigma = 2306''.2181\,T + 0''.30188\,T^2 + 0''.017998\,T^3 \tag{2.158}$$

$$\Theta = 2004''.3109\,T - 0''.42665\,T^2 - 0''.041833\,T^3 \tag{2.159}$$

$$Z = 2306''.2181\,T + 1''.09468\,T^2 + 0''.018203\,T^3 \tag{2.160}$$

Partial derivatives of the VLBI observables with respect to luni-solar and planetary precession are derived from the expressions (2.152-2.157) and given in Section 2.9. The precession matrix completes the standard model for the orientation of the Earth. Numerical checks of direct estimates of precession corrections against similar estimates based on the perturbation rotation (next section) ensure consistency.

2.6.4 PERTURBATION ROTATION

This standard model for the rotation of the Earth as a whole may need a small incremental rotation about any one of the resulting axes. Define this perturbation rotation matrix as

$$\Omega = \Delta_x\Delta_y\Delta_z \tag{2.161}$$

where

$$\Delta_x = \begin{pmatrix} 1 & 0 & 0 \\ 0 & 1 & \delta\Theta_x \\ 0 & -\delta\Theta_x & 1 \end{pmatrix} \tag{2.162}$$

with $\delta\Theta_x$ being a small angle rotation about the x axis, in the sense of carrying y into z;

$$\Delta_y = \begin{pmatrix} 1 & 0 & -\delta\Theta_y \\ 0 & 1 & 0 \\ \delta\Theta_y & 0 & 1 \end{pmatrix} \tag{2.163}$$

with $\delta\Theta_y$ being a small angle rotation about the y axis, in the sense of carrying z into x; and

$$\Delta_z = \begin{pmatrix} 1 & \delta\Theta_z & 0 \\ -\delta\Theta_z & 1 & 0 \\ 0 & 0 & 1 \end{pmatrix} \tag{2.164}$$

with $\delta\Theta_z$ being a small angle rotation about the z axis, in the sense of carrying x into y. For angles on the order of 1 arc second we can neglect terms on the order $\delta\Theta^2 R_E$ as they give effects on the order of 0.015 cm. Thus, in that approximation

$$\Omega = \begin{pmatrix} 1 & \delta\Theta_z & -\delta\Theta_y \\ -\delta\Theta_z & 1 & \delta\Theta_x \\ \delta\Theta_y & -\delta\Theta_x & 1 \end{pmatrix} \tag{2.165}$$

In general,

$$\delta\Theta_i = \delta\Theta_i(t) = \delta\Theta_{i0} + \delta\dot{\Theta}_i T + f_i(T) \tag{2.166}$$

which is the sum of an offset, a time-linear rate, and some higher order or oscillatory terms. Currently, only the offset and linear rate are implemented. In particular, a non-zero value of $\delta\dot{\Theta}_y$ is equivalent to a change in the precession constant, and $\delta\dot{\Theta}_x$ is equivalent to the time rate of change of the obliquity ϵ. Setting

$$\delta\Theta_x = \delta\Theta_y = \delta\Theta_z = 0 \tag{2.167}$$

gives the effect of applying only the standard rotation matrices.

Starting with the Earth-fixed vector, $\mathbf{r}_0$, we have in Sections 2.3 through 2.6 above shown how we obtain the same vector, $\mathbf{r}_c$, expressed in the celestial frame:

$$\mathbf{r}_c = \Omega PNUXY(\mathbf{r}_0 + \Delta) \tag{2.168}$$

2.7 EARTH ORBITAL MOTION

We now wish to transform these station locations from a geocentric reference frame moving with the Earth to a celestial reference frame which is at rest relative to the center of mass of the Solar System. In this Solar System barycentric (SSB) frame we will use these station locations to calculate the geometric delay (see Section 2.1). We will transform the resulting time interval back to the frame in which the time delay is actually measured by the interferometer – the frame moving with the Earth.

Let Σ' be a geocentric frame moving with vector velocity $= \beta c$ relative to a frame, Σ, at rest relative to the Solar System center of mass. Further, let $\mathbf{r}(t)$ be the position of a point (*e.g.*, station location) in space as a function of time, t, as measured in the Σ (SSB) frame. In the Σ' (geocentric) frame, there is a corresponding position $\mathbf{r}'(t')$ as a function of time, t'. We normally observe and model $\mathbf{r}'(t')$ as shown in Sections 2.3 through 2.6. However, in order to calculate the geometric delay in the SSB frame (Σ), we will need the transformations of $\mathbf{r}(t)$ and $\mathbf{r}'(t')$, as well as of t and t', as

we shift frames of reference. Measuring positions in units of light travel time, we have from Jackson (1975):

$$\mathbf{r}'(t') = \mathbf{r}(t) + (\gamma - 1)\mathbf{r}(t) \cdot \frac{\boldsymbol{\beta}\boldsymbol{\beta}}{\beta^2} - \gamma\boldsymbol{\beta}t \tag{2.169}$$

$$t' = \gamma[t - \mathbf{r}(t) \cdot \boldsymbol{\beta}] \tag{2.170}$$

and for the inverse transformation:

$$\mathbf{r}(t) = \mathbf{r}'(t') + (\gamma - 1)\mathbf{r}'(t') \cdot \frac{\boldsymbol{\beta}\boldsymbol{\beta}}{\beta^2} + \gamma\boldsymbol{\beta}t' \tag{2.171}$$

$$t = \gamma[t' + \mathbf{r}'(t') \cdot \boldsymbol{\beta}] \tag{2.172}$$

where

$$\gamma = (1 - \beta^2)^{-1/2} \tag{2.173}$$

Let t_1 represent the time measured in the SSB frame (Σ), at which a wave front crosses antenna 1 at position $\mathbf{r}_1(t_1)$. Let $\mathbf{r}_2(t_1)$ be the position of antenna 2 at this same time, as measured in the SSB frame. Also, let t_2^* be the time measured in this frame at which that same wave front intersects station 2. This occurs at the position $\mathbf{r}_2(t_2^*)$. Following Section 2.1, we can calculate the geometric delay $t_2^* - t_1$. Transforming this time interval back to the geocentric (Σ') frame, we obtain

$$t_2^{*\prime} - t_1' = \gamma(t_2^* - t_1) - \gamma[\mathbf{r}_2(t_2^*) - \mathbf{r}_1(t_1)] \cdot \boldsymbol{\beta} \tag{2.174}$$

Assume further that the motion of station #2 is rectilinear over this time interval. This assumption is not strictly true but, as discussed below, the resulting error is much less than 1 mm in calculated delay. Thus,

$$\mathbf{r}_2(t_2^*) = \mathbf{r}_2(t_1) + \boldsymbol{\beta}_2(t_2^* - t_1) \tag{2.175}$$

which gives:

$$\mathbf{r}_2(t_2^*) - \mathbf{r}_1(t_1) = \mathbf{r}_2(t_1) - \mathbf{r}_1(t_1) + \boldsymbol{\beta}_2(t_2^* - t_1) \tag{2.176}$$

and

$$\begin{aligned} t_2^{*\prime} - t_1' &= \gamma(t_2^* - t_1) - \gamma[\mathbf{r}_2(t_1) - \mathbf{r}_1(t_1)] \cdot \boldsymbol{\beta} - \gamma\boldsymbol{\beta}_2 \cdot \boldsymbol{\beta}[t_2^* - t_1] \\ &= \gamma(1 - \boldsymbol{\beta}_2 \cdot \boldsymbol{\beta})(t_2^* - t_1) - \gamma[\mathbf{r}_2(t_1) - \mathbf{r}_1(t_1)] \cdot \boldsymbol{\beta} \end{aligned} \tag{2.177}$$

This is the expression for the geometric delay that would be observed in the geocentric (Σ') frame in terms of the geometric delay and station positions measured in the SSB system (Σ).

Since our calculation starts with station locations given in the geocentric frame, it is convenient to obtain an expression for $[\mathbf{r}_2(t_1) - \mathbf{r}_1(t_1)]$ in terms of quantities expressed in the geocentric frame. To obtain such an expression consider two events $[\mathbf{r}_1'(t_1'),\ \mathbf{r}_2'(t_1')]$ that are geometrically separate, but simultaneous, in the geocentric frame, and occurring at time t_1'. These two events appear in the SSB frame as:

$$\mathbf{r}_1(t_1) = \mathbf{r}_1'(t_1') + (\gamma - 1)\mathbf{r}_1'(t_1') \cdot \frac{\boldsymbol{\beta}\boldsymbol{\beta}}{\beta^2} + \gamma\boldsymbol{\beta}t_1' \tag{2.178}$$

and as:

$$\mathbf{r}_2(t_2) = \mathbf{r}_2'(t_1') + (\gamma - 1)\mathbf{r}_2'(t_1') \cdot \frac{\boldsymbol{\beta}\boldsymbol{\beta}}{\beta^2} + \gamma\boldsymbol{\beta}t_1' \tag{2.179}$$

where

$$t_2 - t_1 = \gamma[\mathbf{r}_2'(t_1') - \mathbf{r}_1'(t_1')] \cdot \boldsymbol{\beta} \tag{2.180}$$

With these three equations and the expression

$$\mathbf{r}_2(t_2) = \mathbf{r}_2(t_1) + \boldsymbol{\beta}_2[t_2 - t_1] \tag{2.181}$$

we may obtain the vector $\mathbf{r}_2(t_1)$:

$$\mathbf{r}_2(t_1) = \mathbf{r}_2'(t_1') + (\gamma - 1)\mathbf{r}_2'(t_1') \cdot \frac{\boldsymbol{\beta}\boldsymbol{\beta}}{\beta^2} + \gamma\boldsymbol{\beta}t_1' - \gamma\boldsymbol{\beta}_2[\mathbf{r}_2'(t_1') - \mathbf{r}_1'(t_1')] \cdot \boldsymbol{\beta} \tag{2.182}$$

This is the position of station #2 at the time t_1 as observed in Σ. From this we obtain:

$$\begin{aligned}\mathbf{r}_2(t_1) - \mathbf{r}_1(t_1) = \mathbf{r}_2'(t_1') - \mathbf{r}_1'(t_1') + (\gamma - 1)[\mathbf{r}_2'(t_1') - \mathbf{r}_1'(t_1')] \cdot \frac{\boldsymbol{\beta}\boldsymbol{\beta}}{\beta^2} \\ - \gamma\boldsymbol{\beta}_2[\mathbf{r}_2'(t_1') - \mathbf{r}_1'(t_1')] \cdot \boldsymbol{\beta}\end{aligned} \tag{2.183}$$

As shown in Section 2.1, the vectors $[\mathbf{r}_2(t_1) - \mathbf{r}_1(t_1)]$ and $\boldsymbol{\beta}_2$ are all that is needed to obtain $t_2^* - t_1$ for the case of plane waves. For curved wave fronts we will need to know the individual station locations in the barycentric frame as well. These we obtain from (2.178) and (2.182) with t_1' set equal to zero. Setting $t_1' = 0$ is justified since the origin of time is arbitrary when we are trying to obtain time differences.

In the actual coding of these transformations, the relationship for the transformation of velocities is also needed. Taking differentials of (2.171) and (2.172) we have:

$$d\mathbf{r} = d\mathbf{r}' + (\gamma - 1)d\mathbf{r}' \cdot \frac{\boldsymbol{\beta}\boldsymbol{\beta}}{\beta^2} + \gamma\boldsymbol{\beta}dt' \tag{2.184}$$

$$dt = \gamma(dt' + d\mathbf{r}' \cdot \boldsymbol{\beta}) \tag{2.185}$$

Dividing to obtain $d\mathbf{r}/dt$ we obtain for station #2 in the SSB (Σ) frame:

$$\boldsymbol{\beta}_2 = \frac{\boldsymbol{\beta}_2' + (\gamma - 1)\boldsymbol{\beta}_2' \cdot \frac{\boldsymbol{\beta}\boldsymbol{\beta}}{\beta^2} + \gamma\boldsymbol{\beta}}{\gamma(1 + \boldsymbol{\beta}_2' \cdot \boldsymbol{\beta})} \tag{2.186}$$

For station #2 relative to the geocentric origin, we have from (2.98) and (2.99):

$$\boldsymbol{\beta}_2' \approx \Omega PN\frac{dU}{dH}XY\mathbf{r}_{2t}'\omega_E \tag{2.187}$$

where

$$\omega_E = 7.2921151467 \times 10^{-5} \text{ rad/s} \tag{2.188}$$

is the inertial rotation rate of the Earth as specified in Kaplan (1981), p.12. This is not a critical number since it is used only for station velocities, or to extrapolate Earth rotation forward for very small fractions of a day (*i.e.*, typically less than 1000 seconds). Actually, this expression is a better approximation than it might seem from the form since the errors in the approximation, $\frac{dH}{dt} = \omega_E$, are very nearly offset by the effect of ignoring the time dependence of PN.

The assumption of rectilinear motion can be shown to result in negligible errors. Using the plane wave front approximation (2.2), we can estimate the error $\delta\tau$ in the calculated delay due to an error $\Delta\boldsymbol{\beta}_2$ in the above value of $\boldsymbol{\beta}_2$:

$$\delta\tau = \hat{\mathbf{k}} \cdot [\mathbf{r}_2(t_1) - \mathbf{r}_1(t_1)]\left[\frac{1}{1 - \hat{\mathbf{k}} \cdot (\boldsymbol{\beta}_2 + \Delta\boldsymbol{\beta}_2)} - \frac{1}{1 - \hat{\mathbf{k}} \cdot \boldsymbol{\beta}_2}\right] \approx \tau\Delta\boldsymbol{\beta}_2 \tag{2.189}$$

Further, from (2.186) above,

$$\Delta\boldsymbol{\beta}_2 \approx \Delta\boldsymbol{\beta}_2' \tag{2.190}$$

since

$$\gamma \approx 1 + 10^{-8} \tag{2.191}$$

For the vector $\boldsymbol{\beta}_2'$ in a frame rotating with angular velocity ω, the error $\Delta\boldsymbol{\beta}_2'$ that accumulates in the time interval τ due to neglecting the rotation of that frame is

$$\Delta\boldsymbol{\beta}_2' \approx \boldsymbol{\beta}_2 \omega \tau \tag{2.192}$$

Thus for typical Earth-fixed baselines, where $\tau \leq 0.02$ s, neglect of the curvilinear motion of station #2 due to the rotation of the Earth causes an error of $< 4 \times 10^{-14}$ s, or 0.0012 cm, in the calculation of τ. Similarly, neglect of the orbital character of the Earth's motion causes an error on the order of 0.00024 cm maximum.

The position, $\mathbf{R}_E$, and velocity, $\boldsymbol{\beta}_E$, of the Earth's center about the center of mass of the Solar System are:

$$\mathbf{R}_E = -\frac{\sum m_i \mathbf{R}_i}{\sum m_i} \tag{2.193}$$

$$\boldsymbol{\beta}_E = -\frac{\sum m_i \boldsymbol{\beta}_i}{\sum m_i} \tag{2.194}$$

where the index i indicates the Sun, Moon, and all nine Solar System planets. m_i is the mass of the body indexed by i, while $\mathbf{R}_i$ and $\boldsymbol{\beta}_i$ are that body's center-of-mass position and velocity relative to the center of the Earth in the barycentric frame. In a strict sense, the summation should be over all objects in the Solar System. Except for the Earth-Moon system, each planet mass represents not only that planet's mass, but also that of all its satellites. The $\mathbf{R}_i$ and $\boldsymbol{\beta}_i$ are obtained from the JPL planetary ephemeris (DE200 as of May, 1982) for the J2000 frame.

Working in a frame at rest with respect to the center of mass of the Solar System causes relativistic effects due to the motion of the Solar System in a "fixed frame" to be included in the mean position of the sources and in their proper motion. The effects of galactic rotation can be easily estimated. In the vicinity of the Sun, the period for galactic rotation is approximately 2.2×10^8 years. Thus our angular velocity about the galactic center is $\approx 2\pi/2.2 \times 10^8 = 3 \times 10^{-8}$ radians/year. For sources within the Galaxy, at distances approximately equal to our distance from the galactic center, therefore, the apparent positions could change by ≈ 30 nrad/yr. An intercontinental baseline (10,000 km) could thus be in error by as much as 30 cm/yr (1 nrad $\approx$ 1 cm) if measurements were based on sources within the Galaxy. Since our distance from the galactic center is $\approx 2.7 \times 10^4$ light years, and most extragalactic radio sources are believed to be $\approx 10^9$ light years distant, the potential baseline error is scaled by the ratio of these two distances, $\approx 3 \times 10^{-5}$, and becomes ≈ 0.001 cm/year. Even with the present 15-year history of VLBI data, the purely geometric systematic error due to galactic rotation is probably negligible, and only exceeds the millimeter level for sources closer than 100 million light years.

A second contribution to time variability is aberration due to special relativistic effects for observers on a moving platform. Both the galactic latitude and longitude of the Solar System vary sinusoidally with the galactic rotation period $T = 2.2 \times 10^8$ years, amplitudes ranging over $\pm v/c$ (French, 1968), and the latitude variation is also proportional to the sine of the latitude. The amplitude range is 7.5×10^{-4}; thus over half the rotational period at zero galactic latitude, the longitude varies by

$$\Delta\theta = (2v/c)/(0.5T) = 1.4 \times 10^{-11} \text{rad/y} \tag{2.195}$$

Over the present 15-year span of VLBI data, the systematic errors induced by aberration are thus 0.2 nrad (40 μas) in angular measurements, and 2 mm in distance measurements for a 10,000 km baseline. Both are in the range that is currently starting to be detectable, and serious consideration will be given to model enhancements in the near future.

2.8 ANTENNA GEOMETRY

The above work indicates how the time delay model would be calculated for two points fixed with respect to the Earth's crust. In practice, however, an antenna system does not behave as an Earth-fixed point. Not only are there instrumental delays in the system, but portions of the antenna move relative to the Earth. To the extent that instrumental delays are independent of the antenna orientation, they are indistinguishable to the interferometer from clock offsets and secular changes in these offsets. If necessary, these instrumental delays can be separated from clock properties by a careful calibration of each antenna system. That is a separate problem, treated as a calibration correction (*e.g.*, Thomas, 1981), and will not be addressed here.

However, the motions of the antennas relative to the Earth's surface must be considered since they are part of the geometric model. A fairly general antenna pointing system is shown schematically in Figure 5. The unit vector, $\hat{\mathbf{s}}$, to the apparent source position is shown. Usually, a symmetry axis AD will point parallel to $\hat{\mathbf{s}}$. The point A on the figure also represents the end view of an axis which allows rotation in the plane perpendicular to that axis. This axis is offset by some distance H from a second rotation axis BE. All points on this second rotation axis are fixed relative to the Earth. Consequently, any point along that axis is a candidate for the fiducial point which terminates this end of the baseline. The point we actually use is the point P. A plane containing axis A and perpendicular to BE intersects BE at the point P. This is somewhat an arbitrary choice, one of conceptual convenience.

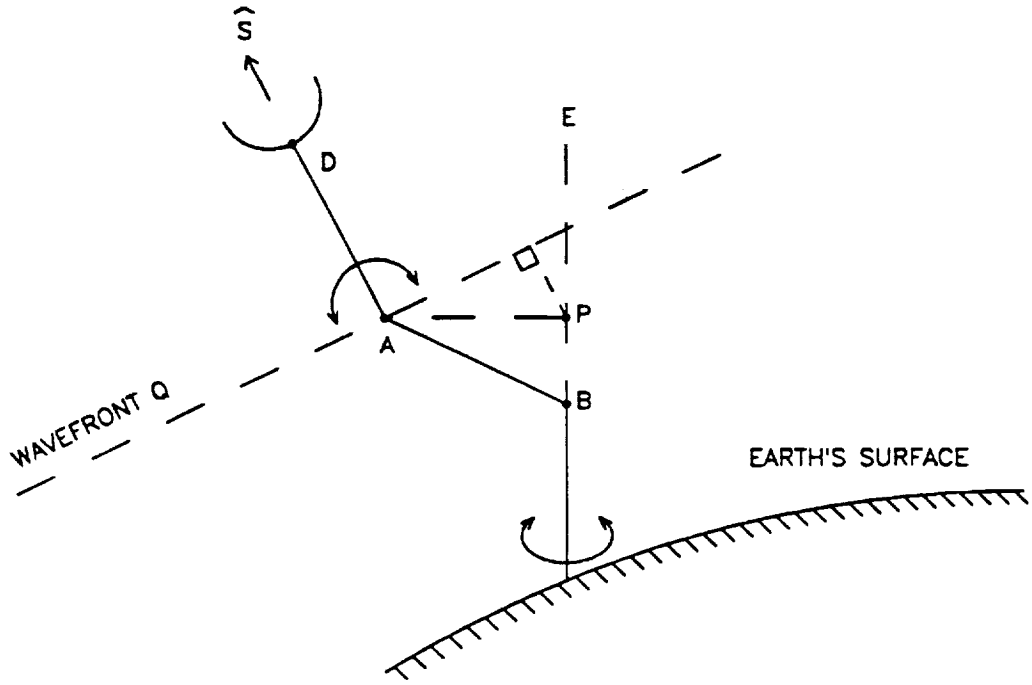

Figure 5. A generalized schematic representation of the geometry of a steerable antenna

Consider the plane Q which is perpendicular to the antenna symmetry axis, AD, and contains the antenna rotation axis A. For plane wave fronts this is an isophase plane (it coincides with the wave front). For curved wave fronts this deviates from an isophase surface by $\approx H^2/(2R)$, where R is the distance to the source, and H is taken as a typical antenna offset AP. For $H \approx 10$ meters,

$R = R_{moon} = 60R_E \approx 3.6 \times 10^8$ m, and the curvature correction $H^2/(2R) \approx 1.4 \times 10^{-7}$ m is totally negligible. R has to be 5 km, or $10^{-3}R_E$, before this deviation approaches 1 cm contribution. Consequently, for all anticipated applications of radio interferometry using high-gain radio antennas, the curvature of the wave front may be neglected in obtaining the effect on the time delay of the antenna orientation.

Provided the instrumental delay of the antenna system is independent of the antenna orientation, the recorded signal is at a constant phase delay, independent of antenna orientation, at any point on the Q plane. Since this delay is indistinguishable from a clock offset, it will be totally absorbed by that portion of our model.

2.8.1 AXIS OFFSET

The advantage of choosing the Q plane rather than some other plane parallel to it is that axis A is contained in this plane, and axis A is fixed relative to the BE axis by the antenna structure. If l is the length of a line from P perpendicular to the Q plane, the wave front will reach the Earth-fixed point P at a time $\Delta t = l/c$ after the wave front passes through axis A. If τ_0 is the model delay for a wave front to pass from P on antenna #1 to a similarly defined point on antenna #2, then the model for the observed delay should be amended as:

$$\tau = \tau_0 - (\Delta t_2 - \Delta t_1) = \tau_0 + (l_1 - l_2)/c \tag{2.196}$$

where the subscripts refer to antennas #1 and #2.

For the inclusion of this effect in the model, we follow a treatment given by Wade (1970). Define a unit vector $\hat{\mathbf{I}}$ along BE, in the sense of positive away from the Earth. Further, define a vector, $\mathbf{L}$, from P to A. Without much loss of generality in this antenna system, we assume that $\hat{\mathbf{s}}, \mathbf{L}$, and $\hat{\mathbf{I}}$ are coplanar. Then:

$$\mathbf{L} = \pm H \frac{\hat{\mathbf{I}} \times [\hat{\mathbf{s}} \times \hat{\mathbf{I}}]}{|\, \hat{\mathbf{I}} \times [\hat{\mathbf{s}} \times \hat{\mathbf{I}}]\,|} \tag{2.197}$$

where the plus or minus sign is chosen to give $\mathbf{L}$ the direction from P to A. The plus sign is used if, when $\hat{\mathbf{s}}$ and $\hat{\mathbf{L}}$ are parallel or antiparallel, the antenna comes closer to the source as H increases. Since

$$\hat{\mathbf{I}} \times [\hat{\mathbf{s}} \times \hat{\mathbf{I}}] = \hat{\mathbf{s}} - \hat{\mathbf{I}}\,[\hat{\mathbf{I}} \cdot \hat{\mathbf{s}}] \tag{2.198}$$

$$l = \hat{\mathbf{s}} \cdot \mathbf{L} = \pm H \sqrt{1 - [\hat{\mathbf{s}} \cdot \hat{\mathbf{I}}]^2} \tag{2.199}$$

where the sign choice above is carried through.

Curvature is always a negligible effect in the determination of $\hat{\mathbf{s}} \cdot \mathbf{L}$. Likewise, gravitational effects are sufficiently constant over a dimension $|\mathbf{L}|$ so as to enable one to obtain a single Cartesian frame over these dimensions, to a very good approximation. Consequently, it is somewhat easier to calculate a proper time $\Delta t = l/c$ in the antenna frame and to include it in the model by adding it to τ_0, taking into account, in principle at least, the time dilation in going from the antenna frame to the frame in which τ_0 is obtained.

2.8.2 REFRACTION

Thus, if $\hat{\mathbf{s}}_0$ is the unit vector to the source from the antenna in a frame at rest with respect to the Solar System center of mass, perform a Lorentz transformation to obtain $\hat{\mathbf{s}}$, the apparent source unit vector in the Earth-fixed celestial frame. Actually, the antenna does not "look" at the apparent source position $\hat{\mathbf{s}}$, but rather at the position of the source after the ray path has been refracted by an angle ε in the Earth's atmosphere. This effect is already included in the tropospheric delay correction (Section 4); however since the antenna model uses the antenna elevation angle E_0, the correction must be made here as well. For the worst case (elevation angle of 6°) at average DSN station altitudes, the deflection can be as large as 2×10^{-3} radians. Thus, $\delta l \approx H\varepsilon \approx 2$ cm for

$H = 10$ meters. A model option permits modification of $\hat{\mathbf{s}}_0$ to take atmospheric refraction into account. The large-elevation-angle approximation is the inverse tangent law:

$$\Delta E = 3.13 \times 10^{-4} / \tan E_0 \tag{2.200}$$

where E is the elevation angle, and ΔE the change in apparent elevation E_0 induced by refraction. This model was implemented only for software comparison purposes, since it gives incorrect results at low elevation angles. In the notation of Section 4.2, a single homogeneous spherical layer approximation yields the bending correction in terms of the zenith troposphere delays ρ_Z, refractivity moment M_{001}, scale height Δ, and Earth radius R:

$$\Delta E = \cos^{-1}[\cos(E_0 + \alpha_0)/(1 + \chi_0)] - \alpha_0 \tag{2.201}$$

where

$$\chi_0 = (\rho z_{dry} + \rho z_{wet}/M_{001})/\Delta \tag{2.202}$$

$$\alpha_0 = \cos^{-1}[(1 + \sigma')/(1 + \sigma)] \tag{2.203}$$

$$\sigma = \Delta/R \tag{2.204}$$

$$\sigma' = \left[\left(1 + \sigma(\sigma + 2)/\sin^2 E_0\right)^{1/2} - 1\right] \sin^2 E_0 \tag{2.205}$$

This formula agrees with ray-tracing results to within 1% at 6° and ≈15% at 1° elevation, while the corresponding comparisons for Eq. (2.200) give ≈25% at 6° and a factor of 3 at 1°.

Since we are given $\hat{\mathbf{I}}$ in terrestrial coordinates, we first perform the coordinate transformation given by Q above:

$$\hat{\mathbf{I}} = Q\hat{\mathbf{I}}_{terrestrial} \tag{2.206}$$

With this done, obtain $\Delta t = l/c$, as shown in Figure 6 for each of the major antenna types. Note that for "nearby" sources we also must include parallax (*e.g.*, geographically separate antennas are not pointing in the same direction). If $\mathbf{R}_0$ is the position of the source as seen from the center of the Earth, and $\mathbf{r}$ is the position of a station in the same frame, then the position of the source relative to that station is

$$\mathbf{R} = \mathbf{R}_0 - \mathbf{r} \tag{2.207}$$

and in (2.199) we make the substitution

$$[\hat{\mathbf{s}} \cdot \hat{\mathbf{I}}]^2 = \left[\frac{[\mathbf{R}_0 - \mathbf{r}] \cdot \hat{\mathbf{I}}}{|\mathbf{R}_0 - \mathbf{r}|}\right]^2 \tag{2.208}$$

2.8.3 UNIQUE ANTENNAS

One of the VLBI antennas employed by the IRIS project of the National Geodetic Survey does not fall into any standard category. It is unique because it is an equatorial mount designed for the latitude of Washington, D.C., but was deployed at Richmond, Florida until it was destroyed in the hurricane of August 1992. The considerable latitude difference, and the axis offset of several meters, make it imperative that the antenna geometry be properly modeled. In the local VEN coordinate frame, the vector $\hat{\mathbf{I}}$ is

$$\begin{pmatrix} \sin\phi_W \\ -\cos\phi_W \sin\epsilon \\ \cos\phi_W \cos\epsilon \end{pmatrix} \tag{2.209}$$

Upon transformation to the Earth-fixed frame via the matrix VW [Eq. (2.71)], it becomes

$$\begin{pmatrix} \cos\lambda(\sin\phi_W \cos\phi - \cos\phi_W \sin\phi \cos\epsilon) + \sin\lambda \cos\phi_W \sin\epsilon \\ \sin\lambda(\sin\phi_W \cos\phi - \cos\phi_W \sin\phi \cos\epsilon) - \cos\lambda \cos\phi_W \sin\epsilon \\ \sin\phi_W \sin\phi + \cos\phi_W \cos\phi \cos\epsilon \end{pmatrix} \tag{2.210}$$

Here (λ, ϕ) are the Richmond longitude and latitude, ϕ_W is the latitude of Washington (39.06°), and $\epsilon = 0.12°$ W of N is the azimuth misalignment.

Two other one-of-a-kind antennas, Arecibo and Nancay, are seldom used in astrometric and geodetic VLBI work. The Arecibo antenna has hardware features which make it equivalent to an azimuth-elevation mount. The Nancay array has been treated by Ortega-Molina (1985), but the model is not presently incorporated in MODEST code.

$$l = \pm H\sqrt{1 - (\hat{S}\cdot\hat{1})^2}$$

AZIMUTH–ELEVATION		HOUR ANGLE–DECLINATION	X–Y
INTERSECTING	OFFSET		
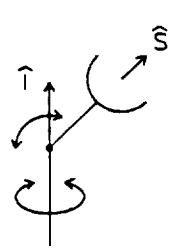	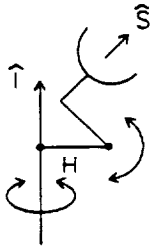	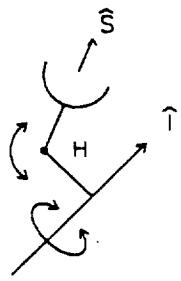	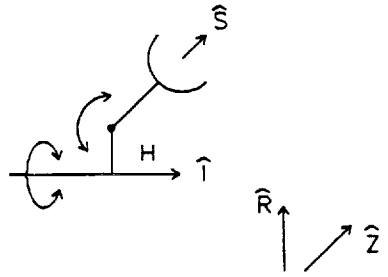
$H = 0$ $\Rightarrow l = 0$	$\hat{1}$ TOWARD GEODETIC VERTICAL $l = \pm H$ COS (ELEVATION ANGLE)	$\hat{1}$ TOWARD NORTH POLE IN NORTHERN HEMISPHERE AND TOWARD SOUTH POLE IN SOUTHERN HEMISPHERE $l = \pm H$ COS (SOURCE DECLINATION)	LET $\hat{Z}$ BE UNIT VECTOR TOWARD EARTH'S NORTH POLE $\hat{R}$ BE UNIT VECTOR TOWARD LOCAL GEODETIC VERTICAL THEN $\hat{1} = \dfrac{\hat{R} \times (\hat{Z} \times \hat{R})}{\lvert\hat{R} \times (\hat{Z} \times \hat{R})\rvert}$ AND $(\hat{S}\cdot\hat{1})^2 = \dfrac{[(\hat{S}\cdot\hat{Z})^2 - 2(\hat{S}\cdot\hat{Z})(\hat{S}\cdot\hat{R})(\hat{R}\cdot\hat{Z}) + (\hat{S}\cdot\hat{R})^2(\hat{R}\cdot\hat{Z})^2]}{1 - (\hat{R}\cdot\hat{Z})^2}$ $l = \pm H\sqrt{1 - (\hat{S}\cdot\hat{1})^2}$

Figure 6. Schematic representations of the four major antenna geometries used in VLBI

2.8.4 SITE VECTORS

In the modeling software is the facility to provide a time-invariant offset vector in local geodetic coordinates (east, north, and local geodetic vertical) from this point (antenna location) to a point elsewhere, such as a benchmark on the ground. This is particularly useful in work involving transportable antennas which may be placed in slightly different places relative to an Earth-fixed benchmark each time a site is reoccupied. In modeling that offset vector, we make the assumption of a plane tangent to the geoid at the reference benchmark and assume that the local geodetic vertical for the antenna is parallel to that for the benchmark. With these assumptions there is an identity in the adjustments of antenna location with changes derived for the benchmark location. The error introduced by these assumptions in a baseline adjustment is approximately $\Delta B \times (d/R_E)$, where ΔB is the baseline adjustment from its *a priori* value, d is the separation of the antenna from the benchmark, and R_E is the radius of the Earth. To keep this error smaller than 0.01 cm for baseline adjustments on the order of 1 meter, $d < 600$ meters is required.

More troublesome is that an error in obtaining the local vertical by an angle $\delta\Theta$, when using an antenna whose intersection of axes is a distance, H, above the ground, can cause an error of $H\sin\delta\Theta \approx H\delta\Theta$ in measuring the baseline to the benchmark (Allen, 1982). Unless this error is already absorbed into the actual measurement of the offset vector, care must be taken in setting up the antenna so as to make $\delta\Theta$ minimal. For a baseline error < 0.1 cm, and an antenna height of 10 meters, $\delta\Theta < 20$ arcseconds is required. Often plumb bobs are used to locate the antenna position relative to a mark on the ground. This mark is, in turn, surveyed to the benchmark. Even the difference in geodetic vertical from the vertical defined by the plumb bob may be as large as 1 arc minute, thus potentially causing an error of 0.3 cm for antennas of height 10 meters. Consequently, great care must be taken in these measurements, particularly if the site is to be repeatedly occupied by antennas of different sizes.

2.8.5 FEED ROTATION

Another physical effect related to antenna structures is the differential feed rotation for circularly polarized receivers. Liewer (1985) has calculated the phase shift θ for various antenna types. It is zero for equatorially mounted antennas. For altazimuth mounts,

$$\tan\theta = \cos\phi\sin h/(\sin\phi\cos\delta - \cos\phi\sin\delta\cos h) \tag{2.211}$$

with ϕ = station latitude, h = hour angle, and δ = declination of the source. For X-Y mounts, two cases are distinguished: orientation $N-S$ or $E-W$. The respective rotation angles are

$$\tan(-\theta) = \sin\phi\sin h/(\cos\phi\cos\delta + \sin\phi\sin\delta\cos h) \quad (N-S) \tag{2.212}$$

$$\tan(-\theta) = -\cos h/(\sin\delta\sin h) \quad (E-W) \tag{2.213}$$

The effect cancels for group delay data, but can be significant for phase delay and delay rate data. The effect on phase delay is

$$\tau = (\theta_2 - \theta_1)/f \tag{2.214}$$

where f is the observing frequency and θ_i the phase rotation at station i. The feed rotation correction is an optional part of the MODEST model.

Finally, another small correction which accounts for the effect of orientation of hour angle-declination (HA-Dec) and X-Y antennas on the tropospheric path delay was considered by Jacobs (1988). Details are given in the troposphere Section, 4.6.

2.8.6 THERMAL EXPANSION

By analogy with the model for atmospheric loading in Sec. 2.4.4, diurnal variations of the temperature cause vertical displacements of the antenna reference point. These can amount to several mm for ordinary day-to-night temperature variations for large antennas. If VLBI data acquired during a variety of weather conditions are to be processed simultaneously, it may be important to account for the vertical motion of the reference point.

A rudimentary model of this effect is implemented in MODEST. It assumes that the vertical displacement Δr of the antenna reference point, a distance h above the ground, is

$$\Delta r = \alpha(T - T_{ref})h \tag{2.215}$$

where α is the coefficient of thermal expansion and T_{ref} is the reference temperature. The height h may be approximated as one half of the antenna diameter. The reference temperature is taken to be equal to the global average temperature at each station, or the universal average 292 K (used in tropospheric mapping in Sec. 4.2) if the former is not available. For steel and concrete, a linear expansion coefficient of 12 ppm is appropriate. Thus for a 70-m antenna, the vertical motion is 0.42 mm/K.

2.8.7 ANTENNA SUBREFLECTOR FOCUSING

For some experiments (notably the Time and Earth Motion Precision Observation [TEMPO] project) which use the DSN Cassegrain antennas, the subreflector is moved in order to maintain focus and to optimize the signal-to-noise ratio. Such motions introduce systematic errors in the antenna position derived from the measurements. For experiments performed in this "slew" mode, the path delay may change by $\approx$8 cm over the $6° - 90°$ elevation range. Simulations show that this effect is almost entirely absorbed by the clock epoch and local station vertical coordinate parameters. For baselines between two 70-m antennas, this causes a potential error of up to 12 cm in length. This effect is most easily modeled as a site vector relating fixed and slewed antenna positions.

2.9 PARTIAL DERIVATIVES OF DELAY WITH RESPECT TO GEOMETRIC MODEL PARAMETERS

With respect to any given parameter, the calculation of the time-delay model must be at least as accurate as the data is sensitive to that parameter. Consequently, such effects as the curvature of the wave fronts were considered. However, such detail is not necessary for determining the derivatives with respect to the relevant model parameters. Here, the plane wave approximation is sufficient. Iteration on the estimated parameters and the rapid convergence of an expansion of the time delay in the relevant parameters about some *a priori* point permit this simplification.

In this plane wave approximation we wish to obtain the parameter derivatives with respect to:

1. the nominal baseline components (actually, station locations),
2. the parameters of the whole Earth orientation matrix Q described in Section 2.6,
3. the solid-Earth tidal parameters,
4. the parameters of source location (right ascension and declination),
5. the antenna axis offsets,
6. the constant, γ_{PPN}, in the retardation of the light ray due to gravitational effects.

The expressions for these derivatives are considerably simplified if tensor notation, with the Einstein summation convention, is employed. Before proceeding any further, we make the following definitions for this section:

τ = time delay modeled in the geocentric frame,
τ_s = this same time delay, but modeled in the Solar System center of mass frame,
$\hat{\mathbf{s}}$ = source unit vector (in the celestial system at rest with respect to the Solar System center of mass),
$\boldsymbol{\beta}$ = velocity of the geocentric frame as measured in the Solar System center of mass frame (remember, all distances are measured in time; thus, this quantity is dimensionless),
$\boldsymbol{\beta}_2$ = velocity of station #2 in Solar System center of mass frame,
ρ = $1 + \hat{\mathbf{s}} \cdot \boldsymbol{\beta}_2$. This is a factor ≈ 1.0001, which arises from the motion of station #2 during the passage of the wave front from station #1 to #2,
γ = $(1 - \boldsymbol{\beta}^2)^{-1/2}$,
γ_2 = $(1 - \boldsymbol{\beta}_2^2)^{-1/2}$,
Q = matrix which transforms from the terrestrial system to the celestial system,
$\mathbf{L}_0$ = the baseline vector in the terrestrial system,
$\mathbf{L}_s$ = this same baseline vector in the celestial system center of mass frame,
$\mathbf{L}$ = this same baseline vector in the celestial system.

With these definitions (2.177) may be written

$$\tau = \gamma(1 - \boldsymbol{\beta} \cdot \boldsymbol{\beta}_2)\tau_s - \gamma \boldsymbol{\beta} \cdot \mathbf{L}_s \tag{2.216}$$

For plane waves from (2.2):

$$\tau_s = \frac{\hat{\mathbf{k}} \cdot [\mathbf{r}_2 - \mathbf{r}_1]}{1 - \hat{\mathbf{k}} \cdot \boldsymbol{\beta}_2} = -\frac{\hat{\mathbf{s}} \cdot \mathbf{L}_s}{1 + \hat{\mathbf{s}} \cdot \boldsymbol{\beta}_2} = -\frac{\hat{\mathbf{s}} \cdot \mathbf{L}_s}{\rho} \tag{2.217}$$

Thus,

$$\tau = -\gamma[1 - \beta_{2_i}\beta_i]\frac{s_k L_{s_k}}{\rho} - \gamma \beta_k L_{s_k} \tag{2.218}$$

For parameters (represented symbolically by η) associated with L_{s_k} only:

$$\frac{\partial \tau}{\partial \eta} = -\left[\gamma(1 - \beta_{2_i}\beta_i)\frac{s_k}{\rho} + \gamma \beta_k\right]\frac{\partial L_{s_k}}{\partial \eta} \tag{2.219}$$

Define the vector:

$$\Psi_k = -\left[\gamma(1 - \beta_{2_i}\beta_i)\frac{s_k}{\rho} + \gamma \beta_k\right] \tag{2.220}$$

Then

$$\frac{\partial \tau}{\partial \eta} = \Psi_k \frac{\partial L_{s_k}}{\partial \eta} \tag{2.221}$$

2.9.1 SOURCE PARAMETERS

For parameters associated with the source position only:

$$\frac{\partial \tau}{\partial \eta} = -\gamma(1 - \beta_{2_i}\beta_i)\frac{L_{s_k}}{\rho}\left[\frac{\partial s_k}{\partial \eta} - \frac{s_k}{\rho}\frac{\partial \rho}{\partial \eta}\right] \tag{2.222}$$

Since

$$\rho = 1 + s_l \beta_{2_l} \tag{2.223}$$

$$\begin{aligned}\frac{\partial \tau}{\partial \eta} &= -\gamma(1 - \beta_{2_i}\beta_i)\frac{L_{s_k}}{\rho}\left[\frac{\partial s_k}{\partial \eta} - \frac{s_k \beta_{2_l}}{\rho}\frac{\partial s_l}{\partial \eta}\right] \\ &= -\gamma(1 - \beta_{2_i}\beta_i)\frac{L_{s_k}}{\rho}\left[\delta_{kl} - \frac{s_k \beta_{2_l}}{\rho}\right]\frac{\partial s_l}{\partial \eta}\end{aligned} \tag{2.224}$$

Define the vector:

$$M_j = -\gamma(1 - \beta_{2_l}\beta_l)\frac{L_{s_i}}{\rho}\left[\delta_{ij} - \frac{s_i \beta_{2_j}}{\rho}\right] \tag{2.225}$$

Then,

$$\frac{\partial \tau}{\partial \eta} = M_j \frac{\partial s_j}{\partial \eta} \tag{2.226}$$

For example:

$$\hat{\mathbf{s}} = [\ \cos\delta\cos\alpha,\ \cos\delta\sin\alpha,\ \sin\delta\ ] \tag{2.227}$$

Then,

$$\frac{\partial \hat{\mathbf{s}}}{\partial \alpha} = [\ -\cos\delta\sin\alpha,\ \cos\delta\cos\alpha,\ 0\ ] = [\ A_1, A_2, A_3\ ] \tag{2.228}$$

and

$$\frac{\partial \hat{\mathbf{s}}}{\partial \delta} = [\ -\sin\delta\cos\alpha,\ -\sin\delta\sin\alpha,\ \cos\delta\ ] = [\ F_1, F_2, F_3\ ] \tag{2.229}$$

and

$$\frac{\partial \tau}{\partial \alpha} = M_i A_i \tag{2.230}$$

$$\frac{\partial \tau}{\partial \delta} = M_i F_i \tag{2.231}$$

Or, if we define the matrices:

$$G = \begin{pmatrix} A_1 & F_1 \\ A_2 & F_2 \\ A_3 & F_3 \end{pmatrix} \tag{2.232}$$

and

$$M = (\ M_1, M_2, M_3\ ) \tag{2.233}$$

then:

$$\left[\frac{\partial \tau}{\partial \alpha},\ \frac{\partial \tau}{\partial \delta}\right] = MG \tag{2.234}$$

For a linear model of source "proper motion" [Eqs. (2.91)-(2.92)], the partials of τ with respect to the time rates of change of right ascension and declination ($\dot{\alpha}$, $\dot{\delta}$) are

$$\left[\frac{\partial\tau}{\partial\dot{\alpha}}, \quad \frac{\partial\tau}{\partial\dot{\delta}}\right] = (t - t_0)MG \tag{2.235}$$

where t_0 is a reference time.

The partials of the observables with respect to the flux ratio K and the baseline projection R for a two-component model are obtained from Charlot's (1990a) expression for the group delay:

$$\frac{\partial\tau}{\partial K} = \frac{2\pi R\left[1 - \cos(2\pi R)\right]}{\omega(1+K)^2} \cdot \frac{K^4 - 2K^3 - 2K^2 - 2K + 1 - 4K^2\cos(2\pi R)}{\left[K^2 + 2K\cos(2\pi R) + 1\right]^2} \tag{2.236}$$

$$\frac{\partial\tau}{\partial R} = \frac{2\pi K(1-K)}{\omega(1+K)} \cdot \frac{(1+K^2) + 2\pi R(1+K)^2\sin(2\pi R) - \left[(1-K)^2 + 2K\cos(2\pi R)\right]\cos(2\pi R)}{\left[K^2 + 2K\cos(2\pi R) + 1\right]^2} \tag{2.237}$$

Finally, the partials with respect to the remaining two structure parameters s and θ are obtained from $\partial\tau/\partial R$ via

$$\frac{\partial\tau}{\partial s} = \frac{\partial\tau}{\partial R}\frac{\partial R}{\partial s} = (u\sin\theta + v\cos\theta)\,\frac{\partial\tau}{\partial R} \tag{2.238}$$

$$\frac{\partial\tau}{\partial\theta} = \frac{\partial\tau}{\partial R}\frac{\partial R}{\partial\theta} = s\,(u\cos\theta - v\sin\theta)\,\frac{\partial\tau}{\partial R} \tag{2.239}$$

2.9.2 STATION PARAMETERS

For station location parameters the algebra is somewhat more complex. Since

$$\begin{aligned}\mathbf{L}_s &= \mathbf{r}_2(t_1) - \mathbf{r}_1(t_1) \\ &= \mathbf{r}_2(t_2) - \mathbf{r}_1(t_1) - \boldsymbol{\beta}_2[t_2 - t_1] \\ &= \mathbf{r}_2(t_2) - \mathbf{r}_1(t_1) - \gamma\boldsymbol{\beta}_2[\mathbf{r}_2'(t_1') - \mathbf{r}_1'(t_1')]\cdot\boldsymbol{\beta} \\ &= [\mathbf{r}_2'(t_1') - \mathbf{r}_1'(t_1')] + (\gamma-1)[\mathbf{r}_2'(t_1') - \mathbf{r}_1'(t_1')]\cdot\hat{\boldsymbol{\beta}}\hat{\boldsymbol{\beta}} - \gamma\boldsymbol{\beta}_2\boldsymbol{\beta}\cdot[\mathbf{r}_2'(t_1') - \mathbf{r}_1'(t_1')]\end{aligned} \tag{2.240}$$

we have:

$$\mathbf{L}_s = \mathbf{L} + (\gamma-1)\mathbf{L}\cdot\hat{\boldsymbol{\beta}}\hat{\boldsymbol{\beta}} - \gamma\boldsymbol{\beta}_2\boldsymbol{\beta}\cdot\mathbf{L} \tag{2.241}$$

or in tensor notation

$$L_{s_i} = \left[\delta_{ij} + \left[\frac{(\gamma-1)\beta_i}{\beta^2} - \gamma\beta_{2_i}\right]\beta_j\right]L_j \tag{2.242}$$

Define the tensor:

$$E_{ij} = \delta_{ij} + \left[\frac{(\gamma-1)\beta_i}{\beta^2} - \gamma\beta_{2_i}\right]\beta_j \tag{2.243}$$

Then

$$L_{s_i} = E_{ij}L_j \tag{2.244}$$

Since

$$L_j = Q_{jk}L_{0_k} \tag{2.245}$$

$$L_{s_i} = E_{ij}Q_{jk}L_{0_k} \tag{2.246}$$

Thus,

$$\tau = \Psi_i E_{ij} Q_{jk} L_{0_k} \tag{2.247}$$

For parameters which are involved with station locations expressed in the terrestrial coordinate system:

$$\frac{\partial \tau}{\partial \eta} = [\Psi_i E_{ij} Q_{jk}] \frac{\partial L_{0_k}}{\partial \eta} = B_k \frac{\partial L_{0_k}}{\partial \eta} \tag{2.248}$$

where the vector element

$$B_k = \Psi_i E_{ij} Q_{jk} \tag{2.249}$$

Such parameters are: $r^0_{sp_i}$ (radius off spin axis), λ^0_i (longitude), z^0_i (height above the equator), $\dot{r}_{sp_i}$, $\dot{\lambda}_i$, $\dot{z}_i$ (the station coordinates' respective time rates), h_{2i} (vertical quadrupole Love number), l_{2i} (horizontal quadrupole Love number), ψ_i (phase lag of maximum tidal amplitude). The subscript refers to station number, *i.e.*, $i = 1, 2$. Define the matrix:

$$W = [-R_1, R_2, -\Lambda_1, \Lambda_2, -Z_1, Z_2, -\dot{R}_1, \dot{R}_2, -\dot{\Lambda}_1, \dot{\Lambda}_2, -\dot{Z}_1, \dot{Z}_2, -V_1, V_2, -H_1, H_2, -\Phi_1, \Phi_2] \tag{2.250}$$

where each column contains the partials of the L_0 component vectors x, y, z with respect to the parameters. For example, for the constant terms in the cylindrical station coordinates [see Eqs. (2.36) through (2.38)]:

$$R_i = \begin{pmatrix} \frac{\partial L_{0_x}}{\partial r^0_{sp_i}} \\ \frac{\partial L_{0_y}}{\partial r^0_{sp_i}} \\ \frac{\partial L_{0_z}}{\partial r^0_{sp_i}} \end{pmatrix} = \begin{pmatrix} \cos\lambda^0_i \\ \sin\lambda^0_i \\ 0 \end{pmatrix} \tag{2.251}$$

$$\Lambda_i = \begin{pmatrix} \frac{\partial L_{0_x}}{\partial \lambda^0_i} \\ \frac{\partial L_{0_y}}{\partial \lambda^0_i} \\ \frac{\partial L_{0_z}}{\partial \lambda^0_i} \end{pmatrix} = \begin{pmatrix} -r^0_{sp_i} \sin\lambda^0_i \\ r^0_{sp_i} \cos\lambda^0_i \\ 0 \end{pmatrix} \tag{2.252}$$

$$Z_i = \begin{pmatrix} \frac{\partial L_{0_x}}{\partial z^0_i} \\ \frac{\partial L_{0_y}}{\partial z^0_i} \\ \frac{\partial L_{0_z}}{\partial z^0_i} \end{pmatrix} = \begin{pmatrix} 0 \\ 0 \\ 1 \end{pmatrix} \tag{2.253}$$

For the station coordinate rates,

$$\dot{R}_i = (t - t_0) R_i \qquad \dot{\Lambda}_i = (t - t_0)\Lambda_i \qquad \dot{Z}_i = (t - t_0) Z_i \tag{2.254}$$

From Eqs. (2.48) through (2.59), and relying on Williams (1970):

$$V_i = \begin{pmatrix} \frac{\partial \delta_{ix}}{\partial h_{2i}} \\ \frac{\partial \delta_{iy}}{\partial h_{2i}} \\ \frac{\partial \delta_{iz}}{\partial h_{2i}} \end{pmatrix} = S(i)V(i)W(i) \begin{pmatrix} g^{(2)}_1(i) \\ 0 \\ 0 \end{pmatrix} \tag{2.255}$$

$$H_i = \begin{pmatrix} \frac{\partial \delta_{ix}}{\partial l_{2i}} \\ \frac{\partial \delta_{iy}}{\partial l_{2i}} \\ \frac{\partial \delta_{iz}}{\partial l_{2i}} \end{pmatrix} = S(i)V(i)W(i) \begin{pmatrix} 0 \\ g_2^{(2)}(i) \\ g_3^{(2)}(i) \end{pmatrix} \tag{2.256}$$

$$\Phi_i = \begin{pmatrix} \frac{\partial \delta_{ix}}{\partial \psi_i} \\ \frac{\partial \delta_{iy}}{\partial \psi_i} \\ \frac{\partial \delta_{iz}}{\partial \psi_i} \end{pmatrix} = S(i)V(i)W(i) \begin{pmatrix} \frac{\partial g_1^{(2)}(i)}{\partial \psi_i} \\ \frac{\partial g_2^{(2)}(i)}{\partial \psi_i} \\ \frac{\partial g_3^{(2)}(i)}{\partial \psi_i} \end{pmatrix} \tag{2.257}$$

where $i = 1$ implies station #1, $i = 2$ implies #2, and $S(1) = -1$, while $S(2) = 1$. These partials of $g^{(2)}$ with respect to ψ are

$$\frac{\partial g_{1_s}^{(2)}}{\partial \psi} = \frac{3\mu_s r_p^2}{R_s^5} h \mathbf{r}_p \cdot \mathbf{R}_s [y_p X_s - x_p Y_s] \tag{2.258}$$

$$\frac{\partial g_{2_s}^{(2)}}{\partial \psi} = \frac{3\mu_s r_p^2}{R_s^5} \, l \, \frac{|\mathbf{r}_p|}{\sqrt{x_p^2 + y_p^2}} \left[[\mathbf{r}_p \cdot \mathbf{R}_s][x_p X_s + y_p Y_s] - [x_p Y_s - y_p X_s]^2 \right] \tag{2.259}$$

$$\frac{\partial g_{3_s}^{(2)}}{\partial \psi} = \frac{3\mu_s r_p^2}{R_s^5} \, l \, [y_p X_s - x_p Y_s] \left[\sqrt{x_p^2 + y_p^2} Z_s - \frac{z_p}{\sqrt{x_p^2 + y_p^2}} [2\mathbf{r}_p \cdot \mathbf{R}_s - z_p Z_s] \right] \tag{2.260}$$

Also, define a vector:

$$D = \left[\frac{\partial \tau}{\partial r_{sp_1}^0}, \frac{\partial \tau}{\partial r_{sp_2}^0}, \frac{\partial \tau}{\partial \lambda_1^0}, \frac{\partial \tau}{\partial \lambda_2^0}, \frac{\partial \tau}{\partial z_1^0}, \frac{\partial \tau}{\partial z_2^0}, \frac{\partial \tau}{\partial \dot{r}_{sp_1}}, \frac{\partial \tau}{\partial \dot{r}_{sp_2}}, \frac{\partial \tau}{\partial \dot{\lambda}_1}, \frac{\partial \tau}{\partial \dot{\lambda}_2}, \frac{\partial \tau}{\partial \dot{z}_1}, \frac{\partial \tau}{\partial \dot{z}_2}, \right.$$
$$\left. \frac{\partial \tau}{\partial b_1}, \frac{\partial \tau}{\partial b_2}, \frac{\partial \tau}{\partial h_{21}}, \frac{\partial \tau}{\partial h_{22}}, \frac{\partial \tau}{\partial l_{21}}, \frac{\partial \tau}{\partial l_{22}}, \frac{\partial \tau}{\partial \psi_1}, \frac{\partial \tau}{\partial \psi_2} \right] \tag{2.261}$$

Then

$$D = BW \tag{2.262}$$

2.9.2.1 Ocean Loading Parameters

Partials with respect to the amplitudes ξ_i^j [Eq. (2.74)] of the ocean loading model are trivial in the local coordinate system. Transformation to geocentric coordinates via (2.68) yields the corresponding partials with respect to the amplitudes, $\frac{\partial \tau}{\partial \xi_i^j}$.

2.9.2.2 Atmosphere Loading Parameter

Partials of the station vertical displacement with respect to the atmosphere loading scale factor f, $\frac{\partial \Delta r}{\partial f} = -0.55\bar{p}$, are transformed via (2.68) to give the observable partials $\frac{\partial \tau}{\partial f}$.

2.9.3 EARTH ORIENTATION PARAMETERS

Certain parameters such as $UT1$, polar motion, precession, and nutation affect Q only. For these parameters, symbolized by η,

$$\frac{\partial \tau}{\partial \eta} = \Psi_i E_{ij} \left(\frac{\partial Q_{ik}}{\partial \eta} \right) L_{0_k} \tag{2.263}$$

Define a vector:

$$K_i = \Psi_k E_{ki} \tag{2.264}$$

Then

$$\frac{\partial \tau}{\partial \eta} = K_i \left(\frac{\partial Q_{ik}}{\partial \eta} \right) L_{0_k} \tag{2.265}$$

for parameters which affect only the orientation of the Earth as a whole.

2.9.3.1 UT1 and Polar Motion

A number of parameter partials are available for the orientation of the Earth. These are for $UT1$, X pole, Y pole, and nutation, as well as the angular offset and angular rate terms in the Earth orientation perturbation matrix Ω. From (2.98):

$$Q = \Omega PNUXY \tag{2.266}$$

Define the matrix:

$$Y' = \frac{\partial Y}{\partial \Theta_2} = \begin{pmatrix} 0 & 0 & 0 \\ 0 & -\sin\Theta_2 & \cos\Theta_2 \\ 0 & -\cos\Theta_2 & -\sin\Theta_2 \end{pmatrix} \tag{2.267}$$

Then, the partial required for the Y polar motion parameter is:

$$\frac{\partial Q}{\partial \Theta_2} = \Omega PNUXY' \tag{2.268}$$

An analogous technique is used for the X pole angle, working with the matrix partials $\frac{\partial X}{\partial \Theta_1}$. Partials with respect to $UT1$ involve a slight complication due to the last three terms in Eq. (2.105). On the assumption that only the term linear in T_u contributes significantly,

$$\frac{\partial U}{\partial (UT1)} = \frac{\partial U}{\partial H}(1 + 1/365.25) \tag{2.269}$$

Partials of time rates of the UTPM parameters are related to those of the parameters themselves:

$$\frac{\partial Q}{\partial \dot{\Theta}_i} = \frac{\partial Q}{\partial \Theta_i}(t - t_0) \tag{2.270}$$

2.9.3.1.1 UTPM Tidal Amplitudes

Partials of τ with respect to the amplitudes of both the solid and ocean tide contributions to UT1 and polar motion are also easily obtained. Again, the required partials of Q are written as

$$\frac{\partial Q}{\partial \eta} = \Omega PN \frac{\partial U}{\partial \eta} XY \tag{2.271}$$

and

$$\frac{\partial Q}{\partial \eta} = \Omega P N U \frac{\partial X}{\partial \eta} Y \tag{2.272}$$

with a similar expression for the Y component. For the solid tide amplitudes A_i (2.113),

$$\frac{\partial U}{\partial A_i} = \frac{\partial U}{\partial (UT1)} \frac{\partial \Theta_3}{\partial A_i} \tag{2.273}$$

and

$$\frac{\partial \Theta_3}{\partial A_i} = \sin\left[\sum_{j=1}^{5} k_{ij}\alpha_j\right] \tag{2.274}$$

For the ocean tidal amplitudes A_i^k and B_i^k of (2.114),

$$\frac{\partial \Theta_k}{\partial A_i^k} = \cos\left[\sum_{j=1}^{5} k_{ij}\alpha_j + n_i(h_\gamma + \pi)\right] \tag{2.275}$$

2.9.3.2 Nutation

Partial derivatives of the VLBI observables with respect to the nutation angles and amplitudes appear formidable at first sight, but are relatively easy to evaluate if the calculation is performed in an organized fashion. Symbolizing the parameters by η, we need to evaluate the partials of the matrix Q with respect to η:

$$\frac{\partial Q}{\partial \eta} = \Omega P \left(\frac{\partial N}{\partial \delta\psi} U + N \frac{\partial U}{\partial \delta\psi} \right) \frac{\partial \delta\psi}{\partial \eta} XY \tag{2.276}$$

$$\frac{\partial Q}{\partial \eta} = \Omega P \left(\frac{\partial N}{\partial \delta\varepsilon} U + N \frac{\partial U}{\partial \delta\varepsilon} \right) \frac{\partial \delta\varepsilon}{\partial \eta} XY \tag{2.277}$$

Since $\delta\varepsilon = \varepsilon - \bar{\varepsilon}$, the first partial on the right hand side of Eq. (2.277) is equal to $\frac{\partial N}{\partial \varepsilon}$. The derivatives of N with respect to the angles $\delta\psi$ and $\delta\varepsilon$ are easily obtained from the expression for N in Eq. (2.120):

$$\frac{\partial N}{\partial \delta\psi} = \begin{pmatrix} -\sin\delta\psi & \cos\varepsilon\cos\delta\psi & \sin\varepsilon\cos\delta\psi \\ -\cos\bar{\varepsilon}\cos\delta\psi & -\cos\bar{\varepsilon}\cos\varepsilon\sin\delta\psi & -\cos\bar{\varepsilon}\sin\varepsilon\sin\delta\psi \\ -\sin\bar{\varepsilon}\cos\delta\psi & -\sin\bar{\varepsilon}\cos\varepsilon\sin\delta\psi & -\sin\bar{\varepsilon}\sin\varepsilon\sin\delta\psi \end{pmatrix} \tag{2.278}$$

and

$$\frac{\partial N}{\partial \delta\varepsilon} = \begin{pmatrix} 0 & -\sin\varepsilon\sin\delta\psi & \cos\varepsilon\sin\delta\psi \\ 0 & -\cos\bar{\varepsilon}\sin\varepsilon\cos\delta\psi + \sin\bar{\varepsilon}\cos\varepsilon & \cos\bar{\varepsilon}\cos\varepsilon\cos\delta\psi + \sin\bar{\varepsilon}\sin\varepsilon \\ 0 & -\sin\bar{\varepsilon}\sin\varepsilon\cos\delta\psi - \cos\bar{\varepsilon}\cos\varepsilon & \sin\bar{\varepsilon}\cos\varepsilon\cos\delta\psi - \cos\bar{\varepsilon}\sin\varepsilon \end{pmatrix} \tag{2.279}$$

From Eq. (2.103), the partials of U with respect to $\delta\psi$ and $\delta\varepsilon$ are

$$\frac{\partial U}{\partial \delta\psi, \delta\varepsilon} = \begin{pmatrix} -\sin H & -\cos H & 0 \\ \cos H & -\sin H & 0 \\ 0 & 0 & 0 \end{pmatrix} \frac{\partial H}{\partial \delta\psi, \delta\varepsilon} \tag{2.280}$$

and, from Eq. (2.108),

$$\frac{\partial H}{\partial \delta\psi} = \cos\varepsilon \;/\; (\cos^2\delta\psi \;+\; \cos^2\varepsilon \sin^2\delta\psi) \tag{2.281}$$

$$\frac{\partial H}{\partial \delta\varepsilon} = -\sin\varepsilon\tan\delta\psi \;/\; (1 \;+\; \cos^2\varepsilon\tan^2\delta\psi) \tag{2.282}$$

the U-dependent terms in Eqs. (2.276) and (2.277) are evaluated.

Partials of $\delta\psi$ and $\delta\varepsilon$ with respect to the parameters A_{ij} and B_{ij} are obtained immediately from Eqs. (2.130-2.133). For the "free nutations",

$$\frac{\partial\delta\psi^f}{\partial A_{00}} = \sin\omega_f T, \qquad \frac{\partial\delta\varepsilon^f}{\partial B_{00}} = \cos\omega_f T \tag{2.283}$$

$$\frac{\partial\delta\psi^f}{\partial A_{10}} = T\sin\omega_f T, \qquad \frac{\partial\delta\varepsilon^f}{\partial B_{10}} = T\cos\omega_f T \tag{2.284}$$

$$\frac{\partial\delta\psi^f}{\partial A_{20}} = \cos\omega_f T, \qquad \frac{\partial\delta\varepsilon^f}{\partial B_{20}} = \sin\omega_f T \tag{2.285}$$

$$\frac{\partial\delta\psi^f}{\partial A_{30}} = T\cos\omega_f T, \qquad \frac{\partial\delta\varepsilon^f}{\partial B_{30}} = T\sin\omega_f T \tag{2.286}$$

and for the 1980 IAU series terms (j = 1 to 106):

$$\frac{\partial\delta\psi}{\partial A_{0j}} = \sin\Big[\sum_{i=1}^{5} k_{ji}\alpha_i(T)\Big], \qquad \frac{\partial\delta\varepsilon}{\partial B_{0j}} = \cos\Big[\sum_{i=1}^{5} k_{ji}\alpha_i(T)\Big] \tag{2.287}$$

$$\frac{\partial\delta\psi}{\partial A_{1j}} = T\sin\Big[\sum_{i=1}^{5} k_{ji}\alpha_i(T)\Big], \qquad \frac{\partial\delta\varepsilon}{\partial B_{1j}} = T\cos\Big[\sum_{i=1}^{5} k_{ji}\alpha_i(T)\Big] \tag{2.288}$$

$$\frac{\partial\delta\psi}{\partial A_{2j}} = \cos\Big[\sum_{i=1}^{5} k_{ji}\alpha_i(T)\Big], \qquad \frac{\partial\delta\varepsilon}{\partial B_{2j}} = \sin\Big[\sum_{i=1}^{5} k_{ji}\alpha_i(T)\Big] \tag{2.289}$$

$$\frac{\partial\delta\psi}{\partial A_{3j}} = T\cos\Big[\sum_{i=1}^{5} k_{ji}\alpha_i(T)\Big], \qquad \frac{\partial\delta\varepsilon}{\partial B_{3j}} = T\sin\Big[\sum_{i=1}^{5} k_{ji}\alpha_i(T)\Big]. \tag{2.290}$$

2.9.3.3 Precession

Partial derivatives of the observables with respect to precession parameters are evaluated in a manner similar to those with respect to nutations. Symbolizing either the luni-solar precession p_{LS} or the planetary precession p_{PL} by π, the partial of the rotation matrix Q is

$$\frac{\partial Q}{\partial\pi} = \Omega\Big[\frac{\partial P}{\partial\pi}NU + PN\frac{\partial U}{\partial\pi}\Big]XY \tag{2.291}$$

The partials $\dfrac{\partial P}{\partial\pi}$ are very complicated, and will be written in terms of the partials of each matrix element P_{ij}:

$$\begin{aligned}\frac{1}{T}\frac{\partial P_{11}}{\partial p_{LS}} = &-\cos\bar{\varepsilon}_0\sin\zeta\cos\Theta\cos Z/2 - \sin\bar{\varepsilon}_0\cos\zeta\sin\Theta\cos Z\\ &-\cos\bar{\varepsilon}_0\cos\zeta\cos\Theta\sin Z/2 - \cos\bar{\varepsilon}_0\cos\zeta\sin Z/2\\ &-\cos\bar{\varepsilon}_0\sin\zeta\cos Z/2\end{aligned} \tag{2.292}$$

$$\begin{aligned}\frac{1}{T}\frac{\partial P_{11}}{\partial p_{PL}} = &\sin\zeta\cos\Theta\cos Z/2 + \cos\zeta\cos\Theta\sin Z/2\\ &+\cos\zeta\sin Z/2 + \sin\zeta\cos Z/2\end{aligned} \tag{2.293}$$

$$\begin{aligned}\frac{1}{T}\frac{\partial P_{12}}{\partial p_{LS}} = &-\cos\bar{\varepsilon}_0\sin\zeta\cos\Theta\sin Z/2 - \sin\bar{\varepsilon}_0\cos\zeta\sin\Theta\sin Z\\ &+\cos\bar{\varepsilon}_0\cos\zeta\cos\Theta\cos Z/2 + \cos\bar{\varepsilon}_0\cos\zeta\cos Z/2\\ &-\cos\bar{\varepsilon}_0\sin\zeta\sin Z/2\end{aligned} \tag{2.294}$$

$$\frac{1}{T}\frac{\partial P_{12}}{\partial p_{PL}} = \sin\varsigma\cos\Theta\sin Z/2 - \cos\varsigma\cos\Theta\cos Z/2 - \cos\varsigma\cos Z/2 + \sin\varsigma\sin Z/2 \tag{2.295}$$

$$\frac{1}{T}\frac{\partial P_{13}}{\partial p_{LS}} = -\cos\bar{\varepsilon}_0\sin\varsigma\sin\Theta/2 + \sin\bar{\varepsilon}_0\cos\varsigma\cos\Theta \tag{2.296}$$

$$\frac{\partial P_{13}}{\partial p_{PL}} = T\sin\varsigma\sin\Theta/2$$

$$\frac{1}{T}\frac{\partial P_{21}}{\partial p_{LS}} = -\cos\bar{\varepsilon}_0\cos\varsigma\cos\Theta\cos Z/2 + \sin\bar{\varepsilon}_0\sin\varsigma\sin\Theta\cos Z + \cos\bar{\varepsilon}_0\sin\varsigma\cos\Theta\sin Z/2 + \cos\bar{\varepsilon}_0\sin\varsigma\sin Z/2 - \cos\bar{\varepsilon}_0\cos\varsigma\cos Z/2 \tag{2.297}$$

$$\frac{1}{T}\frac{\partial P_{21}}{\partial p_{PL}} = \cos\varsigma\cos\Theta\cos Z/2 - \sin\varsigma\cos\Theta\sin Z/2 - \sin\varsigma\sin Z/2 + \cos\varsigma\cos Z/2 \tag{2.298}$$

$$\frac{1}{T}\frac{\partial P_{22}}{\partial p_{LS}} = -\cos\bar{\varepsilon}_0\cos\varsigma\cos\Theta\sin Z/2 + \sin\bar{\varepsilon}_0\sin\varsigma\sin\Theta\sin Z - \cos\bar{\varepsilon}_0\sin\varsigma\cos\Theta\cos Z/2 - \cos\bar{\varepsilon}_0\sin\varsigma\cos Z/2 - \cos\bar{\varepsilon}_0\cos\varsigma\sin Z/2 \tag{2.299}$$

$$\frac{1}{T}\frac{\partial P_{22}}{\partial p_{PL}} = \cos\varsigma\cos\Theta\sin Z/2 + \sin\varsigma\cos\Theta\cos Z/2 + \sin\varsigma\cos Z/2 + \cos\varsigma\sin Z/2 \tag{2.300}$$

$$\frac{1}{T}\frac{\partial P_{23}}{\partial p_{LS}} = -\cos\bar{\varepsilon}_0\cos\varsigma\sin\Theta/2 - \sin\bar{\varepsilon}_0\sin\varsigma\cos\Theta \tag{2.301}$$

$$\frac{\partial P_{23}}{\partial p_{PL}} = T\cos\varsigma\sin\Theta/2 \tag{2.302}$$

$$\frac{1}{T}\frac{\partial P_{31}}{\partial p_{LS}} = -\sin\bar{\varepsilon}_0\cos\Theta\cos Z + \cos\bar{\varepsilon}_0\sin\Theta\sin Z/2 \tag{2.303}$$

$$\frac{\partial P_{31}}{\partial p_{PL}} = -T\sin\Theta\sin Z/2 \tag{2.304}$$

$$\frac{1}{T}\frac{\partial P_{32}}{\partial p_{LS}} = -\sin\bar{\varepsilon}_0\cos\Theta\sin Z - \cos\bar{\varepsilon}_0\sin\Theta\cos Z/2 \tag{2.305}$$

$$\frac{\partial P_{32}}{\partial p_{PL}} = T\sin\Theta\cos Z/2 \tag{2.306}$$

$$\frac{\partial P_{33}}{\partial p_{LS}} = -T\sin\bar{\varepsilon}_0\sin\Theta \tag{2.307}$$

$$\frac{\partial P_{33}}{\partial p_{PL}} = 0 \tag{2.308}$$

A check on the algebra may be performed by noting that

$$\frac{\partial P}{\partial p_{PL}} = -T\Big[\frac{\partial P}{\partial \varsigma} + \frac{\partial P}{\partial Z}\Big]/2 \tag{2.309}$$

and

$$\frac{\partial P}{\partial p_{LS}} = -\cos\bar{\varepsilon}_0 \frac{\partial P}{\partial p_{PL}} + T\sin\bar{\varepsilon}_0 \frac{\partial P}{\partial \Theta} \tag{2.310}$$

The corresponding partials of the U matrix are much simpler:

$$\frac{\partial U}{\partial p_{LS}} = T\cos\bar{\varepsilon}_0 \begin{pmatrix} -\sin H & -\cos H & 0 \\ \cos H & -\sin H & 0 \\ 0 & 0 & 0 \end{pmatrix} \tag{2.311}$$

$$\frac{\partial U}{\partial p_{PL}} = -\left(\frac{\partial U}{\partial p_{LS}}\right) / \cos\bar{\varepsilon}_0 \tag{2.312}$$

2.9.3.4 Rotational Tweaks

Finally, the partials of the nutation matrix with respect to the "tweaks" $\Delta\psi$ and $\Delta\varepsilon$ are obtained by making the replacements (2.134) and (2.135) in N. The partials $\frac{\partial N}{\partial \Delta\psi}$ and $\frac{\partial N}{\partial \Delta\varepsilon}$ are then seen to be identical to Eqs. (2.278) and (2.279), with the same replacements for $\delta\psi$ and $\delta\varepsilon$. Expressions analogous to Eqs. (2.280-2.282) account for the shift of the equinox by nutation changes $\delta\psi$ and $\delta\varepsilon$. If the *a priori* tweaks are zero, the partials are exactly equal to the expressions (2.278) and (2.279).

For the parameters in the perturbation matrix, Ω, from (2.165-2.166):

$$\frac{\partial \Omega}{\partial \delta\Theta_{x0}} = \begin{pmatrix} 0 & 0 & 0 \\ 0 & 0 & 1 \\ 0 & -1 & 0 \end{pmatrix} \tag{2.313}$$

$$\frac{\partial \Omega}{\partial \delta\dot{\Theta}_x} = \begin{pmatrix} 0 & 0 & 0 \\ 0 & 0 & t \\ 0 & -t & 0 \end{pmatrix} \tag{2.314}$$

where t is the number of years from the reference epoch (*e.g.*, J2000). Then, by substituting these matrices for Ω in (2.98), we obtain the appropriate partials of Q for perturbations about the x axis. By analogy, the perturbation parameters about the y and z axes may also readily be obtained.

2.9.4 ADDITIVE PARAMETERS

If we seek the partials of parameters that affect only the "add-on" terms in $\tau = \tau_0 + \Delta\tau$, then from (2.177) we have:

$$\frac{\partial \tau}{\partial \eta} = \gamma(1 - \boldsymbol{\beta}\cdot\boldsymbol{\beta}_2)\frac{\partial(\Delta\tau)}{\partial \eta} \tag{2.315}$$

for terms which were "added on" in the Solar System barycenter. An example is gravitational bending:

$$\frac{\partial \tau}{\partial \gamma_{PPN}} = \gamma(1 - \boldsymbol{\beta}\cdot\boldsymbol{\beta}_2)\frac{\Delta_G}{(1+\gamma_{PPN})} \tag{2.316}$$

For terms "added on" in the geocentric frame, then:

$$\frac{\partial \tau}{\partial \eta} = \frac{\partial \Delta\tau}{\partial \eta} \tag{2.317}$$

An example is the antenna offset vector. In this case:

$$\frac{\partial \tau}{\partial(\text{offset station } \#2)} = -\left[\pm\sqrt{1 - [\hat{\mathbf{s}}\cdot\hat{\mathbf{I}}]^2}\right] \tag{2.318}$$

and

$$\frac{\partial \tau}{\partial(\text{offset station } \#1)} = \pm\sqrt{1 - [\hat{\mathbf{s}}\cdot\hat{\mathbf{I}}]^2} \tag{2.319}$$

where the choice of sign for each station is determined by the choice of sign for that station in the model portion.

SECTION 3

CLOCK MODEL

The frequency standards ("clocks") at each of the two antennas are normally independent of each other. Attempts are made to synchronize them before an experiment by conventional synchronization techniques, but these techniques are accurate to only a few μs in epoch and $\approx 10^{-12}$ in rate. More importantly, clocks often exhibit "jumps" and instabilities at a level that would greatly degrade interferometer accuracy. To account for these clock effects, an additional "delay" τ_c is included in the model delay, a delay that models the behavior of a station clock as a piecewise quadratic function of time throughout an observing session. Usually, however, we use only the linear portion of this model. For each station this clock model is given by:

$$\tau_c = \tau_{c1} + \tau_{c2}(t - t_{ref}) + \tau_{c3}(t - t_{ref})^2/2 \tag{3.1}$$

The term, t_{ref}, may be set by the user as a specific time (Julian date), or by default taken as the midpoint of the interval over which the *a priori* clock parameters, τ_{c1}, τ_{c2}, τ_{c3}, apply.

In addition to the effects of the lack of synchronization of clocks between stations, there are other differential instrumental effects which may contribute to the observed delay. In general, it is adequate to model these effects as if they were "clocklike". However, the instrumental effects on delays measured using the multifrequency bandwidth synthesis technique (Thomas, 1981) may be different from the instrumental effects on delays obtained from phase measurements at a single frequency.

The bandwidth synthesis process obtains group delay from the slope of phase versus frequency $\left(\tau = \frac{\partial \phi}{\partial \nu}\right)$ across multiple frequency segments spanning the receiver passband. Thus, any frequency-independent instrumental contribution to the measured interferometer phase has no effect on the delay determined by the bandwidth synthesis technique. However, if delay is obtained directly from the phase measurement, ϕ, at a given frequency, ν, then this derived phase delay $\left(\tau_{pd} = \frac{\phi}{\nu}\right)$ does have that instrumental contribution.

Because of this difference, it is necessary to augment the "clock" model for phase delay measurements:

$$\tau_{c_{pd}} = \tau_c + \tau_{c4}(t - t_{ref}) + \tau_{c5}(t - t_{ref})^2/2 \tag{3.2}$$

where τ_c is the clock model for bandwidth synthesis observations and is defined in (3.1). Since the present system measures both bandwidth synthesis delay and phase delay rate, all of the clock parameters described above must be used. However, in a "perfectly" calibrated interferometer, $\tau_{c4} = \tau_{c5} = 0$. This particular model implementation allows simultaneous use of delay rate data derived from phase delay, with delay data derived by means of the bandwidth synthesis technique. However, our particular software implementation currently is inconsistent with the simultaneous use of delay derived from bandwidth synthesis and delay obtained from phase delay measurements.

An optional refinement of the clock model is also available. For dual-frequency (S/X) delays, an additional clock offset may be estimated. It originates from the differential instrumental delay and fringe fitting delays for S- and X-band data, which may be sizeable. For dual-frequency observables, the clock model depends on this differential instrumental delay and on the frequencies ω_S, ω_X in the individual bands as

$$\tau_{c6}\ \omega_X^2/(\omega_X^2 - \omega_S^2) \tag{3.3}$$

The differential instrumental delay τ_{c6} is normally highly correlated with the usual clock offset τ_{c1}, but under some circumstances may convey additional information.

To model the interferometer delay on a given baseline, a difference of station clock terms is formed:

$$\tau_c = \tau_{c_{\text{station 2}}} - \tau_{c_{\text{station 1}}} \tag{3.4}$$

Specification of a reference clock is unnecessary until the parameter adjustment step, and need not concern us in the description of the model.

The partial derivatives of model delay with respect to the set of six parameters ($\tau_{c1}, \tau_{c2}, \tau_{c3}, \tau_{c4}, \tau_{c5}$, and τ_{c6}) for each station are so trivial as to need no further explanation.

SECTION 4

TROPOSPHERE MODEL

In order to reach each antenna, the radio wave front must pass through the Earth's atmosphere. This atmosphere is made up of two components: the neutral atmosphere and the ionosphere. In turn, the neutral atmosphere is composed of two major constituents: the dry and the wet. The dry portion, primarily oxygen and nitrogen, is very nearly in hydrostatic equilibrium, and its effects can be accurately estimated simply by measuring the barometric pressure. Typically, at sea level in the local zenith direction, the additional delay that the incoming signal experiences due to the troposphere is approximately 2 meters. Except for winds aloft, unusually strong lee waves behind mountains (*e.g.*, Owens Valley, California), or very high pressure gradients, an azimuthally symmetric model based on measurements of surface barometric pressure is considered adequate. We have not yet investigated where this assumption breaks down, though "back-of-the-envelope" calculations indicate that, except in the unusual cases above, the error in such an assumption causes a less than 1-cm error in the baseline.

Unfortunately, the wet component of the atmosphere (both water vapor and condensed water in the form of clouds) is not so easily modeled. The experimental evidence (Resch, 1983) is that it is "clumpy", and not azimuthally symmetric about the local vertical at a level which can cause many centimeters of error in a baseline measurement. Furthermore, because of incomplete mixing, surface measurements are inadequate in estimating this contribution which even at zenith can reach 20 to 30 cm. Ideally, this tropospheric induced delay should be determined experimentally at each site. This is particularly true for short and intermediate (B < 1000 km) baselines, where the elevation angles of the two antennas are highly correlated in the observations. For long baselines, both the independence of the elevation angles at the two antennas, and the fact that often the mutual visibility requirements of VLBI constrain the antennas to look only in certain azimuthal sectors, allow the use of the interferometer data itself to estimate the effect of the water vapor as part of the parameter estimation process. For this reason, and because state-of-the-art water-vapor measurements are not always available, we also have the capability to model the neutral atmosphere at each station as a two-component effect, with each component being an azimuthally symmetric function of the local geodetic elevation angle.

At each station the delay experienced by the incoming signal due to the troposphere can be modeled using a spherical-shell troposphere consisting of a wet component and a dry component:

$$\tau_{trop\ station\ i} = \tau_{wet\ trop} + \tau_{dry\ trop} \tag{4.1}$$

The total troposphere model for a given baseline is then:

$$\tau_t = \tau_{trop\ station\ 2} - \tau_{trop\ station\ 1} \tag{4.2}$$

If E_i is the apparent geodetic elevation angle of the observed source at station i, we have (dropping the subscript i):

$$\tau_{trop} = \rho z_{dry} R_{dry}(E) + \rho z_{wet} R_{wet}(E) \tag{4.3}$$

where ρz is the additional delay at local zenith due to the presence of the troposphere, and R is an elevation angle mapping function.

For some geodetic experiments, the observed delay has been corrected for the total tropospheric delays at the two stations, which are in turn calculated on the basis of surface pressure measurements for the dry component, and water-vapor radiometer measurements for the wet component. This correction is recorded in the input data stream in such a way that it can be replaced by a new model. In the absence of such external calibrations, it was found that modeling the zenith delay as a linear function of time improves troposphere modeling considerably. The dry and wet zenith parameters are written as

$$\rho z_{d,w} = \rho^0_{z_{d,w}} + \dot{\rho} z_{d,w}(t - t_0) \tag{4.4}$$

where t_0 is a reference time.

Since the model is linear in the parameters ρ^0 and $\dot{\rho}$, the partial derivatives with respect to zenith delays and rates are trivial. They are:

$$\frac{\partial \tau}{\partial \rho^0_{Z_{i\,d\ or\ w}}} = f(i) R_{i\,d\ or\ w} \tag{4.5}$$

and

$$\frac{\partial \tau}{\partial \dot{\rho} z_{i\,d\ or\ w}} = (t - t_0) f(i) R_{i\,d\ or\ w} \tag{4.6}$$

where $f(i) = 1$ for station #2, and -1 for station #1.

4.1 CHAO MAPPING FUNCTION

The simplest mapping function implemented in MODEST code is that obtained by C. C. Chao (1974) through analytic fits to ray tracing, a function which he claims is accurate to the level of 1% at 6° elevation angle and becomes much more accurate at higher elevation angles.

$$R = \frac{1}{\sin E + \dfrac{A}{\tan E + B}} \tag{4.7}$$

where

$$A_{dry} = 0.00143 \tag{4.8}$$
$$B_{dry} = 0.0445 \tag{4.9}$$
$$A_{wet} = 0.00035 \tag{4.10}$$
$$B_{wet} = 0.017 \tag{4.11}$$

The user must specify values for the zenith delays.

The partial derivatives of delay with respect to the parameters A_{dry} and B_{dry} are:

$$\frac{\partial \tau}{\partial A_{dry}} = -f(i) \rho_{Z_{dry}} R^2_{dry} / (\tan E + B_{dry}) \tag{4.12}$$

and

$$\frac{\partial \tau}{\partial B_{dry}} = f(i) \rho_{Z_{dry}} R^2_{dry} A_{dry} / (\tan E + B_{dry})^2 \tag{4.13}$$

where R_{dry} is the Chao mapping function, and E is the elevation angle.

4.2 LANYI MAPPING FUNCTION

Analyses of intercontinental data indicate that the Chao mapping function [Eq. (4.7)] is inadequate. To rectify this situation, two modifications have been made to the MODEST code. First, the dry-troposphere mapping parameters A_{dry} and B_{dry} of the Chao mapping function R_{dry} have been promoted to the status of estimable parameters. Second, the code now permits the use of two more accurate mapping functions. The first of these is the analytic function developed by Lanyi (1984). In its simplest form, this mapping function employs average values of atmospheric constants. Provision is made for specifying surface meteorological data acquired at the time of the VLBI experiments, which may override the average values. Using numerical fits to ray-tracing results, Davis *et al.* (1985) have arrived at another function, designated the CfA-2.2 mapping function. Comparisons indicate that the Lanyi and CfA functions are in agreement to better than 1 cm over an extreme range of atmospheric conditions down to 6° elevation angles. Finally, an approximate partial derivative is obtained with

respect to one parameter in the Lanyi mapping function; this permits adjustment even in the absence of surface data. The Lanyi function was made the default MODEST troposphere model in early 1986.

Motivation for and full details of the development of a new tropospheric mapping function are given by Lanyi (1984). Here we attempt to give a minimal summary of the final formulas. The tropospheric delay is written as:

$$\tau_{trop} = F(E)/\sin E \tag{4.14}$$

where

$$\begin{aligned} F(E) = {} & \rho_{Z_{dry}} F_{dry}(E) + \rho_{Z_{wet}} F_{wet}(E) \\ & + [\rho^2_{Z_{dry}} F_{b1}(E) + 2\rho_{Z_{dry}}\rho_{Z_{wet}} F_{b2}(E) + \rho^2_{Z_{wet}} F_{b3}(E)]/\Delta + \rho^3_{Z_{dry}} F_{b4}(E)/\Delta^2 \end{aligned} \tag{4.15}$$

The quantities $\rho_{Z_{dry}}$ and $\rho_{Z_{wet}}$ have the usual meaning: zenith dry and wet tropospheric delays. Δ is the atmospheric scale height, $\Delta = kT_0/mg_c$, k = Boltzmann's constant, T_0 = average surface temperature, m = mean molecular mass of dry air, and g_c = gravitational acceleration at the center of gravity of the air column. With the standard values $k = 1.38066 \times 10^{-16}$ erg/K, $m = 4.8097 \times 10^{-23}$ g, $g_c = 978.37$ cm/s^2, and the average temperature for DSN stations $T_0 = 292$ K, the scale height $\Delta = 8567$ m.

The dry, wet, and bending contributions to the delay, $F_{dry}(E)$, $F_{wet}(E)$, and $F_{b1,b2,b3,b4}(E)$, are expressed in terms of moments of the refractivity as

$$F_{dry}(E) = A_{10}(E) G(\lambda M_{110}, u) + 3\sigma u M_{210} G^3(M_{110}, u)/2 \tag{4.16}$$

$$F_{wet}(E) = A_{01}(E) G(\lambda M_{101}/M_{001}, u)/M_{001} \tag{4.17}$$

$$F_{b1}(E) = [\sigma G^3(M_{110}, u)/\sin^2 E - M_{020} G^3(M_{120}/M_{020}, u)]/2\tan^2 E \tag{4.18}$$

$$F_{b2}(E) = -M_{011} G^3(M_{111}/M_{011}, u)/2M_{001}\tan^2 E \tag{4.19}$$

$$F_{b3}(E) = -M_{002} G^3(M_{102}/M_{002}, u)/2M^2_{001}\tan^2 E \tag{4.20}$$

$$F_{b4}(E) = M_{030} G^3(M_{130}/M_{030}, u)/\tan^4 E \tag{4.21}$$

A misprinted sign in the last of Eqs. (5) of Appendix B of Lanyi (1984) has been corrected in Eq. (4.21). Here $G(q,u)$ is a geometric factor given by

$$G(q, u) = (1 + qu)^{-1/2} \tag{4.22}$$

with

$$u = 2\sigma/\tan^2 E \tag{4.23}$$

where $\sigma = \Delta/R$ is a measure of the curvature of the Earth's surface with standard value 0.001345.

The quantities $A_{lm}(E)$ and M_{ilm} are related to moments of the atmospheric refractivity, and are defined below. $A_{10}(E)$ involves the dry refractivity, while $A_{01}(E)$ is the corresponding wet quantity. The $A_{lm}(E)$ are given by

$$A_{lm}(E) = M_{0lm} + \sum_{n=1}^{10}\sum_{k=0}^{n} \frac{(-1)^{n+k}(2n-1)!!\, M_{n-k,l,m}}{2^n k!(n-k)!} \left[\frac{u}{1 + \lambda u M_{1lm}/M_{0lm}}\right]^n \left[\frac{\lambda M_{1lm}}{M_{0lm}}\right]^k \tag{4.24}$$

with the scale factor $\lambda = 3$ for $E < 10°$ and $\lambda = 1$ for $E > 10°$. Only the two combinations $(l, m) = (0,1)$ and $(1,0)$ are needed for the $A_{lm}(E)$. The moments of the dry and wet refractivities are defined as

$$M_{nij} = \int_0^\infty dq\; q^n f^i_{dry}(q) f^j_{wet}(q) \tag{4.25}$$

where $f_{dry,\,wet}(q)$ are the surface-normalized refractivities. Here, n ranges from 0 to 10, i from 0 to 3, and j from 0 to 2; not all combinations are needed. Carrying out the integration in Eq. (4.25) for a three-section temperature profile gives an expression for the general moment M_{nij}:

$$\begin{aligned} M_{nij}/n! = {} & (1 - e^{-aq_1})/a^{n+1} + e^{-aq_1}\left[1 - T_2^{b+n+1}(q_1, q_2)\right] \prod_{i=0}^{n} \frac{\alpha}{b+i+1} \\ & + e^{-aq_1} T_2^{b+n+1}(q_1, q_2)/a^{n+1} \end{aligned} \tag{4.26}$$

Here,

$$T_2(q_1, q_2) = 1 - (q_2 - q_1)/\alpha \tag{4.27}$$

The quantities q_1 and q_2 are the scale-height normalized inversion and tropopause altitudes, respectively. For the standard atmospheric model, $q_1 = 0.1459$ and $q_2 = 1.424$. The constants a and b are functions of the dry ($\alpha = 5.0$) and wet ($\beta = 3.5$) model parameters, as well as of the powers of the refractivities (i and j) in the moment definitions. Table IX gives the necessary a's and b's.

Table IX

Dependence of the Constants a and b
on Tropospheric Model Parameters

i	j	a	b
1	0	1	$\alpha - 1$
0	1	β	$\alpha\beta - 2$
2	0	2	$2(\alpha - 1)$
1	1	$\beta + 1$	$\beta(\alpha + 1) - 3$
0	2	2β	$2(\alpha\beta - 2)$
3	0	3	$3(\alpha - 1)$

Note that the normalization is such that $M_{010} = 1$; this moment has therefore not been explicitly written in Eqs. (4.16) through (4.21).

At present, provision is made for input of four meteorological parameters to override the default (average) values of the Lanyi model. These are: 1) the surface temperature T_0, which determines the atmosphere scale height; 2) the temperature lapse rate W, which determines the dry model parameter α; 3) the inversion altitude h_1, which determines q_1; and 4) the tropopause altitude h_2, which determines q_2. A fifth parameter, the surface pressure p_0, is not used at present. Table X summarizes the four parameters and derived quantities, and their default values. Approximate sensitivities of the tropospheric delay (at 6° elevation) to the meteorological parameters are given in the last column.

Table X

Surface Meteorological Parameters in the Lanyi Mapping Function

Parameter	Default	Derived parameter and value	Sensitivity (6°)
T_0	292 K	$\Delta = kT_0/mg_c = 8.567$ km	−7 mm/K
W	6.8165 K/km	$\alpha = 100T_0/W\Delta = 5.0$	20 mm/K/km
h_1	1.25 km	$q_1 = h_1/\Delta = 0.1459$	−20 mm/km
h_2	12.2 km	$q_2 = h_2/\Delta = 1.424$	5 mm/km

Partials of the delay with respect to the dry and wet zenith delays are obtained from Eqs. (4.14) and (4.15):

$$\frac{\partial \tau}{\partial \rho z_{dry}} = f(i)\left[F_{dry}(E) + 2\rho z_{dry} F_{b1}(E)/\Delta\right]/\sin E + \left[2\rho z_{wet} F_{b2}(E)/\Delta + 3\rho_{z_{dry}}^2 F_{b4}(E)/\Delta^2\right]/\sin E \tag{4.28}$$

$$\frac{\partial \tau}{\partial \rho z_{wet}} = f(i)\left[F_{wet}(E) + 2\rho z_{dry} F_{b2}(E)/\Delta + 2\rho z_{wet} F_{b3}(E)/\Delta\right]/\sin E \tag{4.29}$$

In analysis of data for which meteorological parameters are not available, it is convenient to introduce an approximation into the mapping function [Eqs. (4.14) and (4.15)] which involves a one-parameter estimate. This parameter p accounts for deviations from standard meteorological conditions. The tropospheric delay is expressed as

$$\tau_{trop} = (\rho z_{dry} + \rho z_{wet})/\sin E + p\frac{\partial \tau_{trop}}{\partial p} \tag{4.30}$$

where the partial derivative is

$$\frac{\partial \tau_{trop}}{\partial p} = -\frac{(\rho z_{dry} + \rho z_{wet}) u M_{110}}{G(M_{110}, u)\left[1 + G(M_{110}, u)\right]\sin E} + \frac{\rho z_{wet} u (M_{110} - M_{101}/M_{001})}{G(M_{110}, u) G(M_{101}/M_{001}, u)\left[G(M_{110}, u) + G(M_{101}/M_{001}, u)\right]\sin E} \tag{4.31}$$

4.3 CfA MAPPING FUNCTION

Another approach to improved modeling of tropospheric delay was published by Davis *et al.* (1985). Analytic fits to ray-tracing results yield the CfA-2.2 mapping function

$$R = \cfrac{1}{\sin E + \cfrac{a}{\tan E + \cfrac{b}{\sin E + c}}} \tag{4.32}$$

where E is the elevation angle. The three parameters a, b, c are expressed in terms of meteorological data as

$$a = 0.0002723\ (\ 1 + 2.642 \times 10^{-4} p_0 - 6.400 \times 10^{-4} e_0 + 1.337 \times 10^{-2} T_0 - 8.550 \times 10^{-2}\alpha - 2.456 \times 10^{-2} h_2\ ) \tag{4.33}$$

$$b = 0.0004703\ (\ 1 + 2.832 \times 10^{-5} p_0 + 6.799 \times 10^{-4} e_0 + 7.563 \times 10^{-3} T_0 - 7.390 \times 10^{-2}\alpha - 2.961 \times 10^{-2} h_2\ ) \tag{4.34}$$

$$c = -0.0090 \tag{4.35}$$

Here, p_0 is the surface pressure and e_0 the surface partial water vapor pressure, both measured in millibars. The quantities T_0, α, and h_2 have the same meaning and units as in Section 4.2. This function is one of five optional mapping functions in the MODEST model. In connection with testing parameter estimation for the Lanyi function, the partial derivative of delay with respect to surface temperature T_0 in the CfA-2.2 function was also evaluated. It is

$$\frac{\partial \tau}{\partial T_0} = -\frac{\rho z_{dry} R_{dry}^2 \left[3.641 \times 10^{-6}(\sin E + c)\left[\tan E + b/(\sin E + c)\right] - 3.557 \times 10^{-6} a\right]}{(\sin E + c)\left[\tan E + b/(\sin E + c)\right]^2} \tag{4.36}$$

4.4 HERRING 1992 (MTT) MAPPING FUNCTION

A further refinement of the CfA approach by Herring (1992) has yielded the following mapping functions for the dry and wet tropospheric delays, respectively:

$$R_{dry,wet} = \frac{1 + \dfrac{a_{dry,wet}}{1 + \dfrac{b_{dry,wet}}{1 + c_{dry,wet}}}}{\sin E + \dfrac{a_{dry,wet}}{\sin E + \dfrac{b_{dry,wet}}{\sin E + c_{dry,wet}}}} \tag{4.37}$$

The parameters $(a, b, c)_{dry,wet}$ depend on the site latitude (ϕ), altitude (H, km), and surface temperature (T_0, K) via

$$a_{dry} = 0.0006232\ (\ 1 + 0.02230\cos\phi - 0.03354H + 0.003450T_0\ ) \tag{4.38}$$
$$b_{dry} = 0.0025779\ (\ 1 - 0.06207\cos\phi - 0.01284H + 0.000799T_0\ ) \tag{4.39}$$
$$c_{dry} = 0.071839\ (\ 1 - 0.05976\cos\phi - 0.00207H - 0.000029T_0\ ) \tag{4.40}$$

$$a_{wet} = 0.000187\ (\ 1 - 0.0590\cos\phi - 0.2787H + 0.00750T_0\ ) \tag{4.41}$$
$$b_{wet} = 0.000836\ (\ 1 - 0.1221\cos\phi - 0.1209H + 0.00239T_0\ ) \tag{4.42}$$
$$c_{wet} = 0.04160\ (\ 1 - 0.0459\cos\phi - 0.0310H + 0.00036T_0\ ) \tag{4.43}$$

This function is becoming known in the literature as the "MTT" function.

4.5 NIELL MAPPING FUNCTION

Two new mapping functions (wet and dry) which use no surface meteorological data have recently been introduced by Niell (1994). They take the same continued fraction form as the Herring functions above (4.37). The parameters $(a, b, c)_{dry,wet}$ have a more complicated latitude and seasonal dependence, and there is also a (dry only) altitude correction. For latitudes within 15° of the poles, the parameters are constant, while in mid-latitudes they vary both with latitude and day of year (with proper adjustments for the reversal of seasons in the Southern Hemisphere). The altitude correction is proportional to altitude, and has an elevation dependence similar to that of (4.37). Because of the complicated functional dependences and numerous coefficients, the Niell mapping functions are not presented here. They are, however, one of the options in MODEST.

4.6 ANTENNA AXIS OFFSET ALTITUDE CORRECTION

Antennas with non-zero axis offsets, whose second rotation axis (A in Figure 5) moves vertically with changing orientation, have zenith troposphere delays that may vary by 1 to 2 mm. Equatorial and X-Y mounts fall in this class (see Figure 6). At low elevation angles this zenith variation is magnified by the mapping function to 1-2 cm. These variations must be modeled in experiments whose accuracies are at the millimeter level (*e.g.* short-baseline phase delay measurements). Memoranda by Jacobs (1988, 1991) derive the corrections based on considering only the dry troposphere component, and include all terms necessary to achieve an accuracy of a few millimeters. The correction to be added to the zenith dry tropospheric delay is

$$\delta\tau = -\rho_{Z_{dry}}(H/\Delta)\ \psi \tag{4.44}$$

where H is the antenna axis offset, Δ the dry troposphere scale height ($\approx$ 8.6 km), and ψ is an angular factor that varies with the type of mount. For equatorial mounts,

$$\psi = \cos\phi\cos h \tag{4.45}$$

where ϕ is the geodetic latitude and h the local hour angle east of the meridian. The Richmond antenna correction has this form with ϕ replaced by ϕ_W and h by a pseudo-hour angle h_R (see Section 2.8.3), where

$$h_R = \arctan\left[\cos E \sin(\theta - \epsilon)/\left[\cos\phi_W \sin E - \sin\phi_W \cos E \cos(\theta + \epsilon)\right]\right] \tag{4.46}$$

For north-south oriented X-Y mounts,

$$\psi = \sin E/(1 - \cos^2\theta \cos^2 E)^{1/2} \tag{4.47}$$

where E is the elevation angle and θ the azimuth (E of N). Finally, for east-west oriented X-Y mounts,

$$\psi = \sin E/(1 - \sin^2\theta \cos^2 E)^{1/2} \tag{4.48}$$

4.7 OBSERVATION CORRELATIONS VIA THE TROPOSPHERE

An alternative description of the effects of the turbulent non-hydrostatic part of the troposphere is obtained by introducing correlations between observations into the least-squares formalism. The mathematical details of this method will be described by Branson (1994). It is based on the paper of Treuhaft and Lanyi (1987), as implemented by Edwards (1988). A future revision of this document will include a summary of the model for tropospheric correlations. For the present, Table XI gives the default values of the Treuhaft-Lanyi parameters that are used in MODEST. It should be emphasized that the present MODEST code is only capable of treating single-baseline observing sessions.

Table XI

Troposphere Turbulence Parameters

Parameter	Symbol	Value
Scale factor	C	1.7×10^{-7} m$^{-1/3}$
Wind speed	v	8 m/s
Wind direction	...	East
Wet troposphere scale height	h	2 km
Decorrelation length	L	3000 km

SECTION 5

IONOSPHERE MODEL

The second component of the Earth's atmosphere, the ionosphere, is a layer of plasma at about 350 km altitude, created primarily by the ultraviolet portion of the sunlight. In the quasi-longitudinal approximation (Spitzer, 1962) the refractive index of this medium is

$$n = \left[1 - \left(\frac{\nu_p}{\nu}\right)^2 \left(1 \pm \frac{\nu_g}{\nu} \cos\Theta\right)^{-1}\right]^{1/2} \tag{5.1}$$

where the plasma frequency, ν_p, is

$$\nu_p = \left(\rho c^2 r_0/\pi\right)^{1/2} \approx 8.97 \times 10^3 \rho^{1/2} \tag{5.2}$$

the electron gyrofrequency, ν_g, is

$$\nu_g = \frac{eB}{2\pi mc} \tag{5.3}$$

and Θ is the angle between the magnetic field B and the direction of propagation of the wave front. Here ρ is the number density of the electrons, e and m are the electron charge and mass, r_0 is the classical electron radius, and c is the speed of light.

Tables XII and XIII give the plasma, ν_p, and gyro frequencies, ν_g, for the three regimes of a radio signal's ray path: Earth, interplanetary, and interstellar space. Given the S-band ($\nu_S = 2.3$ GHz) and X-band ($\nu_X = 8.4$ GHz) frequencies typically used for geodetic and astrometric VLBI, the importance of correcting for plasma and gyrofrequency can be parameterized by the ratios of ν_p and ν_g to ν_S and to ν_X respectively.

Table XII

Plasma Effects

Plasma	ρ (e/m^3)	ν_p (kHz)	(ν_p/ν_S)	(ν_p/ν_X)
Earth's ionosphere	10^{12}	8900	4×10^{-3}	10^{-3}
Interplanetary	$10^7 - 10^8$	28-89	4×10^{-5}	10^{-5}
Interstellar	10^5	3	1.2×10^{-6}	3×10^{-7}

Table XIII

Electron Gyrofrequency Effects

Magnetic field	B (gauss)	ν_g (kHz)	(ν_g/ν_S)	(ν_g/ν_X)
Earth	0.2	600	3×10^{-4}	7.5×10^{-5}
Interplanetary	10^{-4}	0.3	1.5×10^{-7}	3.2×10^{-8}
Interstellar	10^{-6}	0.003	1.5×10^{-9}	3.2×10^{-10}

Relative to vacuum as a reference, the phase delay of a monochromatic signal transiting this medium of refractive index n is

$$\tau_{pd} = \frac{1}{c}\int (n-1)dl \approx -\frac{1}{2c}\int \left(\frac{\nu_p'}{\nu}\right)^2 \left[1 + \frac{1}{4}\left(\frac{\nu_p'}{\nu}\right)^2 + \frac{1}{8}\left(\frac{\nu_p'}{\nu}\right)^3 + ...\right]dl \tag{5.4}$$

where

$$\frac{\nu_p'}{\nu} = \left(\frac{\nu_p}{\nu}\right)\left[1 \pm \left(\frac{\nu_g}{\nu}\right)\cos\Theta\right]^{-1/2} \tag{5.5}$$

For 8.4 GHz, we may approximate this effect to parts in $10^6 - 10^7$ by:

$$\Delta_{pd} \approx \frac{-q}{\nu^2}\left[1 \pm \overline{\left(\frac{\nu_g}{\nu}\right)\cos\Theta}\right]^{-1} \approx \frac{-q}{\nu^2}\left[1 - \overline{\left(\frac{\pm\nu_g}{\nu}\right)\cos\Theta}\right] \tag{5.6}$$

where

$$q = \frac{cr_0}{2\pi}\int \rho dl = \frac{cr_0 I_e}{2\pi} \tag{5.7}$$

and where I_e is the total number of electrons per unit area along the integrated line of sight. The bar symbolizes a geometrical average. If we also neglect the term $\overline{(\nu_g \cos\Theta)}/\nu$, then the expression for Δ_{pd} becomes simple and independent of the geometry of the traversal of the wave front through the ionosphere:

$$\Delta_{pd} = -q/\nu^2 \tag{5.8}$$

This delay is negative. Thus, a phase advance actually occurs for a monochromatic signal. Since phase delay is obtained at a single frequency, observables derived from phase delay (*e.g.*, phase delay rates) experience an increment which is negative (the observable with the medium present is smaller than it would be without the medium). In contrast, group delays measured by a technique such as bandwidth synthesis $\left(\tau = \frac{\partial\phi}{\partial\nu}\right)$ experience an additive delay which can be derived from (5.8) by differentiating $\phi = \nu\Delta_{pd}$ with respect to frequency:

$$\Delta_{gd} = q/\nu^2 \tag{5.9}$$

Notice that the sign is now positive, though the group delay is of the same magnitude as the phase delay advance. For group delay measurements, the measured delay is larger with the medium present than without the medium.

For a typical ionosphere, $\tau \approx 1$ to 20×10^{-10} s at local zenith for $\nu = 8.4$ GHz. This effect has a maximum at approximately 1400 hours local time and a broad minimum during local night. For long baselines, the effects at each station are quite different. Thus, the differential effect may be of the same order as the maximum.

For the interplanetary medium and at an observing frequency of 8.4 GHz, a single ray path experiences a delay of approximately 6×10^{-7} s in transiting the Solar System. However, the differential between the ray paths to the two stations on the Earth is considerably less, since the gradient between the two ray paths should also be inversely proportional to the dimensions of the plasma region (*e.g.*, one astronomical unit as opposed to a few thousand kilometers). The ray path from a source at a distance of 1 megaparsec (3×10^7 km) experiences an integrated plasma delay of approximately 5000 seconds for a frequency of 8.4 GHz. In this case, however, the typical dimension is also that much greater, and so the differential effect on two ray paths separated by one Earth radius is still not as great as the differential delays caused by the Earth's ionosphere.

5.1 DUAL-FREQUENCY CALIBRATION

These plasma effects can best be removed by the technique of observing the sources at two frequencies, ν_1 and ν_2, where $\nu_{1,2} \gg \nu_p$ and where $|\nu_2 - \nu_1|/(\nu_2 + \nu_1) \approx 1$. Then at the two frequencies ν_1 and ν_2 we obtain

$$\tau_{\nu 1} = \tau + q/\nu_1^2 \tag{5.10}$$

and

$$\tau_{\nu 2} = \tau + q/\nu_2^2 \tag{5.11}$$

Multiplying each expression by the square of the frequency involved and subtracting, we obtain

$$\tau = a\tau_{\nu 2} + b\tau_{\nu 1} \tag{5.12}$$

where

$$a = \frac{\nu_2^2}{\nu_2^2 - \nu_1^2} \tag{5.13}$$

and

$$b = \frac{-\nu_1^2}{\nu_2^2 - \nu_1^2} \tag{5.14}$$

This linear combination of the observables at two frequencies thus removes the charged particle contribution to the delay.

For uncorrelated errors in the frequency windows, the overall error in the derived delay can be modeled as

$$\sigma_\tau^2 = a^2\sigma_{\tau_{\nu 2}}^2 + b^2\sigma_{\tau_{\nu 1}}^2 \tag{5.15}$$

Modeling of other error types is more difficult and will not be treated in this report. Since the values of a and b are independent of q, these same coefficients apply both to group delay and to phase delay.

If we had not neglected the effect of the electron gyrofrequency in the ionosphere, then instead of (5.12) above, we would have obtained

$$\tau = a\tau_{\nu 2} + b\tau_{\nu 1} + \frac{q\,\overline{\nu_g \cos\Theta}}{\nu_2\nu_1(\nu_2 - \nu_1)} \tag{5.16}$$

where a and b are defined as in (5.13) and (5.14), respectively.

If we express the third term on the right-hand side in units of the contribution of the ionosphere at frequency ν_2, we obtain

$$\tau = a\tau_{\nu 2} + b\tau_{\nu 1} + \frac{\Delta_{pd}\nu_2\,\overline{\nu_g \cos\Theta}}{\nu_1(\nu_2 + \nu_1)} \tag{5.17}$$

For X band $\Delta_{pd} \approx 1$ to 20 $\times 10^{-10}$ s at the zenith. When using S band as the other frequency in the pair, this third term is $\approx 2 \times 10^{-4}\Delta_{pd}\cos\Theta \approx 2$ to 40 $\times 10^{-13}$ s at zenith. In the worst case of high ionospheric electron content, and at low elevation angles, this effect could reach 0.1 cm of total error in determining the total delay using the simple formula (5.12) above. Notice that the effect becomes much more significant at lower frequencies.

In the software chain used at the Jet Propulsion Laboratory, the dual-frequency correction is performed prior to the processing step "MODEST" (Lowe, 1992). MODEST does not have the facility to perform this correction. However, the process is described here because it is important to understanding the data input to MODEST. For millimeter accuracy, or for lower observing frequencies even at centimeter accuracy levels, a correction for the gyrofrequency effect is necessary.

5.2 TOTAL ELECTRON CONTENT

In the absence of the dual-frequency observation capability described above, one can improve the model of the interferometer by modeling the ionosphere, using whatever measurements of the total electron content are available. The model we have chosen to implement is very simple. Its formalism is similar to that of the troposphere model, except that the ionosphere is modeled as a spherical shell for which the bottom is at the height h_1, above the geodetic surface of the Earth, and the top of the shell is at the height h_2, above that same surface (see Figure 7). For each station the ionospheric delay is modeled as

$$\tau_i = kgI_eS(E)/\nu^2 \tag{5.18}$$

where

$$k = \frac{0.1 c r_0}{2\pi} \tag{5.19}$$

I_e is the total electron content at zenith (in electrons per meter squared $\times 10^{-17}$), and $g = 1(-1)$ for group (phase) delay. E is the apparent geodetic elevation angle of the source, $S(E)$ is a slant range factor discussed below, and ν is the observing frequency in gigahertz.

The slant range factor (see Figure 7) is

$$S(E) = \frac{\sqrt{R^2 \sin^2 E + 2Rh_2 + h_2^2} - \sqrt{R^2 \sin^2 E + 2Rh_1 + h_1^2}}{h_2 - h_1} \tag{5.20}$$

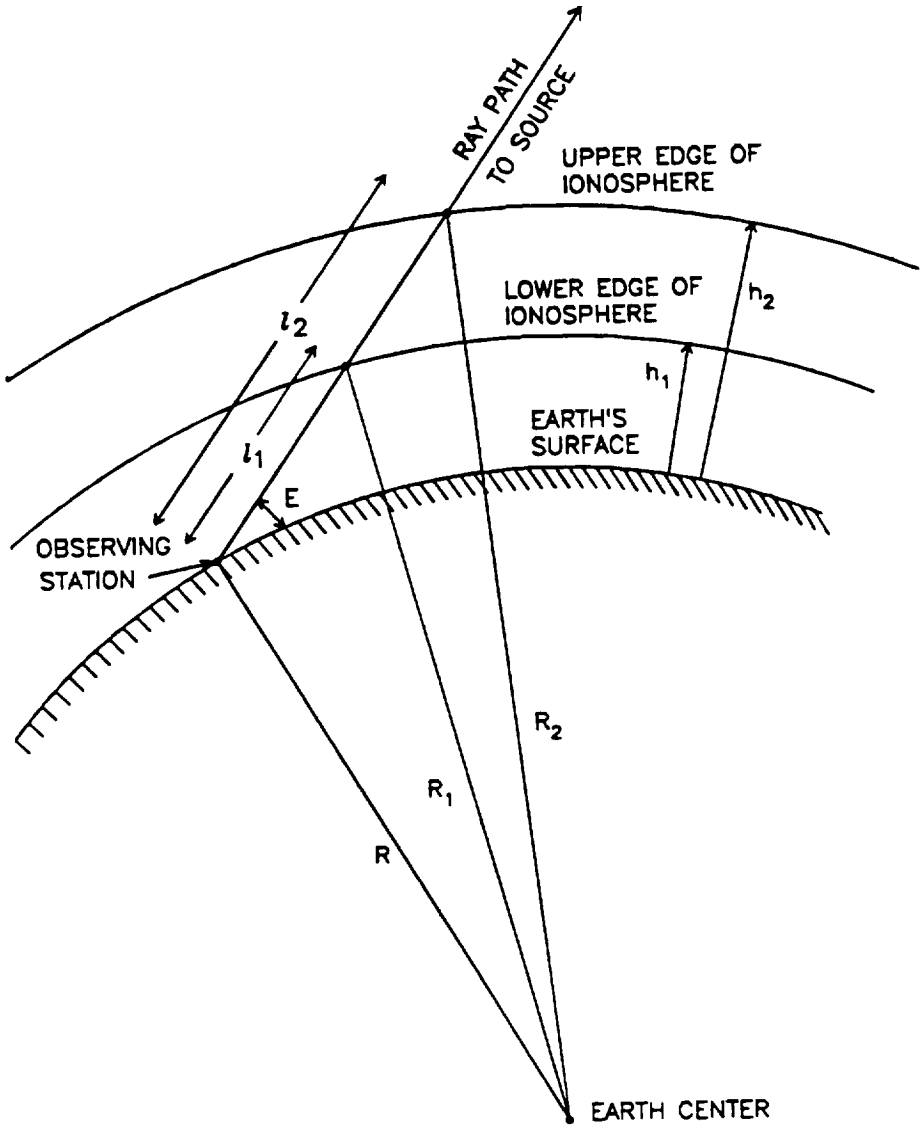

Figure 7. The geometry of the spherical ionospheric shell used for ionospheric corrections

This expression is strictly correct for a spherical Earth of radius R, and a source at apparent elevation angle E. The model employed uses this expression, with the local radius of curvature of the geoid surface at the receiving station R taken to be equal to the distance from the station to the center of

the Earth. The model also assumes this same value of R can be used at the ionospheric penetration points, *e.g.*:

$$R_i = R + h_i \tag{5.21}$$

This is not strictly true, but is a very close approximation, particularly compared to the crude nature of the total electron content determinations on which the model also depends. The total ionospheric contribution on a given baseline is

$$\tau_I = \tau_{i_{station\ 2}} - \tau_{i_{station\ 1}} \tag{5.22}$$

We assume that the ionospheric total electron content, I_e, is the sum of two parts, one obtained by some external set of measurements such as Faraday rotation or GPS techniques, and the other by some specified additive constant:

$$I_e = I_{e\ meas} + I_{e\ add} \tag{5.23}$$

These external measurements, in general, are not along directions in the ionosphere coincident with the ray paths to the interferometer. Thus, for each antenna, it is necessary to map a measurement made along one ray path to the ray paths used by the interferometer. Many different techniques to do this mapping have been suggested and tried; all of them are of dubious accuracy. In the light of these problems, and in the anticipation that dual-frequency observations will be employed for the most accurate interferometric work, we have implemented only a simple hour-angle mapping of the time history of the measurements of I_e at a given latitude and longitude to the point of interest. In this model we allow the user to adjust the "height", h, of the ionosphere, but require

$$\begin{aligned} h_1 &= h - 35 \text{ km} \\ h_2 &= h + 70 \text{ km} \end{aligned} \tag{5.24}$$

Nominally, this "height" is taken to be 350 km. Setting this height to zero causes the program to ignore the ionosphere model, as is required if dual-frequency observations have already been used to remove the plasma effects. As in the troposphere model, these corrections can also be incorporated into the input data stream. Then the user is free to accept the passed correction, and use this model as a small alteration of the previously invoked model, or to remove the passed corrections.

The deficiencies of these ionosphere models for single-frequency observations are compounded by the lens effect of the solar plasma. In effect, the Solar System is a spherical plasma lens which will cause the apparent positions of the radio sources to be shifted from their actual positions by an amount which depends on the solar weather and on the Sun-Earth-source angle. Since both the solar weather and the Sun-Earth-source angle change throughout the year, very accurate observations over the time scale of a year will be virtually impossible.

Only one parameter is present in the ionosphere portion of the model. Again, the model is linear in the parameter $I_{e\ add}$. Thus, the partial derivative with respect to this parameter is

$$\frac{\partial \tau}{\partial I_{e\ add}} = \frac{k\ f(\text{station \#})\ g(\text{data type})\ S(E)}{\nu^2} \tag{5.25}$$

with $f(2) = 1$ and $f(1) = -1$.

SECTION 6

MODELING THE PHASE DELAY RATE (FRINGE FREQUENCY)

The interferometer is capable of producing several data types: group delay, phase delay, and the time rate of change of phase delay. Actually, the time rate of change of group delay is also available. However, it is not accurate enough to be of significance for geodetic uses. The models discussed above are directly applicable either to group delay or to phase delay. However, the model for the time rate of change of phase delay (fringe frequency) must be either constructed separately, or its equivalent information content obtained by forming the time difference of two phase delay values constructed from the delay-rate measurements as shown below. We chose the latter route since then only models of delay are needed. The two phase delay values, $\tau_{pd}(t \pm \Delta)$, used to represent the delay-rate measurement information content are obtained from the expression

$$\tau_{pd}(t \pm \Delta) = \tau_m(t \pm \Delta) + \tau_r(t) \pm \dot{\tau}_r \Delta \tag{6.1}$$

where $\tau_m(t)$ is the model used in the delay extraction processing step, $\tau_r(t)$ is the residual of the observations from that model, and $\dot{\tau}_r$ is the residual delay rate of the data relative to that model. This modeling for the delay extraction step is covered in Thomas (1981), and is done in analysis steps prior to and completely separate from the modeling described in this report. The output of those previous steps is such that the details of all processing prior to the modeling described here are transparent to this step. Only total interferometer delays and differenced total interferometer phase delays (these phase delays are divided by the time interval of the difference) are reported to this step. One of the requirements of these previous processing steps is that the model delay used be accurate enough to provide a residual phase that is a linear function of time over the observation interval required to obtain the delay information. A linear fit to this residual phase yields the value of $\dot{\tau}_r$, the residual delay rate. Using these two values of τ_{pd}, obtained by (6.1) above, the quantity, R, is constructed by the following algorithm:

$$R = \frac{[\tau_{pd}(t + \Delta) - \tau_{pd}(t - \Delta)]}{2\Delta} \tag{6.2}$$

This value and the group delay measurement, τ_{gd}, are the two data types that normally serve as the interferometer data input to be explained by the model described in this report. The software, however, also has the option to model phase delay, τ_{pd}, directly. In the limit $\Delta \rightarrow 0$, this expression for differenced phase delay approaches the instantaneous time rate of change of phase delay (fringe frequency) at time t. In practice, Δ must be large enough to avoid roundoff errors that arise from taking small differences of large numbers, but should also be small enough to allow R to be a reasonably close approximation to the instantaneous delay rate. A suitable compromise appears to be $\Delta \approx 2$ seconds. Fortunately, Δ has a wide range of allowed values, and the capability to model interferometer performance accurately is relatively insensitive to this choice.

SECTION 7

PHYSICAL CONSTANTS USED

In the software that has been implemented we have tried to use the constants recommended by the IERS Standards (1992). Those that have not been previously defined in the text, but which have an effect on the results that are obtained using the JPL software, are given below:

Symbol	Value	Quantity
c	299792.458	Velocity of light (km/s)
r_0	2.817938×10^{-15}	Classical radius of the electron (meters)
R_E	6378.140	Equatorial radius of the Earth (km)
ω_E	$7.2921151467 \times 10^{-5}$	Rotation rate of the Earth (rad/s)
f	298.257	Flattening factor of the geoid
h_2	0.609	Vertical quadrupole Love number
l_2	0.0852	Horizontal quadrupole Love number
h_3	0.292	Vertical octupole Love number
l_3	0.0151	Horizontal octupole Love number
g	980.665	Surface acceleration due to gravity (cm/s^2)
γ_{PPN}	1	Post-Newtonian relativistic gamma factor

Another group of constants is read from the planetary ephemeris file (presently JPL DE200) when MODEST is executed. These constants include all planetary masses and radii; those most important in VLBI modeling are:

AU	1.4959787066×10^8	Astronomical unit (km)
GM_S	$1.3271243993544841 \times 10^{11}$	Mass of Sun (km^3/s^2)
GM_E	398600.4480734463	Mass of Earth (km^3/s^2)
R_S	696000.0	Radius of Sun (km)
M_E/M_M	81.300587	Earth/Moon mass ratio

SECTION 8

POSSIBLE IMPROVEMENTS TO THE CURRENT MODEL

This section lists areas in which the current model can be improved.

General Relativity:

Second-order effects have not been carefully investigated, and could possibly contribute at the picosecond level.

Variations of the Earth's gravitational potential must be taken into account in defining proper lengths. This correction is estimated by Thomas (1991) to amount to 0.2 cm for a 10,000 km baseline.

Earth Tidal Models:

In addition to the eight frequencies considered in the JPL92 model of Section 2.6.1.1.2, short-period variations of UTPM may have components significant at the mm level that will emerge as data analyses are refined.

Empirical estimates of ocean loading amplitudes for several IRIS stations (Sovers, 1994) indicate that the best theoretically derived amplitudes might be in error by several mm. Future refinements in data analyses are expected to improve the accuracy of the ocean loading model to the mm level.

Resonance with the free core nutation may modify some of the amplitude corrections for nearly diurnal frequencies by $\approx$1 mm.

Tides cause motion of the center of mass of the solid Earth due to motion of the center of mass of the oceans (Brosche and Wünsch, 1993). The amplitude of this displacement can be as large as 1 cm at the usual diurnal and semidiurnal tidal frequencies. Its effect on VLBI observations must be assessed.

The retarded tidal potential effect mentioned in Section 2.4.1 can be as large as several tenths of mm. Thus, for correct modeling at the mm level, the light travel time should be accounted for.

Source Structure:

Estimates of parameters for simplified structural models might provide improved data analyses via "poor man's mapping".

Earth Orientation Models:

There are short-period deficiencies in the present IAU models for the orientation of the Earth in space that may be as large as 1 to 2 milliarcseconds, and longer-term deficiencies of the order of 1 milliarcsecond per year (3 cm at one Earth radius). VLBI measurements made during the past decade indicate the need for revisions of this order of the annual nutation terms and the precession constant [Eubanks *et al.* (1985), Herring *et al.* (1986)]. The 18.6-year components of the IAU nutation series are also in error, and present data spans are just approaching durations long enough to separate them from precession. To provide an improved nutation model, we have implemented MODEST options to use the nutation series of Zhu *et al.*, ZMOA 1990-2, or Kinoshita and Souchay (discussed in Section 2.6.2.1). Any of these constitute a provisionally improved model, especially for the annual and semiannual nutations, until the IAU series is officially revised.

Antenna Deformation:

Gravity loading may cause variations in the position of the reference point of a large antenna that are as large as 1 cm in the local vertical direction. Liewer (1986) presents evidence that this causes systematic errors and that their dependence on antenna orientation and temperature may be modeled.

Antenna Alignment:

Hour angle misalignment on the order of 1 arc minute can cause 1 mm delay effects for DSN HA-Dec antennas with 7-m axis offsets.

Troposphere:

New techniques for characterizing the atmosphere are expected to allow more realistic modeling of the tropospheric delay than the simple spherical-shell model underlying all the results of Section 4. When comprehensive atmospheric data from a region surrounding each observing site are available, present computer speeds permit estimating the tropospheric delay by means of a complete ray-tracing solution. Meanwhile, improvements in tropospheric mapping should be sought by modeling details such as the global, seasonal, and diurnal variation of the inversion layer height and troposphere azimuthal asymmetry.

Ionosphere:

Corrections for the gyrofrequency effect may be of millimeter order.

Thermal Effects:

Thermal expansion of the portion of an antenna above the reference point will induce delay signatures that are $\approx$9 ps (3 mm) peak-to-peak for a 34-m dish.

Phase Delay Rate:

Rather than modeling the delay rates as finite differences of model delays, direct analytic expressions for derivatives of delays could be implemented. This would eliminate questions concerning the choice of the time difference Δ discussed in Section 6. Care must be exercised, however, to ensure consistency between definitions of modeled and observed delay rates.

SECTION 9

REFERENCES

Allen, S. L., "Mobile Station Locations", IOM 335.1-71 (JPL internal document), Jet Propulsion Laboratory, Pasadena, California, Dec. 6, 1982.

Aoki, S., B. Guinot, G. H. Kaplan, H. Kinoshita, D. D. McCarthy, and P. K. Seidelmann, "The New Definition of Universal Time", *Astron. Astrophys.*, Vol. 105, pp. 359-361, 1982.

Argus, D. F., and R. G. Gordon, "No-Net-Rotation Model of Current Plate Velocities Incorporating Plate Motion Model NUVEL-1", *Geophys. Res. Let.*, Vol. 18, pp. 2039-2042, 1991.

Branson, R. P. *Parameter Estimation Methods and Algorithms for the JPL VLBI Parameter Estimation Software "MODEST" – 1994*, JPL Publication in preparation, 1994.

Brosche, P., U. Seiler, J. Sundermann, and J. Wünsch, "Periodic Changes in Earth's Rotation due to Oceanic Tides", *Astron. Astrophys.*, Vol. 220, pp. 318-20, 1989.

Brosche, P., J. Wünsch, J. Campbell, and H. Schuh, "Ocean Tide Effects in Universal Time Detected by VLBI", *Astron. Astrophys.*, Vol. 245, pp. 676-682, 1991.

Brosche, P. and J. Wünsch, "Variations of the Solid Earth's Center of Mass due to Oceanic Tides", *Astron. Nachr.*, Vol. 314, pp. 87-90, 1993.

Bureau International de l'Heure, Annual Report for 1982, Paris, France, 1983 (typical for all years).

Bureau International des Poids et Mesures, Circular T30, 1 August 1990, Sèvres, France, 1990.

Cannon, W. H., *A Survey of the Theory of the Earth's Rotation*, JPL Publication 82-38, Jet Propulsion Laboratory, Pasadena, California, Nov. 1, 1981.

Cartwright, D. E. and A. C. Edden, "Corrected Tables of Tidal Harmonics", *Geophys. J. Roy. Astron. Soc.*, Vol. 33, pp. 253-264, 1973.

Chao, C. C., *The Troposphere Calibration Model for Mariner Mars 1971*, Technical Report 32-1587, Jet Propulsion Laboratory, Pasadena, California, pp. 61-76, March, 1974.

Charlot, P., "Structure des Sources Radio Extragalactiques dans les Observations VLBI d'Astrométrie et de Géodynamique", Ph. D. thesis, Paris Observatory, Paris, France, 1989.

Charlot, P., "Radio-Source Structure in Astrometric and Geodetic Very Long Baseline Interferometry", *Astron. J.*, Vol. 99, pp. 1309-1326, 1990a.

Charlot, P., "Fourteen Extragalactic Radio Sources Mapped at 2.3 and 8.4 GHz with a 24-hour Crustal Dynamics Program VLBI Experiment", *Astron. Astrophys.*, Vol. 229, pp. 51-63, 1990b.

Charlot, P., "Evidence for Source Structure Effects Caused by the Quasar 3C273 in Geodetic VLBI Data", to appear in *VLBI Technology – Progress and Future Observational Possibilities, Proc. URSI/IAU Symp.*, Kyoto, Japan, 1993.

Davis, J. L., T. A. Herring, I. I. Shapiro, A. E. E. Rogers, and G. Elgered, "Geodesy by Radio Interferometry: Effects of Atmospheric Modeling Errors on Estimated Baseline Length", *Radio Science*, Vol. 20, pp. 1593-1607, 1985.

DeMets, C., R. G. Gordon, D. F. Argus, and S. Stein, "Current Plate Motions", *Geophys. J. Int.*, Vol. 101, pp. 425-478, 1990.

DeMets, C., R. G. Gordon, D. F. Argus, and S. Stein, "Effect of Recent Revisions to the Geomagnetic Reversal Time Scale on Estimates of Current Plate Motions", *Geophys. Res. Let.*, in press, 1994.

Dewey, R. J. (private communication to O. J. Sovers in 1991), Jet Propulsion Laboratory, Pasadena, California.

Edwards, C. D., "The Effect of Spatial and Temporal Wet Troposphere Fluctuations on Connected Element Interferometry", IOM 335.3-88-98 (JPL internal document), Jet Propulsion Laboratory, Pasadena, California, September 6, 1988.

Eubanks, T. M., J. A. Steppe, and O. J. Sovers, "An Analysis and Intercomparison of VLBI Nutation Estimates", *Proc. Int. Conf. on Earth Rotation and the Terrestrial Reference Frame*, Ohio State University, Columbus, Ohio, Vol. 1, pp. 326-340, 1985.

Explanatory Supplement to the Astronomical Almanac, pp. 39-93, ed. P. K. Seidelmann, University Science Books, Mill Valley, CA, 1992.

Fanselow, J. L., *Observation Model and Parameter Partials for the JPL VLBI Parameter Estimation Software 'MASTERFIT' - V1.0*, JPL Publication 83-39, Jet Propulsion Laboratory, Pasadena, California, 1983.

Folkner, W. M., P. Charlot, M. H. Finger, J. G. Williams, O. J. Sovers, X X Newhall, and E. M. Standish, "Determination of the Extragalactic-Planetary Frame Tie from Joint Analysis of Radio Interferometric and Lunar Laser Ranging Measurements", *Astron. Astrophys.*, Vol. 287, pp. 279-289, 1994.

French, A. P., *Special Relativity*, MIT Introductory Physics Series, pp. 41, 44, 132, Norton, New York, New York, 1968.

Goad, C. C., in IAU, IUGG Joint Working Group on the Rotation of the Earth, "Project MERIT Standards", *United States Naval Observatory Circular No.167*, pp. A7-1 to A7-25, U.S. Naval Observatory, Washington, D.C., Dec. 27, 1983.

Gross, R. S., "A Combination of Earth Orientation Data: SPACE91", *IERS Technical Note 11*, pp. 113-119, Ed. P. Charlot, Paris, France, 1992.

Gross, R. S., "The Effect of Ocean Tides on the Earth's Rotation as Predicted by the Results of an Ocean Tide Model", *Geophys. Res. Let.*, Vol. 20, pp. 293-296, 1993.

Herring, T. A., C. R. Gwinn, and I. I. Shapiro, "Geodesy by Radio Interferometry: Studies of the Forced Nutations of the Earth. Part I: Data Analysis", *J. Geophys. Res.*, Vol. 91, pp. 4745-4754, 1986.

Herring, T. A. and D. Dong, "Current and Future Accuracy of Earth Rotation Measurements", *Proc. of the AGU Chapman Conference on Geodetic VLBI: Monitoring Global Change*, pp. 306-324, *NOAA Tech. Rept. NOS 137 NGS 49*, Rockville, MD, 1991.

Herring, T. A., "Modeling Atmospheric Delays in the Analysis of Space Geodetic Data", in *Refraction of Transatmospheric Signals in Geodesy*", Eds. J. C. DeMunck and T. A. Th. Spoelstra, Netherlands Commission on Geodesy, Delft, Netherlands, 1992.

Herring, T. A., "Diurnal and Semidiurnal Variations in Earth Rotation", paper presented at World Space Congress 92, Washington, D.C., in "The Orientation of the Planet Earth as Observed by Modern Space Techniques", *Advances in Space Research*, pp. 147-156, Pergamon Press, New York, 1993.

International Association of Geodesy, *International Radio Interferometric Surveying (IRIS) Bulletin A*, no. 116, Oct., 1993.

International Earth Rotation Service, *IERS Standards, IERS Technical Note 3*, pp. 37-44, Ed. D. D. McCarthy, Paris, France, 1989.

International Earth Rotation Service, *IERS Standards, IERS Technical Note 13*, Ed. D. D. McCarthy, Paris, France, 1992.

International Earth Rotation Service, *Annual Report for 1992*, Paris, France, 1993.

Jackson, J. D., *Classical Electrodynamics*, John Wiley & Sons, Inc., New York, New York, p. 517, 1975.

Jacobs, C. S., "Refinement of Troposphere Model for Equatorial Mount Antennas", IOM 335.3-88-019 (JPL internal document), Jet Propulsion Laboratory, Pasadena, California, February 12, 1988.

Jacobs, C. S., "Refinement of Troposphere Model for X-Y Mount and Richmond Antennas", IOM 335.6-91-015 (JPL internal document), Jet Propulsion Laboratory, Pasadena, California, August 16, 1991.

Kaplan, G. H., "The IAU Resolutions of Astronomical Constants, Time Scales, and the Fundamental Reference Frame", *United States Naval Observatory Circular No. 163*, U.S. Naval Observatory, Washington, D.C., Dec. 10, 1981.

Kellermann, K. I., and I. I. K. Pauliny-Toth, "Compact Radio Sources", *Ann. Rev. Astron. Astrophys.*, vol. 19, pp. 373-410, 1981.

Kinoshita, H., and J. Souchay, "The Theory of the Nutation for the Rigid Earth Model at the Second Order", *Cel. Mech. and Dyn. Astron.*, Vol. 48, pp. 187-265, 1990.

Lanyi, G. E., "Tropospheric Delay Effects in Radio Interferometry", *Telecommunications and Data Acquisition Prog. Rept. 42-78*, pp. 152-159, Jet Propulsion Laboratory, Pasadena, California, April-June, 1984.

Lieske, J. H., T. Lederle, W. Fricke, and B. Morando, "Expressions for the Precession Quantities Based upon the IAU (1976) System of Astronomical Constants", *Astron. Astrophys.*, Vol. 58, pp. 1-16, 1977.

Liewer, K. M., "Antenna Rotation Corrections to VLBI Data", IOM 335.4-499 (JPL internal document), Jet Propulsion Laboratory, Pasadena, California, March 29, 1985.

Liewer, K. M. (private communication to O. J. Sovers in 1986), Jet Propulsion Laboratory, Pasadena, California.

Lowe, S. T., *Theory of Post-Block II VLBI Observable Extraction*, JPL Publication 92-7, Jet Propulsion Laboratory, Pasadena, California, July 15, 1992.

Mathews, P. M., B. A. Buffett, T. A. Herring, I. I. Shapiro, "Forced Nutations of the Earth: Influence of Inner Core Dynamics: 1. Theory", *J. Geophys. Res.*, Vol. 96B, pp. 8219-8242, 1991.

Melbourne, W. G., J. D. Mulholland, W. L. Sjogren, and F. M. Sturms, Jr., *Constants and Related Information for Astrodynamic Calculations*, Technical Report 32-1306, Jet Propulsion Laboratory, Pasadena, California, July 15, 1968.

Melbourne, W., R. Anderle, M. Feissel, R. King, D. McCarthy, D. Smith, B. Tapley, R. Vicente, *Project MERIT Standards*, United States Naval Observatory Circular No. 167, U.S. Naval Observatory, Washington, D.C., Dec. 27, 1983.

Melbourne, W., R. Anderle, M. Feissel, R. King, D. McCarthy, D. Smith, B. Tapley, R. Vicente, *Project MERIT Standards*, United States Naval Observatory Circular No. 167, Update #1, U.S. Naval Observatory, Washington, D.C., Dec. 1985.

Melchior, P., *The Earth Tides*, p. 114, Pergamon Press, New York, New York, 1966.

Minster, J. B., and T. H. Jordan, "Present-Day Plate Motions", *J. Geophys. Res.*, Vol. 83, pp. 5331-5354, 1978.

Misner, C. W., K. S. Thorne, and J. A. Wheeler, "Gravitation", W. H. Freeman, New York, 1973.

Moyer, T. D., *Mathematical Formulation of the Double-Precision Orbit Determination Program (DPODP)*, Technical Report 32-1527, Jet Propulsion Laboratory, Pasadena, California, pp. 12-17, May 15, 1971.

Naudet, C. J. (private communication to O. J. Sovers in 1994), Jet Propulsion Laboratory, Pasadena, California.

Newhall, X X, Preston, R. A., and Esposito, P. B., "Relating the JPL VLBI Reference Frame and the Planetary Ephemerides", in *Astrometric Techniques, Proc. IAU Symp. 109*, H. K. Eichhorn and R. J. Leacock, eds., Reidel, 1986.

Niell, A. E. (private communication to O. J. Sovers in 1994), Haystack Observatory, Westford, Massachusetts.

Ortega-Molina, A., "Détermination du Centre de Phase du Radiotélescope de Nançay pour les Observations VLBI", Report of Observatoire de Paris-Meudon, Meudon, France, Feb. 1985.

Pagiatakis, S. D., R. B. Langley, and P. Vanicek, "Ocean Tide Loading: A Global Model for the Analysis of VLBI Observations", presented at the 3rd International Symposium on the Use of Artificial Satellites for Geodesy and Geodynamics, National Technical University, Athens, Greece, Sept. 1982.

Pagiatakis, S. D., *Ocean Tide Loading, Body Tide and Polar Motion Effects on Very Long Baseline Interferometry*, Technical Report No. 92, Dept. of Surveying Engineering, University of New Brunswick, Fredericton, N. B., Canada, Dec. 1982.

Pagiatakis, S. D., "The Response of a Realistic Earth to Ocean Tide Loading", *Geophys. J. Int.*, Vol. 103, pp. 541-560, 1990.

Rabbel, W., and H. Schuh, "The Influence of Atmospheric Loading on VLBI Experiments", *J. Geophysics*, Vol. 59, pp. 164-170, 1986.

Ray, J. R., C. Ma, J. W. Ryan, T. E. Clark, R. J. Eanes, M. M. Watkins, B. E. Schutz, and B. D. Tapley, "Comparison of VLBI and SLR Geocentric Site Coordinates", *Geophys. Res. Let.*, Vol. 18, pp. 231-234, 1991.

Resch, G. M., and R. B. Miller, "Water Vapor Radiometry in Geodetic Applications", *Geodetic Aspects of Electromagnetic Wave Propagation through the Atmosphere*, Ed. F. K. Brunner, Springer Verlag, Berlin, Germany, 1983.

Scherneck, H. G., *Crustal Loading Affecting VLBI Sites*, University of Uppsala, Institute of Geophysics, Dept. of Geodesy, Report No. 20, Uppsala, Sweden, 1983.

Scherneck, H. G. (private communication to O. J. Sovers in 1990), University of Uppsala, Institute of Geophysics, Dept. of Geodesy, Uppsala, Sweden.

Scherneck, H. G., "A Parameterised Solid Earth Tide Model and Ocean Tide Loading Effects for Global Geodetic Baseline Measurements", *Geophys. J. Int.*, Vol. 106, pp. 677-694, 1991.

Scherneck, H. G. (private communication to O. J. Sovers in 1993), University of Uppsala, Institute of Geophysics, Dept. of Geodesy, Uppsala, Sweden.

Seidelmann, P. K., "1980 IAU Theory of Nutation: The Final Report of the IAU Working Group on Nutation", *Celestial Mechanics*, Vol. 27, pp. 79-106, 1982.

Seiler, U., "An Investigation of the Tides of the World Ocean and their Instantaneous Angular Momentum Budget", *Mitteilungen Institut für Meereskunde, Univ. Hamburg*, 101 pp., 1989.

Seiler, U., "Variations of the Angular Momentum Budget for Tides of the Present Ocean", in *Earth's Rotation from Eons to Days*, ed. P. Brosche and J. Sündermann, 81-94, Springer Verlag, New York, 1990.

Seiler, U., "Periodic Changes of the Angular Momentum Budget due to the Tides of the World Ocean", *J. Geophys. Res.*, 96, 10287-10300, 1991.

Shahid-Saless, B., R. W. Hellings, and N. Ashby, "A Picosecond Accuracy Relativistic VLBI Model Via Fermi Normal Coordinates", *Geophys. Res. Let.*, Vol. 18, pp. 1139-1142, 1991.

Souchay, J. (private communication to O. J. Sovers in 1993), Jet Propulsion Laboratory, Pasadena, California.

Sovers, O. J. and J. L. Fanselow, *Observation Model and Parameter Partials for the JPL VLBI Parameter Estimation Software 'MASTERFIT' - 1987*, JPL Publication 83-39, Rev. 3, Jet Propulsion Laboratory, Pasadena, California, 1987.

Sovers, O. J., C. S. Jacobs, and R. S. Gross, "Measuring Rapid Ocean Tidal Earth Orientation Variations with VLBI", *J. Geophys. Res.*, Vol. 98, No. B11, pp. 19959-19971, 1993.

Sovers, O. J., "Vertical Ocean Loading Amplitudes from VLBI Measurements", *Geophys. Res. Letters*, Vol. 21, pp. 357-360, 1994.

Spitzer, L., Jr., *Physics of Fully Ionized Gases*, Interscience Publishers, New York, New York, 1962.

Thomas, J. B., *An Analysis of Source Structure Effects in Radio Interferometry Measurements*, JPL Publication 80-84, Jet Propulsion Laboratory, Pasadena, California, 1980.

Thomas, J. B., *An Analysis of Radio Interferometry with the Block 0 System*, JPL Publication 81-49, Jet Propulsion Laboratory, Pasadena, California, 1981.

Thomas, J. B., *Interferometry Theory for the Block II Processor*, JPL Publication 87-29, Jet Propulsion Laboratory, Pasadena, California, 1987.

Thomas, J. B. (private communication to O. J. Sovers in 1991), Jet Propulsion Laboratory, Pasadena, California.

Thompson, A. R., J. M. Moran, and G. W. Swenson, Jr., "Interferometry and Synthesis in Radio Astronomy", Wiley, New York, 1986.

Treuhaft, R. N. (private communication to O. J. Sovers in 1991), Jet Propulsion Laboratory, Pasadena, California.

Treuhaft, R. N., and G. E. Lanyi, "The Effect of the Dynamic Wet Troposphere on Radio Interferometric Measurements", *Radio Science*, Vol. 22, pp. 251-265, March-April 1987.

Treuhaft, R. N., and S. T. Lowe, "A Measurement of Planetary Relativistic Deflection", *Astron. J.*, Vol. 102, pp. 1879-1888, 1991.

Treuhaft, R. N., and J. B. Thomas, "Incorporating Atmospheric Delay into the Relativistic VLBI Time Delay", IOM 335.6-91-016 (JPL internal document), Jet Propulsion Laboratory, Pasadena, California, August 15, 1991.

Ulvestad, J. S., "Effects of Source Structure on Astrometry and Geodesy", IAU Symposium 129 Proceedings, Reidel, Cambridge, Mass., 1988.

Wade, C. M., "Precise Positions of Radio Sources", *Astrophys. J.*, Vol. 162, p. 381, 1970.

Wahr, J. M., "The Tidal Motions of a Rotating, Elliptical, Elastic, and Oceanless Earth", Ph. D. Thesis, University of Colorado, 1979.

Wahr, J. M., "Deformation Induced by Polar Motion", *J. Geophys. Res.*, Vol. 90, pp. 9363-9368, 1985.

Williams, J. G., "Solid Earth Tides", IOM 391-109 (JPL internal document), Jet Propulsion Laboratory, Pasadena, California, July 14, 1970.

Yoder, C. F., J. G. Williams, and M. E. Parke, "Tidal Variations of Earth Rotation", *J. Geophys. Res.*, Vol. 86, B2, pp. 881-891, 1981.

Yoder, C. F. (private communication to J. L. Fanselow in 1982), Jet Propulsion Laboratory, Pasadena, California.

Yoder, C. F. (private communication to O. J. Sovers in 1983), Jet Propulsion Laboratory, Pasadena, California.

Yoder, C. F. (private communication to O. J. Sovers in 1984), Jet Propulsion Laboratory, Pasadena, California.

Zensus, J. A., and T. J. Pearson, eds., *Superluminal Radio Sources*, Cambridge Univ. Press, New York, New York, 1987.

Zhu, S. Y., and E. Groten, "Various Aspects of Numerical Determination of Nutation Constants. I. Improvement of Rigid-Earth Nutation", *Astron. J.*, Vol. 98, pp. 1104-1111, September, 1989.

Zhu, S. Y., E. Groten, and Ch. Reigber, "Various Aspects of Numerical Determination of Nutation Constants. II. An Improved Nutation Series for the Deformable Earth", *Astron. J.*, Vol. 99, pp. 1024-1044, March, 1990.

APPENDIX A

NUTATION MODELS

The five nutation series available in MODEST are tabulated here: Table A.I gives the standard 1980 IAU series; Tables A.II, A.III, and A.IV contain the results of Zhu *et al.* (1990); Tables A.V, A.VI, and A.VII contain the ZMOA 1990-2 series; Tables A.VIII and A.IX contain the Kinoshita-Souchay series; for completeness, the old (Woolard) nutation series is given in Table A.X.

Table A.I

1980 IAU Theory of Nutation

Index j	Period (days)	Argument coefficient k_{j1}	k_{j2}	k_{j3}	k_{j4}	k_{j5}	A_{0j} ($0''.0001$)	A_{1j}	B_{0j} ($0''.0001$)	B_{1j}
1	6798.4	0	0	0	0	1	-171996	-174.2	92025	8.9
2	3399.2	0	0	0	0	2	2062	0.2	-895	0.5
3	1305.5	-2	0	2	0	1	46	0.0	-24	0.0
4	1095.2	2	0	-2	0	0	11	0.0	0	0.0
5	1615.7	-2	0	2	0	2	-3	0.0	1	0.0
6	3232.9	1	-1	0	-1	0	-3	0.0	0	0.0
7	6786.3	0	-2	2	-2	1	-2	0.0	1	0.0
8	943.2	2	0	-2	0	1	1	0.0	0	0.0
9	182.6	0	0	2	-2	2	-13187	-1.6	5736	-3.1
10	365.3	0	1	0	0	0	1426	-3.4	54	-0.1
11	121.7	0	1	2	-2	2	-517	1.2	224	-0.6
12	365.2	0	-1	2	-2	2	217	-0.5	-95	0.3
13	177.8	0	0	2	-2	1	129	0.1	-70	0.0
14	205.9	2	0	0	-2	0	48	0.0	1	0.0
15	173.3	0	0	2	-2	0	-22	0.0	0	0.0
16	182.6	0	2	0	0	0	17	-0.1	0	0.0
17	386.0	0	1	0	0	1	-15	0.0	9	0.0
18	91.3	0	2	2	-2	2	-16	0.1	7	0.0
19	346.6	0	-1	0	0	1	-12	0.0	6	0.0
20	199.8	-2	0	0	2	1	-6	0.0	3	0.0
21	346.6	0	-1	2	-2	1	-5	0.0	3	0.0
22	212.3	2	0	0	-2	1	4	0.0	-2	0.0
23	119.6	0	1	2	-2	1	4	0.0	-2	0.0
24	411.8	1	0	0	-1	0	-4	0.0	0	0.0
25	131.7	2	1	0	-2	0	1	0.0	0	0.0
26	169.0	0	0	-2	2	1	1	0.0	0	0.0
27	329.8	0	1	-2	2	0	-1	0.0	0	0.0
28	409.2	0	1	0	0	2	1	0.0	0	0.0
29	388.3	-1	0	0	1	1	1	0.0	0	0.0
30	117.5	0	1	2	-2	0	-1	0.0	0	0.0

Table A.I cont.

1980 IAU Theory of Nutation

Index j	Period (days)	Argument coefficient k_{j1}	k_{j2}	k_{j3}	k_{j4}	k_{j5}	A_{0j} ($0''.0001$)	A_{1j}	B_{0j} ($0''.0001$)	B_{1j}
31	13.7	0	0	2	0	2	-2274	-0.2	977	-0.5
32	27.6	1	0	0	0	0	712	0.1	-7	0.0
33	13.6	0	0	2	0	1	-386	-0.4	200	0.0
34	9.1	1	0	2	0	2	-301	0.0	129	-0.1
35	31.8	1	0	0	-2	0	-158	0.0	-1	0.0
36	27.1	-1	0	2	0	2	123	0.0	-53	0.0
37	14.8	0	0	0	2	0	63	0.0	-2	0.0
38	27.7	1	0	0	0	1	63	0.1	-33	0.0
39	27.4	-1	0	0	0	1	-58	-0.1	32	0.0
40	9.6	-1	0	2	2	2	-59	0.0	26	0.0
41	9.1	1	0	2	0	1	-51	0.0	27	0.0
42	7.1	0	0	2	2	2	-38	0.0	16	0.0
43	13.8	2	0	0	0	0	29	0.0	-1	0.0
44	23.9	1	0	2	-2	2	29	0.0	-12	0.0
45	6.9	2	0	2	0	2	-31	0.0	13	0.0
46	13.6	0	0	2	0	0	26	0.0	-1	0.0
47	27.0	-1	0	2	0	1	21	0.0	-10	0.0
48	32.0	-1	0	0	2	1	16	0.0	-8	0.0
49	31.7	1	0	0	-2	1	-13	0.0	7	0.0
50	9.5	-1	0	2	2	1	-10	0.0	5	0.0
51	34.8	1	1	0	-2	0	-7	0.0	0	0.0
52	13.2	0	1	2	0	2	7	0.0	-3	0.0
53	14.2	0	-1	2	0	2	-7	0.0	3	0.0
54	5.6	1	0	2	2	2	-8	0.0	3	0.0
55	9.6	1	0	0	2	0	6	0.0	0	0.0
56	12.8	2	0	2	-2	2	6	0.0	-3	0.0
57	14.8	0	0	0	2	1	-6	0.0	3	0.0
58	7.1	0	0	2	2	1	-7	0.0	3	0.0
59	23.9	1	0	2	-2	1	6	0.0	-3	0.0
60	14.7	0	0	0	-2	1	-5	0.0	3	0.0
61	29.8	1	-1	0	0	0	5	0.0	0	0.0
62	6.9	2	0	2	0	1	-5	0.0	3	0.0
63	15.4	0	1	0	-2	0	-4	0.0	0	0.0
64	26.9	1	0	-2	0	0	4	0.0	0	0.0
65	29.5	0	0	0	1	0	-4	0.0	0	0.0
66	25.6	1	1	0	0	0	-3	0.0	0	0.0
67	9.1	1	0	2	0	0	3	0.0	0	0.0
68	9.4	1	-1	2	0	2	-3	0.0	1	0.0
69	9.8	-1	-1	2	2	2	-3	0.0	1	0.0
70	13.7	-2	0	0	0	1	-2	0.0	1	0.0

Table A.I cont.

1980 IAU Theory of Nutation

Index j	Period (days)	Argument coefficient k_{j1}	k_{j2}	k_{j3}	k_{j4}	k_{j5}	A_{0j} (0".0001)	A_{1j}	B_{0j} (0".0001)	B_{1j}
71	5.5	3	0	2	0	2	-3	0.0	1	0.0
72	7.2	0	-1	2	2	2	-3	0.0	1	0.0
73	8.9	1	1	2	0	2	2	0.0	-1	0.0
74	32.6	-1	0	2	-2	1	-2	0.0	1	0.0
75	13.8	2	0	0	0	1	2	0.0	-1	0.0
76	27.8	1	0	0	0	2	-2	0.0	1	0.0
77	9.2	3	0	0	0	0	2	0.0	0	0.0
78	9.3	0	0	2	1	2	2	0.0	-1	0.0
79	27.3	-1	0	0	0	2	1	0.0	-1	0.0
80	10.1	1	0	0	-4	0	-1	0.0	0	0.0
81	14.6	-2	0	2	2	2	1	0.0	-1	0.0
82	5.8	-1	0	2	4	2	-2	0.0	1	0.0
83	15.9	2	0	0	-4	0	-1	0.0	0	0.0
84	22.5	1	1	2	-2	2	1	0.0	-1	0.0
85	5.6	1	0	2	2	1	-1	0.0	1	0.0
86	7.3	-2	0	2	4	2	-1	0.0	1	0.0
87	9.1	-1	0	4	0	2	1	0.0	0	0.0
88	29.3	1	-1	0	-2	0	1	0.0	0	0.0
89	12.8	2	0	2	-2	1	1	0.0	-1	0.0
90	4.7	2	0	2	2	2	-1	0.0	0	0.0
91	9.6	1	0	0	2	1	-1	0.0	0	0.0
92	12.7	0	0	4	-2	2	1	0.0	0	0.0
93	8.7	3	0	2	-2	2	1	0.0	0	0.0
94	23.8	1	0	2	-2	0	-1	0.0	0	0.0
95	13.1	0	1	2	0	1	1	0.0	0	0.0
96	35.0	-1	-1	0	2	1	1	0.0	0	0.0
97	13.6	0	0	-2	0	1	-1	0.0	0	0.0
98	25.4	0	0	2	-1	2	-1	0.0	0	0.0
99	14.2	0	1	0	2	0	-1	0.0	0	0.0
100	9.5	1	0	-2	-2	0	-1	0.0	0	0.0
101	14.2	0	-1	2	0	1	-1	0.0	0	0.0
102	34.7	1	1	0	-2	1	-1	0.0	0	0.0
103	32.8	1	0	-2	2	0	-1	0.0	0	0.0
104	7.1	2	0	0	2	0	1	0.0	0	0.0
105	4.8	0	0	2	4	2	-1	0.0	0	0.0
106	27.3	0	1	0	1	0	1	0.0	0	0.0

Table A.II

Zhu *et al.* Theory of Nutation: 1980 IAU Terms

Index j	Period (days)	Argument coefficient k_{j1}	k_{j2}	k_{j3}	k_{j4}	k_{j5}	A_{0j} (0".00001)	A_{1j}	B_{0j} (0".00001)	B_{1j}
1	6798.38	0	0	0	0	1	-1720618	-1743	920530	90
2	3399.19	0	0	0	0	2	20743	2	-8975	5
3	1305.48	-2	0	2	0	1	460	1	-243	0
4	1095.18	2	0	-2	0	0	110	0	1	0
5	1615.75	-2	0	2	0	2	-31	0	14	0
6	3232.86	1	-1	0	-1	0	-33	0	0	0
7	6786.32	0	-2	2	-2	1	-15	0	8	0
8	943.23	2	0	-2	0	1	7	0	-4	0
9	182.62	0	0	2	-2	2	-131720	-16	57320	-31
10	365.26	0	1	0	0	0	14735	-35	719	-2
11	121.75	0	1	2	-2	2	-5176	12	2247	-7
12	365.22	0	-1	2	-2	2	2161	-5	-961	3
13	177.84	0	0	2	-2	1	1293	1	-699	0
14	205.89	2	0	0	-2	0	479	0	5	0
15	173.31	0	0	2	-2	0	-218	0	-1	0
16	182.63	0	2	0	0	0	168	-1	2	0
17	386.00	0	1	0	0	1	-140	0	86	0
18	91.31	0	2	2	-2	2	-158	1	69	0
19	346.64	0	-1	0	0	1	-127	0	64	0
20	199.84	-2	0	0	2	1	-58	0	30	0
21	346.60	0	-1	2	-2	1	-48	0	27	0
22	212.32	2	0	0	-2	1	41	0	-22	0
23	119.61	0	1	2	-2	1	36	0	-20	0
24	411.78	1	0	0	-1	0	-43	0	-6	0
25	131.67	2	1	0	-2	0	11	0	0	0
26	169.00	0	0	-2	2	1	9	0	-4	0
27	329.79	0	1	-2	2	0	-9	0	0	0
28	409.23	0	1	0	0	2	7	0	-3	0
29	388.27	-1	0	0	1	1	9	0	-4	0
30	117.54	0	1	2	-2	0	-6	0	0	0
31	13.66	0	0	2	0	2	-22824	-2	9806	-5
32	27.55	1	0	0	0	0	7122	1	-70	0
33	13.63	0	0	2	0	1	-3885	-4	2011	0
34	9.13	1	0	2	0	2	-3023	0	1293	-1
35	31.81	1	0	0	-2	0	-1572	0	-13	0
36	27.09	-1	0	2	0	2	1238	0	-535	0
37	14.77	0	0	0	2	0	635	0	-13	0
38	27.67	1	0	0	0	1	633	1	-332	0
39	27.44	-1	0	0	0	1	-580	-1	315	0
40	9.56	-1	0	2	2	2	-598	0	256	0

Index j	Period (days)	Argument coefficient k_{j1}	k_{j2}	k_{j3}	k_{j4}	k_{j5}	A_{0j} ($0''.00001$)	A_{1j}	B_{0j} ($0''.00001$)	B_{1j}
41	9.12	1	0	2	0	1	-517	0	265	0
42	7.10	0	0	2	2	2	-386	0	165	0
43	13.78	2	0	0	0	0	293	0	-6	0
44	23.94	1	0	2	-2	2	286	0	-124	0
45	6.86	2	0	2	0	2	-311	0	132	0
46	13.61	0	0	2	0	0	259	0	-5	0
47	26.98	-1	0	2	0	1	205	0	-107	0
48	31.96	-1	0	0	2	1	152	0	-80	0
49	31.66	1	0	0	-2	1	-129	0	70	0
50	9.54	-1	0	2	2	1	-103	0	53	0
51	34.85	1	1	0	-2	0	-74	0	-1	0
52	13.17	0	1	2	0	2	76	0	-33	0
53	14.19	0	-1	2	0	2	-71	0	31	0
54	5.64	1	0	2	2	2	-77	0	32	0
55	9.61	1	0	0	2	0	66	0	-3	0
56	12.81	2	0	2	-2	2	65	0	-28	0
57	14.80	0	0	0	2	1	-64	0	33	0
58	7.09	0	0	2	2	1	-66	0	34	0
59	23.86	1	0	2	-2	1	58	0	-30	0
60	14.73	0	0	0	-2	1	-50	0	28	0
61	29.80	1	-1	0	0	0	47	0	-1	0
62	6.85	2	0	2	0	1	-53	0	27	0
63	15.39	0	1	0	-2	0	-44	0	-1	0
64	26.88	1	0	-2	0	0	41	0	1	0
65	29.53	0	0	0	1	0	-40	0	1	0
66	25.62	1	1	0	0	0	-34	0	1	0
67	9.11	1	0	2	0	0	34	0	-1	0
68	9.37	1	-1	2	0	2	-29	0	12	0
69	9.81	-1	-1	2	2	2	-29	0	12	0
70	13.75	-2	0	0	0	1	-23	0	13	0
71	5.49	3	0	2	0	2	-29	0	12	0
72	7.24	0	-1	2	2	2	-26	0	11	0
73	8.91	1	1	2	0	2	25	0	-10	0
74	32.61	-1	0	2	-2	1	-20	0	11	0
75	13.81	2	0	0	0	1	22	0	-11	0
76	27.78	1	0	0	0	2	-20	0	8	0
77	9.18	3	0	0	0	0	16	0	-1	0
78	9.34	0	0	2	1	2	16	0	-7	0
79	27.33	-1	0	0	0	2	14	0	-6	0
80	10.08	1	0	0	-4	0	-14	0	-1	0

Table A.II cont.

Zhu *et al.* Theory of Nutation: 1980 IAU Terms

Index j	Period (days)	Argument coefficient k_{j1}	k_{j2}	k_{j3}	k_{j4}	k_{j5}	A_{0j} ($0''.00001$)	A_{1j}	B_{0j} ($0''.00001$)	B_{1j}
81	14.63	-2	0	2	2	2	13	0	-6	0
82	5.80	-1	0	2	4	2	-15	0	6	0
83	15.91	2	0	0	-4	0	-13	0	0	0
84	22.47	1	1	2	-2	2	13	0	-5	0
85	5.64	1	0	2	2	1	-13	0	7	0
86	7.35	-2	0	2	4	2	-12	0	5	0
87	9.06	-1	0	4	0	2	11	0	-5	0
88	29.26	1	-1	0	-2	0	9	0	0	0
89	12.79	2	0	2	-2	1	10	0	-5	0
90	4.68	2	0	2	2	2	-11	0	5	0
91	9.63	1	0	0	2	1	-10	0	5	0
92	12.66	0	0	4	-2	2	9	0	-4	0
93	8.75	3	0	2	-2	2	9	0	-4	0
94	23.77	1	0	2	-2	0	-7	0	0	0
95	13.41	0	1	2	0	1	8	0	-4	0
96	35.03	-1	-1	0	2	1	7	0	-4	0
97	13.58	0	0	-2	0	1	-6	0	3	0
98	25.42	0	0	2	-1	2	-7	0	3	0
99	14.19	0	1	0	2	0	-6	0	0	0
100	9.53	1	0	-2	-2	0	-6	0	0	0
101	14.16	0	-1	2	0	1	-7	0	3	0
102	34.67	1	1	0	-2	1	-6	0	3	0
103	32.76	1	0	-2	2	0	-6	0	0	0
104	7.13	2	0	0	2	0	6	0	0	0
105	4.79	0	0	2	4	2	-7	0	3	0
106	27.32	0	1	0	1	0	5	0	0	0

Table A.III

Zhu *et al.* Theory of Nutation: Out-of-Phase Terms

Index j	Period (days)	Argument coefficient k_{j1}	k_{j2}	k_{j3}	k_{j4}	k_{j5}	A_{2j} ($0''.00001$)	B_{2j}
1	6798.38	0	0	0	0	1	221	112
2	182.62	0	0	2	-2	2	-153	-61
3	365.26	0	1	0	0	0	-55	22
4	13.66	0	0	2	0	2	-5	-2

Table A.IV

Zhu *et al.* Theory of Nutation: Additional Terms

Index j	Period (days)	Argument coefficient k_{j1}	k_{j2}	k_{j3}	k_{j4}	k_{j5}	A_{0j} (0".00001)	B_{0j} (0".00001)
1	5.49	3	0	2	0	1	-5	2
2	5.73	1	-1	2	2	2	-6	2
3	6.96	0	1	2	2	2	5	-2
4	6.99	2	-1	2	0	2	-5	2
5	7.38	0	0	0	4	0	5	0
6	9.31	-1	1	2	2	2	6	-2
7	9.80	-1	-1	2	2	1	-5	2
8	9.87	1	-1	0	2	0	5	0
9	14.83	0	0	0	2	2	-5	2
10	29.93	1	-1	0	0	1	5	-3
11	73.05	0	3	2	-2	2	-5	2
12	177.84	0	0	2	-2	1	-9	7
13	187.66	0	0	2	-2	3	13	-2
14	3230.13	-1	-1	2	-1	2	13	-5
15	3231.50	-1	0	1	0	1	15	3
16	6164.10	-1	1	0	1	1	7	-4
17	4.00	3	0	2	2	2	-1	1
18	4.08	1	0	2	4	2	-2	1
19	4.58	4	0	2	0	2	-3	1
20	4.68	2	0	2	2	1	-2	1
21	4.79	0	0	2	4	1	-1	1
22	5.56	1	1	2	2	2	1	-1
23	5.80	-1	0	2	4	1	-3	1
24	5.90	-1	-1	2	4	2	-2	1
25	6.73	2	1	2	0	2	4	-2
26	6.82	0	0	4	0	2	2	-1
27	6.85	2	0	2	0	0	3	0
28	6.98	1	0	2	1	2	3	-1
29	7.08	0	0	2	2	0	4	0
30	7.13	2	0	0	2	1	-1	1
31	7.23	0	-1	2	2	1	-4	2
32	7.34	-2	0	2	4	1	-2	1
33	7.38	0	-2	2	2	2	-1	1
34	7.39	0	0	0	4	1	-2	1
35	8.68	1	0	4	-2	2	2	-1
36	8.73	3	0	2	-2	1	2	-1
37	8.90	1	1	2	0	1	4	-2
38	9.05	-1	0	4	0	1	2	-1
39	9.11	0	1	2	1	2	-2	1
40	9.17	-3	0	0	0	1	-1	1

Table A.IV cont.

Zhu *et al.* Theory of Nutation: Additional Terms

Index j	Period (days)	Argument coefficient k_{j1}	k_{j2}	k_{j3}	k_{j4}	k_{j5}	A_{0j} ($0''.00001$)	B_{0j} ($0''.00001$)
41	9.33	0	0	2	1	1	3	-1
42	9.35	1	-1	2	0	1	-4	2
43	9.60	-1	0	0	-2	1	-4	3
44	10.07	1	0	0	-4	1	-1	1
45	10.10	-1	0	0	4	1	-2	1
46	10.37	-1	-1	0	4	0	1	0
47	12.38	2	1	2	-2	2	3	-1
48	12.64	0	0	4	-2	1	2	-1
49	13.22	1	0	2	-1	2	-3	1
50	13.28	2	1	0	0	0	-3	0
51	13.63	0	0	2	0	1	-1	0
52	13.69	0	0	2	0	3	2	0
53	14.22	0	1	0	2	1	2	-1
54	14.25	1	0	0	1	0	-3	0
55	14.32	2	-1	0	0	0	4	0
56	14.60	-2	0	2	2	1	2	-1
57	14.70	0	0	0	-2	2	1	-1
58	15.35	0	1	0	-2	1	-3	2
59	15.42	0	-1	0	2	1	-2	1
60	15.87	2	0	0	-4	1	-1	1
61	15.94	-2	0	0	4	1	1	-1
62	16.06	0	-2	0	2	0	2	0
63	16.10	0	0	2	-4	1	-1	1
64	22.40	1	1	2	-2	1	3	-1
65	25.22	-1	1	2	0	2	4	-2
66	25.53	-1	-1	0	0	1	2	-1
67	25.72	1	1	0	0	1	-3	2
68	26.77	1	0	-2	0	1	3	-1
69	27.32	0	0	1	0	1	-2	0
70	29.26	-1	-1	2	0	2	-2	1
71	29.39	-1	1	0	2	1	-1	1
72	29.40	0	0	0	-1	1	3	-2
73	29.66	0	0	0	1	1	-4	2
74	29.67	-1	1	0	0	1	-2	2
75	31.52	1	0	0	-2	2	3	-1
76	32.11	-1	0	0	2	2	-4	2
77	32.45	-1	0	2	-2	2	3	-1
78	35.80	-1	1	2	-2	1	-1	1
79	38.52	-1	-2	0	2	0	3	0
80	38.74	1	0	2	-4	1	-4	2

Table A.IV cont.

Zhu *et al.* Theory of Nutation: Additional Terms

Index j	Period (days)	Argument coefficient k_{j1}	k_{j2}	k_{j3}	k_{j4}	k_{j5}	A_{0j} ($0''.00001$)	B_{0j} ($0''.00001$)
81	121.75	0	3	0	0	0	3	0
82	129.17	-2	-1	0	2	1	-2	1
83	177.85	0	-2	0	0	1	-1	1
84	219.17	2	0	0	-2	2	-3	1
85	285.41	-2	1	2	0	1	-1	0
86	297.91	-2	1	2	0	2	-1	0
87	313.04	-1	0	2	-1	1	-4	1
88	329.82	0	-1	0	0	2	4	-1
89	438.33	1	0	0	-1	1	3	-1
90	471.95	-2	-1	2	0	2	1	-1
91	507.16	-2	-1	2	0	1	3	0
92	552.62	-3	0	2	1	2	2	-1
93	2266.13	0	0	0	0	3	-2	0
94	6159.14	-1	0	1	0	2	3	-1
95	4.74	2	-1	2	2	2	-1	0
96	4.86	0	-1	2	4	2	-1	0
97	5.58	3	-1	2	0	2	-1	0
98	5.73	1	-1	2	2	1	-1	0
99	5.82	1	0	0	4	0	1	0
100	6.64	4	0	2	-2	2	1	0
101	6.73	2	1	2	0	1	1	0
102	6.89	4	0	0	0	0	1	0
103	6.95	0	1	2	2	1	1	0
104	6.97	1	0	2	1	1	1	0
105	6.98	2	-1	2	0	1	-1	0
106	7.22	-1	0	2	3	2	1	0
107	7.50	-2	-1	2	4	2	-1	0
108	7.54	0	-1	0	4	0	1	0
109	8.94	2	0	2	-1	2	-1	0
110	9.10	1	0	2	0	-1	1	0
111	9.20	3	0	0	0	1	1	0
112	9.30	-1	1	2	2	1	1	0
113	9.37	1	1	0	2	0	-1	0
114	9.89	1	-1	0	2	1	-1	0
115	10.08	-1	-2	2	2	2	-1	0
116	12.35	2	1	2	-2	1	1	0
117	12.71	0	2	2	0	2	1	0
118	12.76	2	0	2	-2	0	-1	0
119	13.49	-2	0	4	0	2	-1	0
120	13.72	1	1	0	1	0	1	0

Table A.IV cont.

Zhu *et al.* Theory of Nutation: Additional Terms

Index j	Period (days)	Argument coefficient k_{j1}	k_{j2}	k_{j3}	k_{j4}	k_{j5}	A_{0j} ($0''.00001$)	B_{0j} ($0''.00001$)
121	13.83	2	0	0	0	2	-1	0
122	14.13	-1	0	2	1	2	1	0
123	14.16	0	1	0	2	-1	-1	0
124	14.76	0	-2	2	0	2	-1	0
125	14.93	2	0	-2	2	-1	1	0
126	15.24	-2	-1	2	2	2	1	0
127	15.31	-1	0	0	3	0	-1	0
128	16.63	-2	-1	0	4	0	1	0
129	23.43	-1	0	4	-2	2	-1	0
130	23.94	1	2	0	0	0	-1	0
131	25.13	-1	1	2	0	-1	1	0
132	25.32	0	0	2	-1	1	-1	0
133	25.52	1	-1	2	-2	1	-1	0
134	25.62	1	-1	2	-2	2	-1	0
135	25.83	2	0	0	-1	0	1	0
136	27.09	-1	2	0	2	0	-1	0
137	27.32	0	-1	2	-1	2	1	0
138	28.15	3	0	-2	0	-1	1	0
139	29.14	-1	-1	2	0	1	-1	0
140	29.14	-1	1	0	2	-1	-1	0
141	31.06	-3	0	2	2	1	1	0
142	32.45	1	-2	0	0	0	1	0
143	34.48	-2	0	0	3	0	-1	0
144	37.62	-3	0	0	4	0	1	0
145	38.52	-1	0	-2	4	-2	-1	0
146	38.96	-1	0	-2	4	0	-1	0
147	43.06	-1	-1	-2	4	-2	1	0
148	43.34	1	1	2	-4	1	-1	0
149	90.10	0	2	2	-2	1	1	0
150	96.78	2	0	2	-4	2	-1	0
151	134.27	2	1	0	-2	1	1	0
152	156.52	-2	0	4	-2	2	-1	0
153	164.08	-2	2	2	0	2	-1	0
154	187.67	0	2	0	0	1	-1	0
155	193.56	1	-1	2	-3	2	1	0
156	235.96	-4	0	2	2	2	-1	0

C1-2

Table A.V

ZMOA 1990-2 Theory of Nutation: 1980 IAU Terms

Index j	Period (days)	Argument coefficient k_{j1}	k_{j2}	k_{j3}	k_{j4}	k_{j5}	A_{0j} ($0''.00001$)	A_{1j}	B_{0j} ($0''.00001$)	B_{1j}
1	6798.38	0	0	0	0	1	-1720670	-1743	920525	90
2	3399.19	0	0	0	0	2	20751	2	-8977	5
3	1305.48	-2	0	2	0	1	460	0	-243	0
4	1095.18	2	0	-2	0	0	110	0	1	0
5	1615.75	-2	0	2	0	2	-31	0	14	0
6	3232.86	1	-1	0	-1	0	-33	0	0	0
7	6786.32	0	-2	2	-2	1	-15	0	8	0
8	943.23	2	0	-2	0	1	7	0	-4	0
9	182.62	0	0	2	-2	2	-131714	-16	57305	-31
10	365.26	0	1	0	0	0	14764	-36	732	-2
11	121.75	0	1	2	-2	2	-5168	12	2244	-7
12	365.22	0	-1	2	-2	2	2161	-5	-960	3
13	177.84	0	0	2	-2	1	1291	1	-698	0
14	205.89	2	0	0	-2	0	479	0	5	0
15	173.31	0	0	2	-2	0	-219	0	-1	0
16	182.63	0	2	0	0	0	168	-1	2	0
17	386.00	0	1	0	0	1	-140	0	86	0
18	91.31	0	2	2	-2	2	-158	1	69	0
19	346.64	0	-1	0	0	1	-128	0	64	0
20	199.84	-2	0	0	2	1	-58	0	31	0
21	346.60	0	-1	2	-2	1	-48	0	28	0
22	212.32	2	0	0	-2	1	41	0	-22	0
23	119.61	0	1	2	-2	1	36	0	-20	0
24	411.78	1	0	0	-1	0	-45	0	-7	0
25	131.67	2	1	0	-2	0	11	0	0	0
26	169.00	0	0	-2	2	1	9	0	-4	0
27	329.79	0	1	-2	2	0	-9	0	0	0
28	409.23	0	1	0	0	2	7	0	-3	0
29	388.27	-1	0	0	1	1	10	0	-4	0
30	117.54	0	1	2	-2	0	-6	0	0	0
31	13.66	0	0	2	0	2	-22756	-2	9779	-5
32	27.55	1	0	0	0	0	7111	1	-67	0
33	13.63	0	0	2	0	1	-3871	-4	2006	0
34	9.13	1	0	2	0	2	-3012	0	1289	-1
35	31.81	1	0	0	-2	0	-1570	0	-13	0
36	27.09	-1	0	2	0	2	1235	0	-533	0
37	14.77	0	0	0	2	0	636	0	-12	0
38	27.67	1	0	0	0	1	632	1	-332	0
39	27.44	-1	0	0	0	1	-581	-1	315	0
40	9.56	-1	0	2	2	2	-596	0	255	0

Table A.V cont.

ZMOA 1990-2 Theory of Nutation: 1980 IAU Terms

Index j	Period (days)	Argument coefficient k_{j1}	k_{j2}	k_{j3}	k_{j4}	k_{j5}	A_{0j} ($0''.00001$)	A_{1j}	B_{0j} ($0''.00001$)	B_{1j}
41	9.12	1	0	2	0	1	-515	0	264	0
42	7.10	0	0	2	2	2	-384	0	164	0
43	13.78	2	0	0	0	0	293	0	-6	0
44	23.94	1	0	2	-2	2	286	0	-124	0
45	6.86	2	0	2	0	2	-309	0	132	0
46	13.61	0	0	2	0	0	259	0	-5	0
47	26.98	-1	0	2	0	1	205	0	-107	0
48	31.96	-1	0	0	2	1	152	0	-80	0
49	31.66	1	0	0	-2	1	-129	0	70	0
50	9.54	-1	0	2	2	1	-102	0	52	0
51	34.85	1	1	0	-2	0	-74	0	-1	0
52	13.17	0	1	2	0	2	76	0	-33	0
53	14.19	0	-1	2	0	2	-76	0	33	0
54	5.64	1	0	2	2	2	-77	0	32	0
55	9.61	1	0	0	2	0	66	0	-2	0
56	12.81	2	0	2	-2	2	65	0	-28	0
57	14.80	0	0	0	2	1	-64	0	33	0
58	7.09	0	0	2	2	1	-66	0	34	0
59	23.86	1	0	2	-2	1	58	0	-30	0
60	14.73	0	0	0	-2	1	-50	0	28	0
61	29.80	1	-1	0	0	0	47	0	-1	0
62	6.85	2	0	2	0	1	-53	0	26	0
63	15.39	0	1	0	-2	0	-44	0	-1	0
64	26.88	1	0	-2	0	0	41	0	1	0
65	29.53	0	0	0	1	0	-40	0	1	0
66	25.62	1	1	0	0	0	-34	0	1	0
67	9.11	1	0	2	0	0	34	0	-1	0
68	9.37	1	-1	2	0	2	-29	0	12	0
69	9.81	-1	-1	2	2	2	-29	0	12	0
70	13.75	-2	0	0	0	1	-23	0	13	0
71	5.49	3	0	2	0	2	-29	0	12	0
72	7.24	0	-1	2	2	2	-26	0	11	0
73	8.91	1	1	2	0	2	24	0	-10	0
74	32.61	-1	0	2	-2	1	-20	0	11	0
75	13.81	2	0	0	0	1	21	0	-11	0
76	27.78	1	0	0	0	2	-20	0	8	0
77	9.18	3	0	0	0	0	16	0	-1	0
78	9.34	0	0	2	1	2	16	0	-7	0
79	27.33	-1	0	0	0	2	14	0	-6	0
80	10.08	1	0	0	-4	0	-14	0	-1	0

Table A.V cont.

ZMOA 1990-2 Theory of Nutation: 1980 IAU Terms

Index j	Period (days)	Argument coefficient k_{j1}	k_{j2}	k_{j3}	k_{j4}	k_{j5}	A_{0j} (0".00001)	A_{1j}	B_{0j} (0".00001)	B_{1j}
81	14.63	-2	0	2	2	2	13	0	-6	0
82	5.80	-1	0	2	4	2	-15	0	6	0
83	15.91	2	0	0	-4	0	-13	0	0	0
84	22.47	1	1	2	-2	2	13	0	-5	0
85	5.64	1	0	2	2	1	-13	0	7	0
86	7.35	-2	0	2	4	2	-12	0	5	0
87	9.06	-1	0	4	0	2	11	0	-5	0
88	29.26	1	-1	0	-2	0	9	0	0	0
89	12.79	2	0	2	-2	1	10	0	-5	0
90	4.68	2	0	2	2	2	-11	0	5	0
91	9.63	1	0	0	2	1	-10	0	5	0
92	12.66	0	0	4	-2	2	9	0	-4	0
93	8.75	3	0	2	-2	2	9	0	-4	0
94	23.77	1	0	2	-2	0	-7	0	0	0
95	13.41	0	1	2	0	1	8	0	-4	0
96	35.03	-1	-1	0	2	1	7	0	-4	0
97	13.58	0	0	-2	0	1	-6	0	3	0
98	25.42	0	0	2	-1	2	-7	0	3	0
99	14.19	0	1	0	2	0	-6	0	0	0
100	9.53	1	0	-2	-2	0	-6	0	0	0
101	14.16	0	-1	2	0	1	-7	0	3	0
102	34.67	1	1	0	-2	1	-6	0	3	0
103	32.76	1	0	-2	2	0	-6	0	0	0
104	7.13	2	0	0	2	0	6	0	0	0
105	4.79	0	0	2	4	2	-7	0	3	0
106	27.32	0	1	0	1	0	5	0	0	0

Table A.VI

ZMOA 1990-2 Theory of Nutation: Additional Terms

Index j	Period (days)	Argument coefficient k_{j1}	k_{j2}	k_{j3}	k_{j4}	k_{j5}	A_{0j} ($0''.00001$)	B_{0j} ($0''.00001$)
1	5.49	3	0	2	0	1	-5	2
2	5.73	1	-1	2	2	2	-6	2
3	6.96	0	1	2	2	2	5	-2
4	6.99	2	-1	2	0	2	-5	2
5	7.38	0	0	0	4	0	5	0
6	9.31	-1	1	2	2	2	6	-2
7	9.80	-1	-1	2	2	1	-5	2
8	9.87	1	-1	0	2	0	5	0
9	14.83	0	0	0	2	2	-5	2
10	29.93	1	-1	0	0	1	5	-3
11	73.05	0	3	2	-2	2	-5	2
12	187.66	0	0	2	-2	3	13	-2
13	3230.13	-1	-1	2	-1	2	13	-5
14	3231.50	-1	0	1	0	1	-15	3
15	6164.10	-1	1	0	1	1	7	-4
16	4.00	3	0	2	2	2	-1	1
17	4.08	1	0	2	4	2	-2	1
18	4.58	4	0	2	0	2	-3	1
19	4.68	2	0	2	2	1	-2	1
20	4.79	0	0	2	4	1	-1	1
21	5.56	1	1	2	2	2	1	-1
22	5.80	-1	0	2	4	1	-3	1
23	5.90	-1	-1	2	4	2	-2	1
24	6.73	2	1	2	0	2	4	-2
25	6.82	0	0	4	0	2	2	-1
26	6.85	2	0	2	0	0	3	0
27	6.98	1	0	2	1	2	3	-1
28	7.08	0	0	2	2	0	4	0
29	7.13	2	0	0	2	1	-1	1
30	7.23	0	-1	2	2	1	-4	2
31	7.34	-2	0	2	4	1	-2	1
32	7.39	0	0	0	4	1	-2	1
33	8.68	1	0	4	-2	2	2	-1
34	8.73	3	0	2	-2	1	2	-1
35	8.90	1	1	2	0	1	4	-2
36	9.05	-1	0	4	0	1	2	-1
37	9.11	0	1	2	1	2	-2	1
38	9.17	-3	0	0	0	1	-1	1
39	9.33	0	0	2	1	1	3	-1
40	9.35	1	-1	2	0	1	-4	2

Table A.VI cont.

ZMOA 1990-2 Theory of Nutation: Additional Terms

Index j	Period (days)	Argument coefficient k_{j1}	k_{j2}	k_{j3}	k_{j4}	k_{j5}	A_{0j} ($0''.00001$)	B_{0j} ($0''.00001$)
41	9.60	-1	0	0	-2	1	-4	3
42	10.07	1	0	0	-4	1	-1	1
43	10.10	-1	0	0	4	1	-2	1
44	10.37	-1	-1	0	4	0	1	0
45	12.38	2	1	2	-2	2	3	-1
46	12.64	0	0	4	-2	1	2	-1
47	13.22	1	0	2	-1	2	-3	1
48	13.28	2	1	0	0	0	-3	0
49	13.69	0	0	2	0	3	2	0
50	14.22	0	1	0	2	1	2	-1
51	14.25	1	0	0	1	0	-3	0
52	14.32	2	-1	0	0	0	4	0
53	14.60	-2	0	2	2	1	2	-1
54	14.70	0	0	0	-2	2	1	-1
55	15.35	0	1	0	-2	1	-3	2
56	15.42	0	-1	0	2	1	-2	1
57	15.87	2	0	0	-4	1	-1	1
58	15.94	-2	0	0	4	1	1	-1
59	16.06	0	-2	0	2	0	2	0
60	16.10	0	0	2	-4	1	-1	1
61	22.40	1	1	2	-2	1	3	-1
62	25.22	-1	1	2	0	2	4	-2
63	25.53	-1	-1	0	0	1	2	-1
64	25.72	1	1	0	0	1	-3	2
65	26.77	1	0	-2	0	1	3	-1
66	27.32	0	0	1	0	1	-2	0
67	29.26	-1	-1	2	0	2	-2	1
68	29.39	-1	1	0	2	1	-1	1
69	29.40	0	0	0	-1	1	3	-2
70	29.66	0	0	0	1	1	-4	2
71	29.67	-1	1	0	0	1	-2	2
72	31.52	1	0	0	-2	2	3	-1
73	32.11	-1	0	0	2	2	-4	2
74	32.45	-1	0	2	-2	2	3	-1
75	35.80	-1	1	2	-2	1	-1	1
76	38.52	-1	-2	0	2	0	3	0
77	38.74	1	0	2	-4	1	-4	2
78	121.75	0	3	0	0	0	3	0
79	129.17	-2	-1	0	2	1	-2	1
80	177.85	0	-2	0	0	1	-1	1

Table A.VI cont.

ZMOA 1990-2 Theory of Nutation: Additional Terms

Index j	Period (days)	Argument coefficient k_{j1}	k_{j2}	k_{j3}	k_{j4}	k_{j5}	A_{0j} ($0''.00001$)	B_{0j} ($0''.00001$)
81	219.17	2	0	0	-2	2	-3	1
82	285.41	-2	1	2	0	1	-1	0
83	297.91	-2	1	2	0	2	-1	0
84	313.04	-1	0	2	-1	1	-4	1
85	329.82	0	-1	0	0	2	4	-1
86	438.33	1	0	0	-1	1	3	-1
87	471.95	-2	-1	2	0	2	2	-1
88	507.16	-2	-1	2	0	1	3	0
89	552.62	-3	0	2	1	2	2	-1
90	2266.13	0	0	0	0	3	-2	0
91	6159.14	-1	0	1	0	2	3	-1

Table A.VII

ZMOA 1990-2 Theory of Nutation: Out-of-Phase Terms

Index j	Period (days)	Argument coefficient k_{j1}	k_{j2}	k_{j3}	k_{j4}	k_{j5}	A_{2j} ($0''.00001$)	B_{2j} ($0''.00001$)
1	6798.38	0	0	0	0	1	375	168
2	182.62	0	0	2	-2	2	-150	-52
3	365.26	0	1	0	0	0	82	-28
4	13.66	0	0	2	0	2	-2	1
5	3399.19	0	0	0	0	2	-8	-3
6	27.56	1	0	0	0	0	-3	3
7	121.75	0	1	2	-2	2	-6	-2
8	13.63	0	0	2	0	1	-1	0
9	9.13	1	0	2	0	2	3	1
10	365.22	1	-1	2	-2	2	1	1
11	31.81	1	0	0	-2	0	-1	-1
12	177.84	0	0	2	-2	1	2	0
13	27.09	-1	0	2	0	2	1	0
14	386.00	0	1	0	0	1	1	0
15	346.64	0	-1	0	0	1	1	0
16	411.78	1	0	0	-1	0	-3	1

Table A.VIII

Kinoshita-Souchay Non-rigid Earth Theory of Nutation

Index j	Period (days)	Argument coefficient k_{j1}	k_{j2}	k_{j3}	k_{j4}	k_{j5}	A_{0j} (μas)	A_{1j}	B_{0j} (μas)	B_{1j}
1	6798.38	0	0	0	0	1	-17199635	-17416	9203279	884
2	3399.19	0	0	0	0	2	207281	21	-89691	47
3	1305.48	-2	0	2	0	1	4596	5	-2425	-1
4	1095.18	2	0	-2	0	0	1100	0	11	0
5	1615.75	-2	0	2	0	2	-312	0	131	0
6	3232.86	1	-1	0	-1	0	-327	0	-1	0
7	6786.32	0	-2	2	-2	1	-130	0	69	0
8	943.23	2	0	-2	0	1	71	0	-37	0
9	182.62	0	0	2	-2	2	-1318678	-155	573570	-305
10	365.26	0	1	0	0	0	142639	-351	5312	-13
11	121.75	0	1	2	-2	2	-51735	123	22459	-68
12	365.22	0	-1	2	-2	2	21686	-50	-9571	30
13	177.84	0	0	2	-2	1	12851	14	-6900	-1
14	205.89	2	0	0	-2	0	4768	0	43	0
15	173.31	0	0	2	-2	0	-2177	0	-14	0
16	182.63	0	2	0	0	0	1670	-8	13	0
17	386.00	0	1	0	0	1	-1449	-2	841	0
18	91.31	0	2	2	-2	2	-1579	7	685	-4
19	346.64	0	-1	0	0	1	-1211	1	619	0
20	199.84	-2	0	0	2	1	-576	-1	303	0
21	346.60	0	-1	2	-2	1	-482	-1	270	0
22	212.32	2	0	0	-2	1	402	0	-220	0
23	119.61	0	1	2	-2	1	355	0	-194	0
24	411.78	1	0	0	-1	0	-382	0	-28	0
25	131.67	2	1	0	-2	0	115	0	1	0
26	169.00	0	0	-2	2	1	87	0	-44	0
27	329.79	0	1	-2	2	0	-88	0	2	0
28	409.23	0	1	0	0	2	71	0	-32	0
29	388.27	-1	0	0	1	1	88	0	-44	0
30	117.54	0	1	2	-2	0	-66	0	0	0
31	13.66	0	0	2	0	2	-227422	-24	97765	-48
32	27.56	1	0	0	0	0	71162	7	-669	0
33	13.63	0	0	2	0	1	-38700	-37	20065	2
34	9.13	1	0	2	0	2	-30078	-4	12875	-6
35	31.81	1	0	0	-2	0	-15710	-1	-123	0
36	27.09	-1	0	2	0	2	12350	1	-5333	3
37	14.77	0	0	0	2	0	6340	1	-121	0
38	27.67	1	0	0	0	1	6311	6	-3323	0
39	27.44	-1	0	0	0	1	-5807	-6	3144	0
40	9.56	-1	0	2	2	2	-5951	-1	2550	-1

Table A.VIII cont.

Kinoshita-Souchay Non-rigid Earth Theory of Nutation

Index j	Period (days)	Argument coefficient k_{j1}	k_{j2}	k_{j3}	k_{j4}	k_{j5}	A_{0j} (μas)	A_{1j}	B_{0j} (μas)	B_{1j}
41	9.12	1	0	2	0	1	-5147	-4	2631	0
42	7.10	0	0	2	2	2	-3842	0	1638	-1
43	13.78	2	0	0	0	0	2925	0	-60	0
44	23.94	1	0	2	-2	2	2861	0	-1234	1
45	6.86	2	0	2	0	2	-3091	0	1319	-1
46	13.61	0	0	2	0	0	2586	0	-54	0
47	26.98	-1	0	2	0	1	2042	2	-1076	0
48	31.96	-1	0	0	2	1	1516	1	-801	0
49	31.66	1	0	0	-2	1	-1288	-1	695	0
50	9.54	-1	0	2	2	1	-1018	-1	521	0
51	34.85	1	1	0	-2	0	-735	0	-5	0
52	13.17	0	1	2	0	2	756	-2	-325	0
53	14.19	0	-1	2	0	2	-713	2	307	0
54	5.64	1	0	2	2	2	-765	0	324	0
55	9.61	1	0	0	2	0	658	0	-20	0
56	12.81	2	0	2	-2	2	642	0	-277	0
57	14.80	0	0	0	2	1	-630	-1	327	0
58	7.09	0	0	2	2	1	-661	-1	334	0
59	23.86	1	0	2	-2	1	571	1	-307	0
60	14.73	0	0	0	-2	1	-494	-1	273	0
61	29.80	1	-1	0	0	0	471	0	-4	0
62	6.85	2	0	2	0	1	-531	0	268	0
63	15.39	0	1	0	-2	0	-435	0	-8	0
64	26.88	1	0	-2	0	0	404	0	4	0
65	29.53	0	0	0	1	0	-422	0	3	0
66	25.62	1	1	0	0	0	-338	0	3	0
67	9.11	1	0	2	0	0	334	0	-11	0
68	9.37	1	-1	2	0	2	-287	0	123	0
69	9.81	-1	-1	2	2	2	-281	0	122	0
70	13.75	-2	0	0	0	1	-229	0	126	0
71	5.49	3	0	2	0	2	-288	0	123	0
72	7.24	0	-1	2	2	2	-263	0	114	0
73	8.91	1	1	2	0	2	246	0	-106	0
74	32.61	-1	0	2	-2	1	-200	0	107	0
75	13.81	2	0	0	0	1	218	0	-114	0
76	27.78	1	0	0	0	2	-197	0	85	0
77	9.18	3	0	0	0	0	157	0	-4	0
78	9.34	0	0	2	1	2	165	0	-72	0
79	27.33	-1	0	0	0	2	140	0	-61	0
80	10.08	1	0	0	-4	0	-133	0	-4	0

Table A.VIII cont.

Kinoshita-Souchay Non-rigid Earth Theory of Nutation

Index j	Period (days)	Argument coefficient k_{j1}	k_{j2}	k_{j3}	k_{j4}	k_{j5}	A_{0j} (μas)	A_{1j}	B_{0j} (μas)	B_{1j}
81	14.63	-2	0	2	2	2	139	0	-60	0
82	5.80	-1	0	2	4	2	-151	0	65	0
83	15.91	2	0	0	-4	0	-128	0	1	0
84	22.47	1	1	2	-2	2	128	0	-55	0
85	5.64	1	0	2	2	1	-132	0	66	0
86	7.35	-2	0	2	4	2	-121	0	52	0
87	9.06	-1	0	4	0	2	115	0	-49	0
88	29.26	1	-1	0	-2	0	95	0	0	0
89	12.79	2	0	2	-2	1	101	0	-54	0
90	4.68	2	0	2	2	2	-107	0	47	0
91	9.63	1	0	0	2	1	-95	0	49	0
92	12.66	0	0	4	-2	2	91	0	-39	0
93	8.75	3	0	2	-2	2	93	0	-40	0
94	23.77	1	0	2	-2	0	-77	0	0	0
95	13.14	0	1	2	0	1	81	0	-42	0
96	35.03	-1	-1	0	2	1	75	0	-39	0
97	13.58	0	0	-2	0	1	-68	0	36	0
98	25.42	0	0	2	-1	2	-67	0	31	0
99	14.19	0	1	0	2	0	-67	0	-1	0
100	9.53	1	0	-2	-2	0	-64	0	1	0
101	14.16	0	-1	2	0	1	-65	0	35	0
102	34.67	1	1	0	-2	1	-61	0	32	0
103	32.76	1	0	-2	2	0	-58	0	0	0
104	7.13	2	0	0	2	0	59	0	1	0
105	4.79	0	0	2	4	2	-68	0	29	0
106	27.32	0	1	0	1	0	57	0	0	0
107	66068.15	-1	1	0	1	2	-52	0	23	0
108	65502.23	-1	0	1	0	3	-6	0	0	0
109	6164.10	-1	1	0	1	1	126	0	-68	0
110	6159.14	-1	0	1	0	2	36	0	18	0
111	3396.17	0	2	-2	2	0	-9	0	0	0
112	3231.50	-1	0	1	0	1	-103	0	-89	0
113	2266.13	0	0	0	0	3	-22	0	10	0
114	2190.35	-1	0	1	0	0	33	0	0	0
115	2189.72	1	1	-2	1	-1	-7	0	0	0
116	1616.43	-2	2	0	2	0	-22	0	0	0
117	548.04	-2	-1	2	0	0	-4	0	0	0
118	507.16	-2	-1	2	0	1	6	0	-4	0
119	471.89	-2	1	0	2	0	1	0	4	0
120	438.33	-1	0	0	1	-1	-9	0	-8	0

Table A.VIII cont.

Kinoshita-Souchay Non-rigid Earth Theory of Nutation

Index j	Period (days)	Argument coefficient k_{j1}	k_{j2}	k_{j3}	k_{j4}	k_{j5}	A_{0j} (μas)	A_{1j}	B_{0j} (μas)	B_{1j}
121	329.82	0	-1	0	0	2	57	0	-25	0
122	313.04	1	0	-2	1	-1	23	0	14	0
123	299.26	1	0	-2	1	0	-7	0	0	0
124	285.41	-2	1	2	0	1	9	0	0	0
125	219.17	-2	0	0	2	-2	11	0	0	0
126	194.13	-2	0	0	2	2	17	0	-8	0
127	187.67	0	2	0	0	1	-9	0	5	0
128	187.66	0	0	-2	2	-3	-122	0	-28	0
129	177.85	0	-2	0	0	1	-6	0	0	0
130	134.27	-2	-1	0	2	-1	-8	0	0	0
131	129.17	-2	-1	0	2	1	-13	0	7	0
132	126.51	1	0	2	-3	2	6	0	0	0
133	95.42	-2	0	-2	4	-1	-10	0	-5	0
134	90.10	0	-2	-2	2	-1	-8	0	-5	0
135	73.05	0	3	2	-2	2	-44	0	19	0
136	38.96	-1	0	-2	4	0	-7	0	0	0
137	38.74	-1	0	-2	4	-1	47	0	24	0
138	38.52	-1	-2	0	2	0	27	0	0	0
139	38.52	-1	0	-2	4	-2	-7	0	0	0
140	37.63	-3	0	0	4	0	16	0	0	0
141	35.80	1	-1	-2	2	-1	11	0	5	0
142	35.23	0	0	2	-3	2	-20	0	8	0
143	34.48	-2	0	0	3	0	-5	0	0	0
144	32.45	1	0	-2	2	-2	-36	0	-16	0
145	32.45	1	-2	0	0	0	8	0	0	0
146	32.11	-1	0	0	2	2	-38	0	17	0
147	31.52	-1	0	0	2	-2	-32	0	-14	0
148	29.93	1	-1	0	0	1	51	0	-27	0
149	29.67	1	-1	0	0	-1	31	0	17	0
150	29.66	0	0	0	1	1	-37	0	20	0
151	29.40	0	0	0	1	-1	-33	0	-18	0
152	29.39	-1	1	0	2	1	-10	0	6	0
153	29.26	-1	-1	2	0	2	-16	0	6	0
154	29.14	-1	1	0	2	-1	-6	0	0	0
155	29.14	-1	-1	2	0	1	-6	0	0	0
156	28.15	-3	0	2	0	1	-8	0	0	0
157	27.43	0	1	0	1	1	5	0	0	0
158	27.32	0	1	-2	1	-2	-9	0	0	0
159	27.32	0	0	1	0	1	-17	0	-15	0
160	27.21	0	0	1	0	0	8	0	0	0

Table A.VIII cont.

Kinoshita-Souchay Non-rigid Earth Theory of Nutation

Index j	Period (days)	Argument coefficient k_{j1}	k_{j2}	k_{j3}	k_{j4}	k_{j5}	A_{0j} (μas)	A_{1j}	B_{0j} (μas)	B_{1j}
161	27.09	-1	2	0	2	0	-8	0	0	0
162	26.77	-1	0	2	0	-1	-27	0	-14	0
163	25.72	1	1	0	0	1	-34	0	19	0
164	25.62	-1	1	-2	2	-2	7	0	0	0
165	25.53	1	1	0	0	-1	-21	0	-12	0
166	25.33	0	0	-2	1	-1	10	0	5	0
167	25.22	-1	1	2	0	2	45	0	-20	0
168	25.13	-1	1	2	0	1	9	0	-5	0
169	23.43	1	0	-4	2	-2	9	0	0	0
170	22.40	-1	-1	-2	2	-1	-23	0	-12	0
171	16.63	-2	-1	0	4	0	12	0	0	0
172	16.10	0	0	-2	4	-1	16	0	9	0
173	16.06	0	-2	0	2	0	21	0	0	0
174	15.94	-2	0	0	4	1	11	0	-6	0
175	15.87	-2	0	0	4	-1	11	0	5	0
176	15.42	0	-1	0	2	1	-14	0	7	0
177	15.35	0	-1	0	2	-1	40	0	18	0
178	15.31	-1	0	0	3	0	-11	0	0	0
179	15.24	-2	-1	2	2	2	6	0	0	0
180	14.93	2	0	-2	2	-1	8	0	0	0
181	14.83	0	0	0	2	2	-46	0	20	0
182	14.77	0	-2	2	0	2	-8	0	0	0
183	14.70	0	0	0	2	-2	-13	0	-5	0
184	14.60	-2	0	2	2	1	21	0	-11	0
185	14.57	-2	0	2	2	0	-6	0	0	0
186	14.32	2	-1	0	0	0	38	0	0	0
187	14.25	1	0	0	1	0	-33	0	0	0
188	14.22	0	1	0	2	1	18	0	-9	0
189	14.16	0	1	0	2	-1	-5	0	0	0
190	14.13	-1	0	2	1	2	8	0	0	0
191	13.83	2	0	0	0	2	-8	0	0	0
192	13.72	2	0	0	0	-2	-6	0	0	0
193	13.72	1	1	0	1	0	5	0	0	0
194	13.69	0	0	2	0	3	20	0	0	0
195	13.49	-2	0	4	0	2	-7	0	0	0
196	13.28	2	1	0	0	0	-28	0	0	0
197	13.28	-2	1	-2	2	-2	-5	0	0	0
198	13.22	-1	0	-2	1	-2	33	0	13	0
199	12.76	-2	0	-2	2	0	8	0	0	0
200	12.71	0	2	2	0	2	7	0	0	0

Table A.VIII cont.

Kinoshita-Souchay Non-rigid Earth Theory of Nutation

Index j	Period (days)	Argument coefficient k_{j1}	k_{j2}	k_{j3}	k_{j4}	k_{j5}	A_{0j} (μas)	A_{1j}	B_{0j} (μas)	B_{1j}
201	12.64	0	0	-4	2	-1	-12	0	-7	0
202	12.38	-2	-1	-2	2	-2	-23	0	-10	0
203	10.37	-1	-1	0	4	0	15	0	0	0
204	10.10	-1	0	0	4	1	-18	0	9	0
205	10.08	-1	-2	2	2	2	-9	0	0	0
206	10.07	-1	0	0	4	-1	12	0	6	0
207	9.87	1	-1	0	2	0	48	0	1	0
208	9.80	-1	-1	2	2	1	-46	0	24	0
209	9.60	1	0	0	2	-1	50	0	27	0
210	9.37	1	1	0	2	0	-11	0	0	0
211	9.35	1	-1	2	0	1	-41	0	22	0
212	9.33	0	0	2	1	1	27	0	-14	0
213	9.31	-1	1	2	2	2	56	0	-23	0
214	9.30	-1	1	2	2	1	7	0	0	0
215	9.20	3	0	0	0	1	7	0	0	0
216	9.17	3	0	0	0	-1	14	0	8	0
217	9.11	0	1	2	1	2	-24	0	10	0
218	9.10	1	0	2	0	-1	10	0	5	0
219	9.05	-1	0	4	0	1	19	0	-9	0
220	8.93	-2	0	-2	1	-2	6	0	0	0
221	8.90	1	1	2	0	1	36	0	-18	0
222	8.73	-3	0	-2	2	-1	-12	0	-7	0
223	8.68	-1	0	-4	2	-2	-19	0	-9	0
224	7.53	0	-1	0	4	0	6	0	0	0
225	7.50	-2	-1	2	4	2	-9	0	0	0
226	7.39	0	0	0	4	1	-13	0	7	0
227	7.38	0	0	0	4	0	48	0	1	0
228	7.38	0	-2	2	2	2	-11	0	5	0
229	7.34	-2	0	2	4	1	-14	0	10	0
230	7.23	0	-1	2	2	1	-44	0	23	0
231	7.22	-1	0	2	3	2	8	0	0	0
232	7.13	2	0	0	2	1	-9	0	5	0
233	7.12	2	0	0	2	-1	5	0	0	0
234	7.08	0	0	2	2	0	41	0	1	0
235	6.99	2	-1	2	0	2	-48	0	21	0
236	6.98	1	0	2	1	2	33	0	-14	0
237	6.98	2	-1	2	0	1	-6	0	0	0
238	6.97	1	0	2	1	1	5	0	0	0
239	6.96	0	1	2	2	2	54	0	-16	0
240	6.95	0	1	2	2	1	7	0	0	0

Table A.VIII cont.

Kinoshita-Souchay Non-rigid Earth Theory of Nutation

Index j	Period (days)	Argument coefficient k_{j1}	k_{j2}	k_{j3}	k_{j4}	k_{j5}	A_{0j} (μas)	A_{1j}	B_{0j} (μas)	B_{1j}
241	6.89	4	0	0	0	0	9	0	0	0
242	6.85	2	0	2	0	0	36	0	1	0
243	6.82	0	0	4	0	2	19	0	-8	0
244	6.73	2	1	2	0	2	40	0	-17	0
245	6.73	2	1	2	0	1	5	0	0	0
246	6.64	-4	0	-2	2	-2	-9	0	0	0
247	5.90	-1	-1	2	4	2	-17	0	7	0
248	5.82	1	0	0	4	0	8	0	0	0
249	5.80	-1	0	2	4	1	-26	0	13	0
250	5.73	1	-1	2	2	2	-59	0	25	0
251	5.73	1	-1	2	2	1	-8	0	0	0
252	5.66	3	0	0	2	0	5	0	0	0
253	5.63	1	0	2	2	0	8	0	0	0
254	5.58	3	-1	2	0	2	-5	0	0	0
255	5.56	1	1	2	2	2	15	0	-6	0
256	5.49	3	0	2	0	1	-49	0	25	0
257	4.86	0	-1	2	4	2	-7	0	0	0
258	4.79	0	0	2	4	1	-12	0	6	0
259	4.74	2	-1	2	2	2	-7	0	0	0
260	4.68	2	0	2	2	1	-18	0	10	0
261	4.58	4	0	2	0	2	-26	0	11	0
262	4.08	1	0	2	4	2	-16	0	7	0
263	4.00	3	0	2	2	2	-14	0	0	0

Table A.IX

Kinoshita-Souchay Non-rigid Earth Theory of Nutation: Planetary Terms

Index j	Period (years)	Argument coefficient k_{j1}	k_{j2}	k_{j3}	k_{j4}	k_{j5}	k_{j6}	k_{j7}	k_{j8}	k_{j9}	k_{j10}	$S_{\psi j}$ (μas)	$C_{\psi j}$ (μas)	$S_{\epsilon j}$ (μas)	$C_{\epsilon j}$ (μas)
1	274.21	0	2	0	-2	0	0	2	0	-2	1	30	0	0	-16
2	273.03	18	-16	0	0	0	0	0	0	-1	0	23	10	0	0
3	241.15	8	-12	0	0	0	0	1	-1	0	-1	-120	60	-31	-63
4	104.14	0	0	2	0	0	0	1	-1	0	0	28	-8	0	-15
5	103.72	0	1	-2	0	0	0	0	0	0	-1	45	-42	23	24
6	95.80	3	-4	0	0	0	0	1	0	-1	0	0	12	0	0
7	49.79	5	-6	0	0	0	0	2	-2	0	0	0	24	0	0
8	47.90	6	-8	0	0	0	0	2	0	-2	0	8	0	0	0
9	37.32	0	2	0	-3	0	0	2	0	-2	-1	-9	0	0	-5
10	37.13	0	2	0	-3	0	0	2	0	-2	0	-35	-6	0	0
11	34.86	0	1	0	-1	0	0	1	0	-1	0	-5	0	0	0
12	32.70	0	0	0	1	0	0	0	0	0	1	0	-7	0	0
13	32.70	0	1	0	1	0	0	1	-1	0	0	0	-8	0	0
14	29.49	0	1	0	0	1	0	1	-1	0	-1	-17	9	0	-9
15	29.42	0	1	0	0	-1	0	1	-1	0	-1	7	0	0	0
16	29.40	0	0	0	0	1	2	0	0	0	0	0	-5	0	0
17	20.19	8	-13	0	0	0	0	0	0	0	1	5	7	0	0
18	19.97	18	-16	0	0	0	0	0	0	-1	1	-6	0	0	0
19	19.01	0	0	0	2	-5	0	0	0	0	-1	-8	0	0	0
20	18.81	0	4	-8	3	0	0	0	0	0	-1	-8	30	-16	-4
21	18.63	0	1	0	0	0	0	1	-1	0	-2	-2	6	0	0
22	18.60	0	1	0	0	0	0	1	-1	0	0	7	-17	0	0
23	18.42	0	4	-8	3	0	0	0	0	0	1	-8	29	16	4
24	18.23	0	0	0	2	-5	0	0	0	0	1	-7	0	0	0
25	17.43	0	2	0	-2	0	0	2	0	-2	0	-45	0	0	0

Table A.IX cont.

Kinoshita-Souchay Non-rigid Earth Theory of Nutation: Planetary Terms

Index j	Period (years)	Argument coefficient k_{j1}	k_{j2}	k_{j3}	k_{j4}	k_{j5}	k_{j6}	k_{j7}	k_{j8}	k_{j9}	k_{j10}	$S_{\psi j}$ (μas)	$C_{\psi j}$ (μas)	$S_{\epsilon j}$ (μas)	$C_{\epsilon j}$ (μas)
26	17.43	18	-16	0	0	0	0	0	0	-1	-1	-6	-3	0	0
27	17.27	8	-13	0	0	0	0	0	0	0	-1	4	6	0	0
28	15.79	0	0	2	0	0	0	1	-1	0	-1	-27	8	0	0
29	15.78	0	-1	2	0	0	0	0	0	0	0	2	-3	0	0
30	15.78	0	1	-2	0	0	0	0	0	0	0	-36	40	0	0
31	15.75	0	1	-2	0	0	-2	0	0	0	0	-6	0	0	0
32	14.72	0	0	0	0	2	2	0	0	0	0	-12	0	0	5
33	14.72	0	1	0	0	-2	0	1	-1	0	-1	5	-11	6	0
34	13.55	5	-6	0	0	0	0	2	-2	0	-1	0	-43	23	0
35	12.40	0	2	0	-3	0	0	2	0	-2	1	-5	0	0	3
36	11.87	0	1	0	1	0	0	1	-1	0	-1	5	19	-10	0
37	11.86	0	0	0	1	0	0	0	0	0	0	-38	30	0	0
38	11.86	0	0	0	1	0	0	0	0	0	0	34	-5	0	0
39	9.75	3	-3	0	0	0	0	2	0	-2	0	-14	0	0	0
40	9.00	0	2	0	-2	0	0	2	0	-2	-1	-5	0	0	0
41	8.10	3	-5	0	0	0	0	0	0	0	0	-19	8	0	0
42	8.10	3	-5	0	0	0	-2	0	0	0	0	222	0	12	97
43	8.10	3	-5	0	0	0	-1	0	0	0	0	-10	-45	23	-6
44	7.89	0	2	-4	0	0	0	0	0	0	0	-10	13	0	0
45	7.88	0	2	-4	0	0	-2	0	0	0	0	5	0	0	0
46	7.84	5	-8	0	0	0	-2	0	0	0	0	0	-26	13	0
47	7.84	5	-7	0	0	0	0	1	-1	0	-1	-14	3	0	-7
48	5.92	0	0	0	2	0	2	0	0	0	0	-104	0	0	45
49	5.92	0	0	0	2	0	2	0	0	0	0	-10	3	0	0
50	5.92	0	0	0	2	0	1	0	0	0	0	0	5	0	0

Table A.1X cont.

Kinoshita-Souchay Non-rigid Earth Theory of Nutation: Planetary Terms

Index j	Period (years)	Argument coefficient k_{j1}	k_{j2}	k_{j3}	k_{j4}	k_{j5}	k_{j6}	k_{j7}	k_{j8}	k_{j9}	k_{j10}	$S_{\psi j}$ (μas)	$C_{\psi j}$ (μas)	$S_{\epsilon j}$ (μas)	$C_{\epsilon j}$ (μas)
51	5.92	0	1	0	-2	0	0	1	-1	0	-1	0	-14	8	0
52	5.64	3	-3	0	0	0	0	2	-2	0	-1	-12	2	0	-6
53	4.50	0	2	0	-2	0	0	2	-2	0	-1	-5	0	0	0
54	3.98	2	-3	0	0	0	0	0	0	0	0	0	14	0	0
55	3.98	2	-3	0	0	0	0	0	0	0	0	4	49	0	0
56	3.95	0	0	0	3	0	2	0	0	0	0	-12	0	0	5
57	2.67	1	-2	0	0	0	-2	0	0	0	0	0	-9	0	0
58	2.47	0	2	-3	0	0	0	0	0	0	0	-8	5	0	0
59	2.14	0	1	-1	0	0	0	0	0	0	0	-6	0	0	0
60	2.00	4	-6	0	0	0	-1	0	0	0	0	0	8	-5	1
61	2.00	4	-6	0	0	0	-2	0	0	0	0	-47	0	0	-21
62	2.00	4	-7	0	0	0	-2	0	0	0	0	0	6	0	0
63	1.60	1	-1	0	0	0	0	0	0	0	0	80	0	0	-4
64	1.60	1	-1	0	0	0	-2	0	0	0	0	0	-6	0	0
65	1.60	1	-1	0	0	0	-1	0	0	0	0	0	7	-4	-1
66	1.60	1	-1	0	0	0	0	0	0	0	0	61	0	0	-3
67	1.34	2	-4	0	0	0	-1	0	0	0	0	0	-5	0	1
68	1.34	0	1	0	-3	0	-2	0	0	0	0	-7	0	0	-2
69	1.33	2	-4	0	0	0	-2	0	0	0	0	12	0	0	5
70	1.33	2	-4	0	0	0	-2	0	0	0	0	38	0	0	15
71	1.20	0	1	0	-2	0	0	0	0	0	0	-29	43	0	7
72	1.15	0	3	-4	0	0	0	0	0	0	0	-12	5	0	1
73	1.14	3	-4	0	0	0	0	0	0	0	0	0	37	0	3
74	1.09	0	1	0	-1	0	0	0	0	0	0	-164	-4	0	10
75	1.09	0	1	0	-1	0	0	0	0	0	0	17	0	0	-7

Table A.IX cont.

Kinoshita-Souchay Non-rigid Earth Theory of Nutation: Planetary Terms

Index j	Period (years)	Argument coefficient k_{j1}	k_{j2}	k_{j3}	k_{j4}	k_{j5}	k_{j6}	k_{j7}	k_{j8}	k_{j9}	k_{j10}	$S_{\phi j}$ (μas)	$C_{\phi j}$ (μas)	$S_{\epsilon j}$ (μas)	$C_{\epsilon j}$ (μas)
76	1.03	0	1	0	0	-1	0	0	0	0	0	-9	0	0	0
77	0.94	0	0	2	0	0	2	0	0	0	0	-8	0	0	0
78	0.92	0	1	0	1	0	2	0	0	0	0	-30	0	0	13
79	0.89	3	-6	0	0	0	-2	0	0	0	0	0	-6	0	0
80	0.89	5	-7	0	0	0	-2	0	0	0	0	-25	0	0	-10
81	0.86	0	1	0	2	0	2	0	0	0	0	0	-5	0	0
82	0.80	2	-2	0	0	0	-1	0	0	0	0	0	5	0	0
83	0.80	2	-2	0	0	0	0	0	0	0	0	39	0	0	1
84	0.80	2	-2	0	0	0	0	0	0	0	0	-104	0	0	2
85	0.73	1	-3	0	0	0	-1	0	0	0	0	0	-5	0	0
86	0.73	1	-3	0	0	0	-2	0	0	0	0	-29	0	0	-12
87	0.73	1	-3	0	0	0	-2	0	0	0	0	17	0	0	7
88	0.57	0	2	0	-3	0	0	0	0	0	0	9	-7	0	0
89	0.57	6	-8	0	0	0	-2	0	0	0	0	-13	0	0	-5
90	0.57	2	-5	0	0	0	-2	0	0	0	0	0	-13	6	0
91	0.53	3	-3	0	0	0	0	0	0	0	0	20	0	0	0
92	0.53	3	-3	0	0	0	2	0	0	0	0	6	-2	0	0
93	0.53	3	-3	0	0	0	0	0	0	0	0	-11	-2	0	0
94	0.52	0	3	-2	0	0	2	0	0	0	0	8	-7	0	0
95	0.52	0	2	0	-1	0	2	0	0	0	0	-17	0	0	8
96	0.50	8	-11	0	0	0	2	0	0	0	0	-6	-11	0	0
97	0.50	0	6	-8	3	0	2	0	0	0	0	13	-45	-19	-5
98	0.50	0	2	-8	3	0	-2	0	0	0	0	12	-42	19	5
99	0.50	0	2	0	0	0	2	0	0	0	0	-10	0	0	0
100	0.50	8	-15	0	0	0	-2	0	0	0	0	-6	-11	0	0

Table A.IX cont.

Kinoshita-Souchay Non-rigid Earth Theory of Nutation: Planetary Terms

Index j	Period (years)	Argument coefficient k_{j1}	k_{j2}	k_{j3}	k_{j4}	k_{j5}	k_{j6}	k_{j7}	k_{j8}	k_{j9}	k_{j10}	$S_{\psi j}$ (μas)	$C_{\psi j}$ (μas)	$S_{\epsilon j}$ (μas)	$C_{\epsilon j}$ (μas)
101	0.48	0	1	2	0	0	0	0	0	0	0	-8	-7	0	0
102	0.48	0	2	0	1	0	2	0	0	0	0	17	-1	0	-8
103	0.47	3	-7	0	0	0	-2	0	0	0	0	7	0	0	0
104	0.44	2	-1	0	0	0	2	0	0	0	0	3	-18	-9	0
105	0.42	7	-9	0	0	0	-2	0	0	0	0	-7	0	0	0
106	0.40	4	-4	0	0	0	0	0	0	0	0	12	0	0	0
107	0.38	1	1	0	0	0	2	0	0	0	0	-32	0	0	14
108	0.35	0	3	0	-2	0	2	0	0	0	0	7	-9	0	0
109	0.35	3	-2	0	0	0	2	0	0	0	0	0	-12	-5	0
110	0.34	0	3	0	-1	0	2	0	0	0	0	56	2	0	-24
111	0.34	0	4	-2	0	0	2	0	0	0	0	15	0	0	-6
112	0.33	8	-10	0	0	0	-2	0	0	0	0	-5	0	0	0
113	0.32	5	-5	0	0	0	0	0	0	0	0	7	0	0	0
114	0.31	2	0	0	0	0	2	0	0	0	0	42	0	0	-18
115	0.26	0	4	0	-2	0	2	0	0	0	0	-19	0	0	9
116	0.04	18	-16	0	0	0	0	0	2	-1	2	-14	-7	-5	12
117	0.04	18	-16	0	0	0	0	0	-2	-1	-2	-12	-6	-6	-14

Table A.X

Woolard Theory of Nutation

Index j	Period (days)	Argument coefficient k_{j1}	k_{j2}	k_{j3}	k_{j4}	k_{j5}	A_{0j} ($0''.0001$)	A_{1j} ($0''.0001$)	B_{0j} ($0''.0001$)	B_{1j} ($0''.0001$)
1	6798.4	0	0	0	0	1	-172327	-173.7	92100	9.1
2	3399.2	0	0	0	0	2	2088	0.2	-904	0.4
3	1305.5	-2	0	2	0	1	45	0.0	-24	0.0
4	1095.2	2	0	-2	0	0	10	0.0	0	0.0
5	1615.7	-2	0	2	0	2	-3	0.0	2	0.0
6	3232.9	1	-1	0	-1	0	-2	0.0	0	0.0
7	6786.3	0	-2	2	-2	1	-4	0.0	2	0.0
8	182.6	0	0	2	-2	2	-12729	-1.3	5522	-2.9
9	365.3	0	1	0	0	0	1261	-3.1	0	0.0
10	121.7	0	1	2	-2	2	-497	1.2	216	-0.6
11	365.2	0	-1	2	-2	2	214	-0.5	-93	0.3
12	177.8	0	0	2	-2	1	124	0.1	-66	0.0
13	205.9	2	0	0	-2	0	45	0.0	0	0.0
14	173.3	0	0	2	-2	0	-21	0.0	0	0.0
15	182.6	0	2	0	0	0	16	-0.1	0	0.0
16	386.0	0	1	0	0	1	-15	0.0	8	0.0
17	91.3	0	2	2	-2	2	-15	0.1	7	0.0
18	346.6	0	-1	0	0	1	-10	0.0	5	0.0
19	199.8	-2	0	0	2	1	-5	0.0	3	0.0
20	346.6	0	-1	2	-2	1	-5	0.0	3	0.0
21	212.3	2	0	0	-2	1	4	0.0	-2	0.0
22	119.6	0	1	2	-2	1	3	0.0	-2	0.0
23	411.8	1	0	0	-1	0	-3	0.0	0	0.0
24	13.7	0	0	2	0	2	-2037	-0.2	884	-0.5
25	27.6	1	0	0	0	0	675	0.1	0	0.0
26	13.6	0	0	2	0	1	-342	-0.4	183	0.0
27	9.1	1	0	2	0	2	-261	0.0	113	-0.1
28	31.8	1	0	0	-2	0	-149	0.0	0	0.0
29	27.1	-1	0	2	0	2	114	0.0	-50	0.0
30	14.8	0	0	0	2	0	60	0.0	0	0.0
31	27.7	1	0	0	0	1	58	0.0	-31	0.0
32	27.4	-1	0	0	0	1	-57	0.0	30	0.0
33	9.6	-1	0	2	2	2	-52	0.0	22	0.0
34	9.1	1	0	2	0	1	-44	0.0	23	0.0
35	7.1	0	0	2	2	2	-32	0.0	14	0.0

Table A.X cont.

Woolard Theory of Nutation

Index j	Period (days)	Argument coefficient k_{j1}	k_{j2}	k_{j3}	k_{j4}	k_{j5}	A_{0j} (0".0001)	A_{1j}	B_{0j} (0".0001)	B_{1j}
36	13.8	2	0	0	0	0	28	0.0	0	0.0
37	23.9	1	0	2	-2	2	26	0.0	-11	0.0
38	6.9	2	0	2	0	2	-26	0.0	11	0.0
39	13.6	0	0	2	0	0	25	0.0	0	0.0
40	27.0	-1	0	2	0	1	19	0.0	-10	0.0
41	32.0	-1	0	0	2	1	14	0.0	-7	0.0
42	31.7	1	0	0	-2	1	-13	0.0	7	0.0
43	9.5	-1	0	2	2	1	-9	0.0	5	0.0
44	34.8	1	1	0	-2	0	-7	0.0	0	0.0
45	13.2	0	1	2	0	2	7	0.0	-3	0.0
46	14.2	0	-1	2	0	2	-6	0.0	3	0.0
47	5.6	1	0	2	2	2	-6	0.0	3	0.0
48	9.6	1	0	0	2	0	6	0.0	0	0.0
49	12.8	2	0	2	-2	2	6	0.0	-2	0.0
50	14.8	0	0	0	2	1	-6	0.0	3	0.0
51	7.1	0	0	2	2	1	-5	0.0	3	0.0
52	23.9	1	0	2	-2	1	5	0.0	-3	0.0
53	14.7	0	0	0	-2	1	-5	0.0	3	0.0
54	29.8	1	-1	0	0	0	4	0.0	0	0.0
55	6.9	2	0	2	0	1	-4	0.0	2	0.0
56	15.4	0	1	0	-2	0	-4	0.0	0	0.0
57	26.9	1	0	-2	0	0	4	0.0	0	0.0
58	29.5	0	0	0	1	0	-4	0.0	0	0.0
59	25.6	1	1	0	0	0	-3	0.0	0	0.0
60	9.1	1	0	2	0	0	3	0.0	0	0.0
61	9.4	1	-1	2	0	2	-3	0.0	0	0.0
62	9.8	-1	-1	2	2	2	-2	0.0	0	0.0
63	13.7	-2	0	0	0	1	-2	0.0	0	0.0
64	5.5	3	0	2	0	2	-2	0.0	0	0.0
65	7.2	0	-1	2	2	2	-2	0.0	0	0.0
66	8.9	1	1	2	0	2	2	0.0	0	0.0
67	32.6	-1	0	2	-2	1	-2	0.0	0	0.0
68	13.8	2	0	0	0	1	2	0.0	0	0.0
69	27.8	1	0	0	0	2	-2	0.0	0	0.0

APPENDIX B

GLOSSARY OF "MODEST" PARAMETERS

For the convenience of users of MODEST, Table B.I identifies the names of adjustable parameters in the code with the notation of this document. Brief definitions and either references to equations (in parentheses) or sections (no parentheses) are also given.

Table B.I

Glossary of MODEST Parameters

Parameter	MODEST name	Definition	Reference
r_{sp}	RSPINAX aaaaaaaa	Cylindrical	(2.36)
λ	LONGTUD aaaaaaaa	station	(2.37)
z	POLPROJ aaaaaaaa	coordinates	(2.38)
$\dot{r}_{sp}$	DRSP/DT aaaaaaaa	Time rates of	(2.36)
$\dot{\lambda}$	DLON/DT aaaaaaaa	change of	(2.37)
$\dot{z}$	DPOL/DT aaaaaaaa	station coordinates	(2.38)
x	X aaaaaaaa	Cartesian	(2.39)
y	Y aaaaaaaa	station	(2.40)
z	Z aaaaaaaa	coordinates	(2.41)
$\dot{x}$	DX/DT aaaaaaaa	Time rates of	(2.39)
$\dot{y}$	DY/DT aaaaaaaa	change of	(2.40)
$\dot{z}$	DZ/DT aaaaaaaa	station coordinates	(2.41)
l	AXISOFF aaaaaaaa	Antenna offset	(2.199)
h, l	*LOVE # aaaaaaaa	Love numbers	(2.49) to (2.51)
ψ	TIDEPHZ aaaaaaaa	Tide lag	(2.46)
ξ_i^j	OLAMgCccaaaaaaaaa OLAMgSccaaaaaaaaa	Ocean loading amplitudes	(2.74)
f	ATMOLOADaaaaaaaa	Loading factor	(2.80)
γ_{PPN}	GEN REL GAMMA FACTOR	PPN gamma	(2.16)
α	RIGHT ASCEN.sssssssssss	Source RA	(2.227)
δ	DECLINATION sssssssssss	Source declination	(2.227)
$\dot{\alpha}$	DRASCEN/DT sssssssssss	Time rates of change	(2.91)
$\dot{\delta}$	DDECLIN/DT sssssssssss	of RA, declination	(2.92)
K	FLUX RATIO sssssssssss	Source	(2.93)
s	SEPARATION sssssssssss	structure	to
θ	ORIENTATION sssssssssss	parameters	(2.97)

aaaaaaaa station name
sssssssssss source name
cc component name (alphanumeric)
g geometric direction (U, N, W)
* V or H

Table B.I cont.

Glossary of MODEST Parameters

Parameter	MODEST name	Definition	Reference
$\Theta_{1,2}$ $UT1 - UTC$	† POLE MOTION UT1 MINUS UTC	Pole position UT1 - UTC	(2.101-102) 2.6.1
$\dot{\Theta}_{1,2}$ $\dot{\Theta}_3$	† POLE RATE UT1-UTC RATE	Time rates of change of UTPM	(2.111)
A_{i3}, B_{i3} $A_{i,1-2}, B_{i,1-2}$	UT1 TIDAL AMPLITUDE cnnn †POL TIDAL AMPLITUDE cnnn	Tidal terms in UTPM	(2.114)
$\delta\Theta_{x,y,z}$ $\delta\dot{\Theta}_{x,y,z}$	‡ AXIS TWEAK OFFSET ‡ AXIS TWEAK RATE	Perturbation coefficients	(2.166) (2.166)
p_{LS} p_{PL}	LUNI-SOLAR PRECESSION PLANETARY PRECESSION	Precession constants	(2.156) (2.156)
A_{0j} A_{1j} $A_{2j,3j}$ B_{0j} B_{1j} $B_{2j,3j}$	NUTATION AMPLTD PSI cjjj NUTATION AMPLTD PSITcjjj NUTATION AMPLTD PSIA NUTATION AMPLTD EPS cjjj NUTATION AMPLTD EPSTcjjj NUTATION AMPLTD EPSA	Nutation amplitudes	(2.128) to (2.133)

† X or Y

‡ X, Y, or Z

c	component: S, C for sine, cosine
jjj	nutation series term number
nnn	tidal series term number

Table B.I cont.

Glossary of MODEST Parameters

Parameter	MODEST name	Definition	Reference
τ_{c1}	C EPOCH aaaaaaaa	Coefficients	(3.1)
τ_{c2}	C RATE aaaaaaaa	in clock	(3.1)
τ_{c3}	DCRAT/DTaaaaaaaa	model for	(3.1)
τ_{c4}	F OFFSETaaaaaaaa	delay and	(3.2)
τ_{c5}	F DRIFT aaaaaaaa	delay rate	(3.2)
τ_{c6}	C EPOS/Xaaaaaaaa	S/X clock offset	(3.3)
ρz_{dry}	DRYZTROPaaaaaaaa	Dry zenith delay	(4.3)
ρz_{wet}	WETZTROPaaaaaaaa	Wet zenith delay	(4.3)
$\dot{\rho} z_{dry}$	DDTRP/DTaaaaaaaa	Zenith delay	(4.4)
$\dot{\rho} z_{wet}$	DWTRP/DTaaaaaaaa	time rates	(4.4)
A_{dry}	DRYZMAPAaaaaaaaa	Chao map	(4.7) to
B_{dry}	DRYZMAPBaaaaaaaa	parameters	(4.11)
p	DRYMAPSGaaaaaaaa	Lanyi map parameter	(4.30)
T_0	SURFTEMPaaaaaaaa	CfA map surface temperature	(4.36)
$I_{e\ add}$	Z TECADDaaaaaaaa	Zenith electron content	(5.23)

aaaaaaaa station name

TECHNICAL REPORT STANDARD TITLE PAGE

1. Report No.	2. Government Accession No.	3. Recipient's Catalog No.
JPL Publication 83-39, Rev. 5		

4. Title and Subtitle	5. Report Date
Observation Model and Parameter Partials for the JPL VLBI Parameter Estimation Software "MODEST"---1994	August 1994
	6. Performing Organization Code

7. Author(s)	8. Performing Organization Report No.
O. J. Sovers and C. S. Jacobs	

9. Performing Organization Name and Address	10. Work Unit No.
JET PROPULSION LABORATORY California Institute of Technology 4800 Oak Grove Drive Pasadena, California 91109	11. Contract or Grant No. NAS7-918
	13. Type of Report and Period Covered JPL Publication
12. Sponsoring Agency Name and Address NATIONAL AERONAUTICS AND SPACE ADMINISTRATION Washington, D.C. 20546	14. Sponsoring Agency Code RE 211-BG-314-40-31-30-26D

15. Supplementary Notes

16. Abstract

This report is a revision of the document Observation Model and Parameter Partials for the JPL VLBI Parameter Estimation Software "MODEST"---1991, dated August 1, 1991. It supersedes that document and its four previous versions (1983, 1985, 1986, and 1987). A number of aspects of the very long baseline interferometry (VLBI) model were improved from 1991 to 1994. Treatment of tidal effects is extended to model the effects of ocean tides on universal time and polar motion (UTPM), including a default model for nearly diurnal and semidiurnal ocean tidal UTPM variations, and partial derivatives for all (solid and ocean) tidal UTPM amplitudes. The time-honored "K_1 correction" for solid Earth tides has been extended to include analogous frequency-dependent response of five tidal components. Partials of ocean loading amplitudes are now supplied. The Zhu-Mathews-Oceans-Anisotropy (ZMOA) 1990-2 and Kinoshita-Souchay models of nutation are now two of the modeling choices to replace the increasingly inadequate 1980 International Astronomical Union (IAU) nutation series. A rudimentary model of antenna thermal expansion is provided. Two more troposphere mapping functions have been added to the repertoire. Finally, correlations among VLBI observations via the model of Treuhaft and Lanyi improve modeling of the dynamic troposphere. A number of minor misprints in Rev. 4 have been corrected.

17. Key Words (Selected by Author(s))	18. Distribution Statement
Geodesy	Unclassified – Unlimited

19. Security Classif. (of this report)	20. Security Classif. (of this page)	21. No. of Pages	22. Price
Unclassified	Unclassified	111	